



TNF

Technisch-Naturwissenschaftliche
Fakultät

Doping induced effects in organic semiconductors and bulk heterojunctions

DISSERTATION

zur Erlangung des akademischen Grades

Doktor

im Doktoratsstudium der

TECHNISCHEN WISSENSCHAFTEN

Eingereicht von:

Mag. Jacek Gąsiorowski

Angefertigt am:

Linz Institute for Organic Solar Cells (LIOS)

Beurteilung:

o. Univ. Prof. Mag. Dr. DDr. h.c. Niyazi Serdar Sariciftci

Univ.-Prof. Dr. Achim Walter Hassel

Linz, October 2013

Eidesstattliche Erklärung

I hereby declare under oath that the submitted doctoral dissertation has been written solely by me without any outside assistance, information other than provided sources or aids have not been used and those used have been fully documented. The dissertation here present is identical to the electronically transmitted text document.

Ich erkläre an Eides statt, dass ich die vorliegende Dissertation selbstständig und ohne fremde Hilfe verfasst, andere als die angegebenen Quellen und Hilfsmittel nicht benutzt bzw. die wörtlich oder sinngemäß entnommenen Stellen als solche kenntlich gemacht habe. Die vorliegende Dissertation ist mit dem elektronisch bestimmten Textdokument identisch.

Linz, Jacek Gasiorowski

Acknowledgements

I would like to thank to:

- Prof. Niyazi Serdar Sariciftci for giving me an opportunity to explore the scientific world of organic semiconductors
- Prof. Achim Walter Hassel for advices and showing me a beauty of electro-chemistry
- Prof. Kurt Hingerl for support and for for precious knowledge about the strength of ellipsometry
- Prof. Reghu Menon for support and scientific optimism
- Dr. Helmut Neugebauer for valuable and very critical discussions which led to a beautiful science. I will always try to think first about the "story"...
- Dr. Patchanita Thamyongit and Dr. Alberto Montaigne Ramil for scientific help and for friendship
- Kertin Oppelt, Engelbert Portenkirchner for nice discussions during coffee breaks and for encouragement
- Dr. Andrei Ionut Mardare for patience and support
- Dr. Philipp Stadler for critical discussion
- Jan Kollender for help with SDCM and for long discussions
- present and former members of LIOS: Dr. habil. Daniel Ayuk Mbi Egbe, Dr. Markus Scharber, Dr. Matthew White, Dr. Mihai Irimia-Vladu, Dr. Marek Havlicek, Dr. Elisa Tordin, Dr. Lucia Leonat, Dr. Getachew Adam Workneh, Dr. Eric Gowacki, Dr. Cigdem Yumusak, Dr. Gundula Voss, Dr. Mateusz Bednorz, Dr. Beatriz Meana-Esteban, Dr. Anita Fuchsbauer, Dr. Gebhard Matt, Dr. Martin Egginger, Dr. Rober Köppe, Dr. Valery Bliznyuk, Dr. Elif Arici, Dr. Sandro Lattante, Dr. Almantas Pivrikas, Dr. Christoph Ulbricht, Dogukan Hazar Apaydin, Stefanie Schlager, Christina and Sandra Enengl, Meltem Akcay, Sameh Boudiba and Serpil Tekoglu
- and last but not least special thanks for my parents for their support...

Abstract(English version)

The need for cheap, easily processible electronics has led to the development of organic semiconductors and recently a lot of effort has been put in the processing optimization for tuning their physical and chemical properties. Big effort was put to understand and improve their electrical conductivity which is one of the key points in the construction of organic electronic devices. One of the ways to increase the charge conductivity in an organic semiconductor is via doping. In this work a detailed study on the chemical, photo and electrochemical doping is presented. For this purpose two polymers from the polythiophene family: poly(3-hexylthiophene) (P3HT), which is the model donor material for organic solar cells and newly developed poly[4,8-bis-substituted-benzo [1,2-b:4,5-b0]dithiophene-2,6-diyl-alt-4-substituted-thieno[3, 4-b] thiophene-2,6-diyl] (PBDTTT-c) were chosen.

In order to understand the optical properties of the polymers and the changes occurring upon doping, the variation of the complex dielectric function was determined from spectroscopic ellipsometric measurements. As a result, a change in the optical spectra due to the polaron formation was detected in the visible range of the optical spectrum. Similar changes were found in the infrared part of the spectrum. For this study an ATR-FTIR technique was applied in order to detect the changes in the vibrational structure of the polymers during chemical and photo doping. As a result, upon doping new infrared activated vibrations (IRAVs) and polaron induced broadband absorptions were measured. While vibrational modes (IRAVs) are identical, polaronic transitions were found to be very sensitive to the doping technique. The resulting polaron absorptions detected in the infrared and visible part of the spectrum obeyed the sum rule. Electrochemistry and photoelectrochemistry of organic materials is especially of high interest since it provides easy and flexible variation of redox parameters which allows the study of material properties at different doping conditions. Photoelectrochemical scanning droplet cell microscopy (PE-SDCM), where only a very small electrolyte droplet at the tip of a capillary comes in contact with the working electrode, is an interesting tool for being used in organic semiconductor studies since it provides the means for localized investigations with high reproducibility. One clear advantage of using the PE-SDCM is represented by so far unprecedented small amounts ($\sim ng$) of organic materials which can be quickly and inexpensively applied in various electrochemical studies. A 0.1M

tetra(n-butyl)ammonium hexafluorophosphate ($TBAPF_6$) dissolved in propylene carbonate was used as electrolyte solution for the electrochemical characterization of both polymers. The redox reactions in both materials were studied by cyclic voltammetry. The electrochemical impedance spectroscopy was applied to study electrical properties. The doping level during the oxidation process, investigated by Mott-Schottky analysis had as a result a decrease by a few orders of magnitudes of the film resistance, due to the electrochemical treatment.

Finally, the photovoltaic effect was studied using an electrochemical cell. The sample was electrochemically characterized in the dark and under various irradiation conditions. The photocurrent or/and photovoltage response was studied as a function of the layer or electrolyte composition. Due to localization, on a single sample various parameter combinations could be studied quantitatively and reproducibly.

Abstract (German version)

Zur Realisierung ubiquitärer preiswerter Elektronik wird weltweit intensiv an Alternativen zur Silizium basierten Elektronik geforscht. Im Rahmen dieser Bemühungen sind organische Halbleiter stark in den Blickpunkt gerückt. Dabei wurden in den letzten Jahren grosse Anstrengungen unternommen, um die physikalischen und chemischen Eigenschaften organischer Halbleiter besser zu verstehen und in Hinblick auf mögliche zukünftige elektronische Anwendungen hin zu optimieren. Eine Steigerung der Leitfähigkeit organischer Halbleiter kann dabei durch Dotieren erreicht werden. In dieser Arbeit wird die chemische, elektrochemische und photoinduzierte Dotierung organischer Halbleiter detailliert untersucht. Als Modellsysteme wurden dabei zwei Polymere aus der Gruppe der Polythiophene ausgewählt. Bei den Modellsystemen handelt es sich um das bereits länger bekannte Poly(3-hexylthiophen) (P3HT) und zum anderen um das neu entwickelte Poly[4,8-bis-substituierten-benzo[1,2-b:4,5-b⁰]dithiophen-2,6-diyl-alt-4-substituierten-thieno[3, 4-b]thiophen-2,6-diyl] (PBDTTT-c).

Die durch das Dotieren hervorgerufenen Änderungen der optischen Eigenschaften wurden mittels spektroskopischer Ellipsometrie untersucht. Dabei wurden Änderungen im sichtbaren Bereich des optischen Spektrums gefunden, welche auf die Bildung eines Polarons zurückzuführen sind. Des Weiteren wurden auch Änderungen im infraroten Bereich des Spektrums festgestellt. Diese Änderungen wurden mittels ATR-FTIR Spektroskopie näher untersucht. Mittels dieser Methode können Änderungen in den Schwingungszuständen des Polymers detektiert werden. Dabei wurden infrarot aktive Schwingungszustände (IRAVs) und neue polaroninduzierte breitbandige Absorptionsbanden gemessen. Während die Schwingungszustände (IRAVs) nahezu unabhängig von der Dotierungsart sind, hat die Art der Dotierung großen Einfluss auf die polaronischen Übergänge. Die Polaron basierten Absorptionen im sichtbaren und infraroten Bereich folgen dabei der Summenregel. Mittels Elektrochemie und Fotoelektrochemie lässt sich der Dotierungsgrad organischer Materialien einfach und präzise variieren. Die Fotoelektrochemische Rastertropfenzellen Mikroskopie (PE-SDCM) ermöglicht eine starke Lokalisierung fotoelektrochemischer Experimente mit hoher Genauigkeit und Reproduzierbarkeit. Dabei wird das Substrat mittels eines kleinen Tropfens an der Spitze einer Kapillare kontaktiert. Aufgrund der starken Lokalisierung der Messung können bisher unerreicht geringe Mengen ($\sim ng$) an organischem Halbleitermaterial schnell und kostengünstig elektrochemisch und

fotoelektrochemisch charakterisiert werden. Im Rahmen dieser Arbeit wurden P3HT und PBDTTT-c mittels PE-SDCM detailliert untersucht. Dabei wurden als Elektrolyt eine 0.1M Lösung von Tetra(n-butyl)ammonium Hexafluorophosphat (*TBAPF₆*) in Propylencarbonat verwendet. Das Redoxverhalten der beiden Polymere wurde mittels zyklischer Voltammetrie untersucht. Zur Bestimmung der elektrischen Eigenschaften der Polymere wurde elektrochemische Impedanzspektroskopie (EIS) verwendet. Die Änderung des Dotierungsgrades durch elektrochemische Oxidation der Polymere wurde mittels Mott-Schottky Analyse untersucht. Dabei wurde eine Steigerung der elektrischen Leitfähigkeit um mehrere Größenordnungen gefunden.

Abschliessend wurden die photovoltaischen Eigenschaften der Polymere mittels PE-SDCM untersucht. Dabei wurden die elektrochemischen Eigenschaften der Polymere im Dunkeln und unter Beleuchtung analysiert. Die photoinduzierten Spannungen und Ströme wurden dabei als Funktion der Schichtdicke und der Zusammensetzung des Elektrolyten untersucht. Aufgrund der starken Lokalisierung welche durch PE-SDCM erreicht wird, kann auf einem einzigen Substrat der Einfluss einer Vielzahl elektrochemischer Parameter untersucht werden.

Contents

1	Introduction	1
2	Materials and experimental setups	7
2.1	Materials	7
2.2	Film parameters determination	8
2.3	Spectroscopic ellipsometry	9
2.4	Fourier transform infrared spectroscopy with attenuated total reflection (ATR-FTIR)	13
2.5	Scanning droplet cell microscopy (SDCM)	14
2.5.1	Photoelectrochemical scanning droplet cell microscopy (PE-SDCM)	16
3	Chemical doping of conjugated polymers	21
3.1	Chemical doping of P3HT	22
3.1.1	Optical properties of the pristine and chemically doped P3HT investigated by spectroscopic ellipsometry	22
3.1.2	Chemical doping in ATR-FTIR	23
3.2	Chemical doping of PBDTTT-c	24
3.2.1	Optical properties of the pristine and chemically doped PBDTTT-c investigated by spectroscopic ellipsometry	24
3.2.2	Chemical doping in ATR-FTIR	26
3.3	Electrical conductivity comparison of the pristine/doped P3HT and PBDTTT-c	27
4	Photodoping of conjugated polymers	29
4.1	Photoinduced absorption in ATR-FTIR for P3HT	29
4.2	Photoinduced absorption in ATR-FTIR for PBDTTT-c	30
4.3	Air stability influence on the P3HT and PBDTTT-c spectroscopic response	31
5	Electrochemical doping of conjugated polymers	33
5.1	Electrochemical oxidation of P3HT	33
5.1.1	Cyclic voltametry	33
5.1.2	Potentiostatic characterization	35
5.1.3	Electrochemical impedance spectroscopy	39
5.1.4	Mott-Schottky analysis	43

Contents

5.2	Electrochemical oxidation of PBDTTT-c	44
5.2.1	Cyclic voltammetry	44
5.2.2	Potentiostatic characterization	45
5.2.3	Electrochemical impedance spectroscopy	49
5.2.4	Mott-Schottky analysis	53
6	Photoelectrochemical characterization of conjugated polymers	55
6.1	Photoelectrochemical characterization of P3HT	56
6.1.1	Dark/illumination current transients	56
6.1.2	Photocurrent stability	62
6.1.3	Photoelectrochemical impedance spectroscopy	64
6.2	Photoelectrochemical characterization of PBDTTT-c and PBDTTT-c:PCBM	68
6.2.1	Current transients behavior as a function of the electrolyte composition	68
6.2.2	Dark/illumination current transients	69
6.2.3	Photocurrent stability	76
6.2.4	Photopotential characterization	78
7	Summary	83
8	Outlook	85
	Bibliography	87

1 Introduction

Organic semiconductors were developed especially due to their possible applications as cheap and environmentally friendly materials for organic electronics. Since their morphological [1] and photophysical [2] properties can be easily modified, a great effort is made for the synthesis and characterization of new organic materials, small molecules [3] and polymers [4]. Also their mechanical flexibility is a big advantage [5, 6]. Most of the polymeric, semiconducting materials used in optoelectronics are derivatives of poly(phenylene vinylene)s, poly(phenylene ethynylene)s and polythiophenes [7]. From this family the most successful is poly(3-hexylthiophene) which was successfully used in various applications, e.g. metal coating [8], donor material in organic photovoltaics (OPV) [9, 10], organic light emitting diodes (OLED) [11] and organic field effect transistors (OFETs) [12]. Recently, new low-band gap materials with broad absorption spectrum ranging from ultraviolet to near infrared, combined with good electrical properties, were enhancing the efficiency of the organic solar cells [13, 14]. From many new polymers, poly[4,8-bis-substituted-benzo[1,2-b:4,5-b⁰]dithiophene-2,6-diyl-alt-4-substituted-thieno[3,4-b] thiophene-2,6-diyl] (PBDTTT-c) is one of the first synthesized as a promising candidate for a new generation of organic semiconductors [15–17]. Due to its enhanced absorption in the visible range and air stability this polymer was successfully used as a donor material in organic solar cells reaching nearly 7 % efficiency [18–21] and in photodetectors [22].

The conjugated polymers in their pristine form are either insulating or semiconducting. The presence of the band gap in the conjugated polymers is directly connected with the alternating single/double bonds (σ and π bonds). Their description is based on the quantum mechanical form of the solution of Schrödinger equation using a linear combination of atomic orbitals (LCAO). The hybridization which appears in LCAO calculation is responsible for the presence of the bonding (lower energy)/anti-bonding (higher energy) states. After the molecule is formed, this hybridization leads to formation of a highest occupied molecular orbital (HOMO) and a lower unoccupied molecular orbital (LUMO). The energetic difference between these two orbitals is describing a band gap.

Since the polymer materials can have a number of defects one of the important effects occurring in organic semiconductors is the formation of polymer chain distortions, which can improve the charge transport across the band gap. From

1 Introduction

the chemical point of view such distortion is described in conjugated polymers by a conjugation break. This break is created as a bi-radical usually termed "soliton-anti-soliton" pair. The schematic drawing for a representative conjugated polymer - poly(para-phenylene) - is presented in Fig. 1.1.

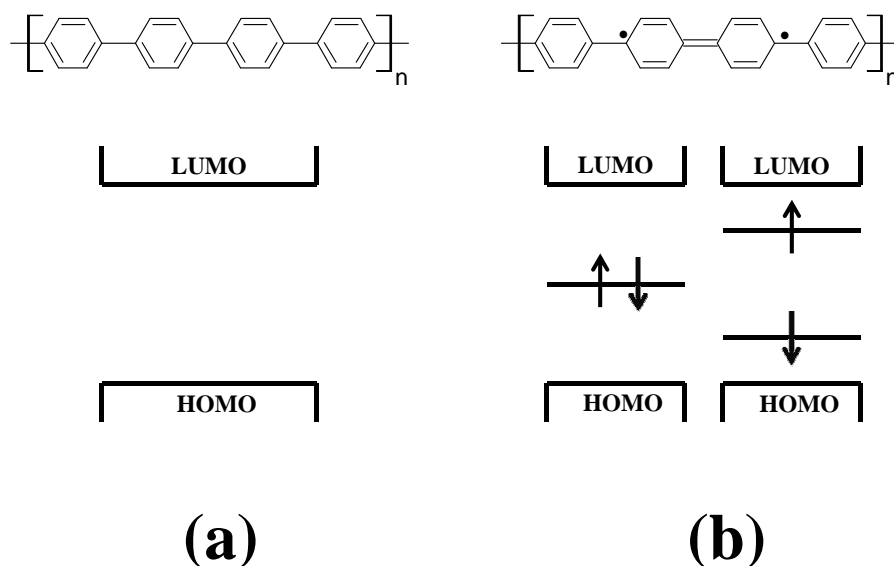


Figure 1.1: Schematic drawing of the (a) poly(para-phenylene) structure and (b) structure with a soliton-anti-soliton pair [23, 24]

Soliton and anti-soliton are defined as neutral radicals connected with an unpaired electron in the polymer chain (e.g. poly(para-phenylene)) which differ with the spin. The soliton has spin $\frac{1}{2}$ while anti-soliton has spin of $-\frac{1}{2}$ and they can annihilate each other. Solitons as chain distortions can be formed in the polymer chain with e.g. thermal energy.

The application in optoelectronics of new materials needs at first an understanding of the electrical and optical properties. Especially big effort was put in understanding and improving electrical conductivity which is one of the key points in construction of organic electronic devices. One of the ways to increase the charge conductivity in an organic semiconductor is via doping [23, 25]. By doping, similar to the inorganic semiconductor case, the amount of the free charge carriers increases, which leads to an increase in the conduction.

The doping considered as an impurity is expected to decrease the energy levels leading to improved charge transport. There are many ways of doping organic materials:

- 1.) Chemical oxidation (reduction) for p- (n) doping
- 2.) Photoinduced doping
- 3.) Electrochemical oxidation (reduction) for p- (n) doping
- 4.) Field induced doping in organic field effect transistors

Doping of organic semiconductors allows the holes and electrons to occupy bands positioned in-the-gap close to HOMO and LUMO level, respectively. If holes are involved in doping, radical cations will be defined, while electron surplus will define radical anions. These radicals can move within the polymer chain as chain distortion defining a polaron. The schematic representation of a polaron in the polymer (e.g. poly(para-phenylene)) as well as the resulting band diagram are presented in Fig. 1.2.

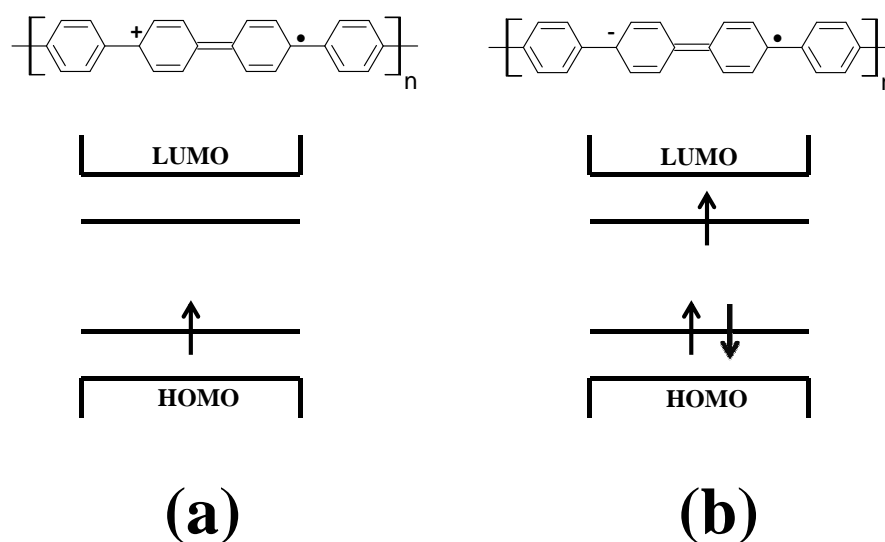


Figure 1.2: Schematic representation of the structure and band diagram of (a) positive and (b) negative polaron in poly(para-phenylene) [23, 24]

In contrast to solitons, the polarons are charged. Moreover, a polaron is always coupled with a soliton. Since the polaron has unpaired charge it will have a $\frac{1}{2}$ spin. The position of the unpaired electron will define a positive polaron (see Fig.1.2(a)) or a negative polaron (see Fig.1.2(b)). When two polarons couple, the solitons from both polarons can be confined resulting in a distortion containing two charged species being formed. The scheme of a bipolaron in poly(para-

phenylene) as well as resulting the band diagram is presented in Fig. 1.3.

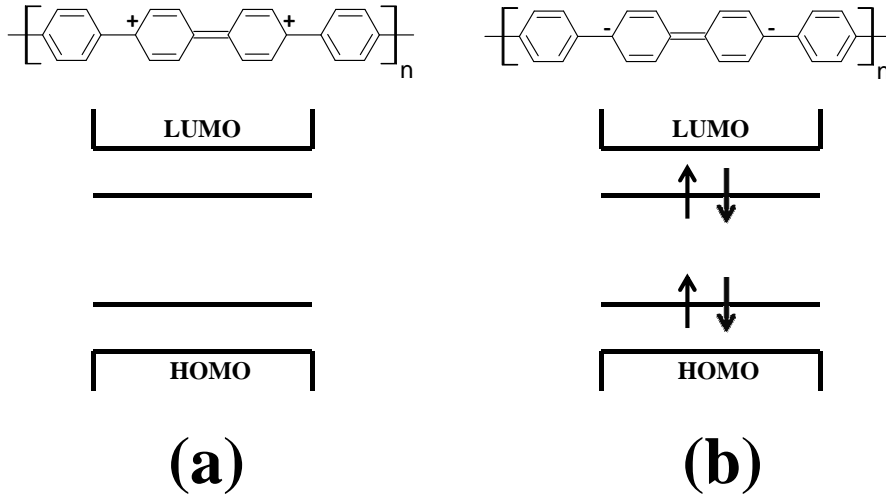


Figure 1.3: Schematic representation of the structure and band diagram of (a) positive and (b) negative bipolaron in poly(para-phenylene) [23, 24]

The bipolaron has twice the charges of a single polaron (± 2) and spin 0. Therefore, during the optical spectroscopy investigations no distinction can be done between a polaron and a bipolaron. The only difference can be found in electron spin resonance measurements, where bipolarons will not be visible. The formation of a bipolaron can be expected in a material containing defects and/or a high doping level.

In their pristine form, polymers are often either dielectric or semiconducting because of the rather large band gap. However, due to the doping, the conducting properties significantly change. Since in the undoped form polymers contain only small amount of free charge carriers, the doping can increase this number by many orders of magnitude. For a very high doping level a transition from dielectric to metallic behaviour can occur. Since the charge density in the polymer layer increases, new effects appear. First of all, a strong increase in the conductivity can be observed. Moreover, this increase is followed by the change of the optical properties. Since the generated charge carriers populate the levels in the gap, by doping the effective band gap decreases. In this work a detailed study of optical and electrical properties of the undoped and doped polymers (P3HT and PBDTTT-c as common family prototypes) as a function of the doping (chemical, photo or electrochemical) are presented.

In order to understand in more detail the change of the optical properties due to doping, the variation of the complex dielectric function or equivalently, the variation of the refractive index as a function of doping has to be measured. The imaginary part of the dielectric function is the characteristic response for

allowed absorption processes, i.e. allowed optical transitions from initial states to excited states. For comparison of different materials this determination of optical constants is also important for applications such as organic light emitting diodes as well as organic photovoltaics, since the optoelectronic properties of semiconducting polymers can be easily tuned by chemical substitution for several applications. Also from fundamental aspects it is of considerable importance to understand how the optical properties in these systems can be modified since the extent of π -conjugation and the stiffness of the backbone of the chains are highly susceptible to changes in the side-groups. These features become even more significant by doping induced variations in the optical spectra, as the electrical (DC) conductivity of these systems changes. The effect of doping on the optical properties during chemical and photodoping was additionally characterized using Fourier Transform Infrared Spectroscopy (FTIR). In this technique the changes in the vibrational structure upon doping were detected.

All electrochemical characterizations presented in this work were done for the first time using a modified version of the scanning droplet cell microscope (SDCM). The SDCM, firstly used more than 15 years ago for localized anodic oxidation of valve metals [26] was continuously developed over time. A small electrolyte droplet coming in direct contact with the surface of the working electrode defines the investigated area, which can easily be in the μm^2 region, offering a very localized area for study. Recent works have proven its capabilities for being used in comprehensive electrochemical investigations with high reproducibility of the wetted area [27]. A complete automation of the system allows scanning over large areas while mapping various surface properties. The electrolyte confinement combined with the scanning capabilities was recently used for analysis of thin film combinatorial libraries [28, 29], grain boundary electrochemistry [30] or electrochemical lithography [31, 32].

2 Materials and experimental setups

2.1 Materials

In this work a detailed study of the doping induced effect in two polymers belonging to the thiophene family is presented. All experiments were performed to characterize a conjugated, donor-acceptor type block co-polymer poly[4,8-bis-substituted-benzo[1,2-b:4,5-b⁰]dithiophene-2,6-diyl-alt-4-substituted-thieno[3,4-b] thiophene-2,6-diyl] and the results were compared to the model organic semiconductor used in photovoltaics, poly(3-hexylthiophene). The structures of the polymers are presented in Figure 2.1.

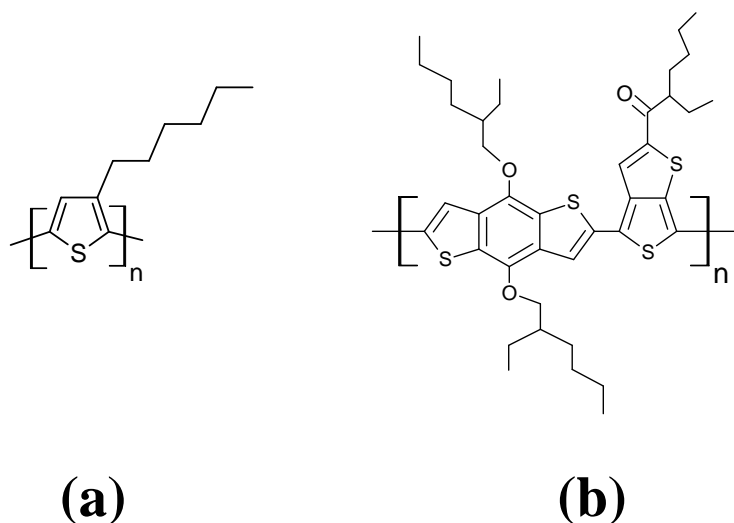


Figure 2.1: The chemical structure of the (a) P3HT and (b) PBDTTT-c

In the part (a) of Figure 2.1 the P3HT is presented. In this study a regioregular form of P3HT was used. Before using, P3HT was cleaned using a recrystallization procedure. A 20gL^{-1} solution of commercially available compound was dissolved in chlorobenzene (99+%, Acros Organics). The newly obtained solution was later slowly dropped in the n-hexan and a purified P3HT was

precipitating. In the part (b) of Figure 2.1 the structure of PBDTTT-c is presented. The polymer was synthesized by co-polymerization of benzothiophene and bithiophene units.

Sample preparation

For all characterizations presented in this study PBDTTT-c purchased from Solarmer Inc. USA was used as received. The polymer was dissolved in chlorobenzene (99+%, Acros Organics) with a concentration of 20 gL^{-1} . For comparison a mixture of PBDTTT-c with (6,6)-phenyl-C61-butyric acid methyl ester (PCBM) was prepared. PCBM, a soluble derivative of buckminsterfullerene was chosen due to the good electron accepting characteristic. The solution was prepared by dissolving PBDTTT-c and PCBM in chlorobenzene (99+ %, Acros Organics) with a total concentration of 20 gL^{-1} and mixing ratio of 1:1 w/w. The P3HT and P3HT:PCBM were dissolved in chlorobenzene (99+%, Acros Organics) with a concentration of 10 gL^{-1} and 20 gL^{-1} (1:1 w/w), respectively. At later stage solutions were spin-casted on $15 \times 15 \text{ mm}^2$ glass/ITO ($15 \text{ } \Omega/\text{sq}$, Kintec Co., China) substrates, and films are formed after drying in air. The glass/ITO substrates were precleaned by sequential sonication in acetone, isopropanol and de-ionized water and dried in nitrogen. For ellipsometric studies the solution was spin coated onto $15 \times 15 \text{ mm}^2$ glass slides, which were precleaned by wiping with toluene and consecutive sonication in acetone (99.8 %, NORMAPUR), isopropanol (99.9 %, NORMAPUR) and deionized water and then dried by purging with air.

2.2 Film parameters determination

Morphological parameters determination

The P3HT and PBDTTT-c thickness was determined by measuring the layer thickness at 4 positions with a stylus DEKTAK system before and after doping. Additionally, in order to determine the surface morphology of the thin polymer layer, an atomic force microscope setup Digital Instruments Dimension 3100 (Veeco Metrology group), working in tapping mode, was used. The root mean square roughness of the PBDTTT-c and P3HT thin films were found below 1 nm .

Electrical conductivity measurement

The conductivity of the thin layer of P3HT and PBDTTT-c in their pristine and chemically doped form were determined using a linear four contact technique. The scheme of the setup is presented in Figure 2.2.

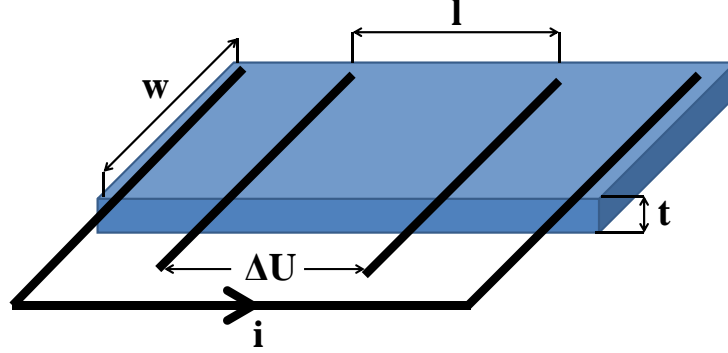


Figure 2.2: The scheme of the four-probe setup

In the technique a current flow (i) between the first and last contact and the drop of the potential (ΔU) between the inner electrodes is measured. Using Ohm's law, the conductivity can be calculated using the following equation

$$\sigma = \frac{1}{\rho} = \frac{il}{\Delta U wt} \quad (2.1)$$

where l is the distance between the inner contacts used to measure the potential drop, w is the width of the sample and t is the film thickness. For this measurement, a Keithley 2400 source/meter was used for measuring the drop of the potential during the current flow.

2.3 Spectroscopic ellipsometry

The spectroscopic investigations of these materials are usually performed either in the UV-Vis [33–35] or in the IR regions [36–38] employing transmission/reflection (T, R) measurements, which are both rather insensitive for an accurate determination of optical properties of thin films. The measured real quantities (T, R) are usually dominated by the reflection of the substrate. Hence, a precise measurement of the optical parameters at various energy scales is very difficult. Also, for the determination of spectral changes, e.g. when comparing spectra of doped samples to undoped ones, the strong transmission/reflection of the substrate can be detrimental. In most of the current literature only the relative variation of transmittance/reflectance is displayed. They show the change

2 Materials and experimental setups

of the significant features after doping, however the dielectric function

$$\epsilon(\omega) = \epsilon_1(\omega) + i\epsilon_2(\omega) \quad (2.2)$$

or equivalently, the refractive index

$$\tilde{n}(\omega) = n(\omega) + ik(\omega) \quad (2.3)$$

were not determined [39–41]. The dielectric function represents a direct causal response function, which is not the case for a transmission / reflection measurement. In order to determine the "absolute" (intrinsic, independent from measurement and geometry influences) material properties, these measurements have to be interpreted in terms of material response functions and the dielectric function is giving the linear optical response. Since the dielectric function of pure substrates can be determined independently with spectroscopic ellipsometry, for thin unknown layers the dielectric function is obtainable easier by modeling (variable angle) the spectroscopic ellipsometry data rather than from normal incidence reflection and transmission data. Despite of the considerable work on the understanding and control of the optical properties of semiconducting polymers done in the past [42–46], this crucial wide spectral range characterization in semiconducting polymers is often missing in detail. Usually UV-Vis (R,T) measurements detect relative changes in the absorption spectrum upon doping. The main absorption peak of the undoped material decreases with the appearance of new peaks related to electronic changes in the semiconducting polymer. From FTIR (R,T) spectra also only relative changes due to the alterations in the vibrational structure as well as from formation of polaronic states are usually obtained. Furthermore, if the spectra in these regions are taken separately, the response may appear at different scales, and a mismatch in the overall characterization of the optical properties in the broad spectral range can occur. Additionally, intensity measurements (R,T) require background measurements or a light path and detector system calibration and the experimental results sometimes show a non-linear dependence on the intensity of the light beam. For the determination of the absorption coefficient α from R, T measurements usually Beer's law is used,

$$I(r_2) = I(r_1)exp(-\alpha |r_2 - r_1|) \quad (2.4)$$

where α is defined by

$$\alpha = \frac{4\pi k}{\lambda_0} \quad (2.5)$$

or equivalently for thin films by

$$\alpha = \frac{\epsilon_2\omega}{cn} \quad (2.6)$$

$I(r_2)$ denotes the intensity at point r_2 and describes the light absorbed by passing from r_1 to r_2 , λ_0 is the wavelength of the light (in vacuum), ω is the frequency

and c the speed of light. However, this formula is only valid for thick films, where the coherent superposition of the fields between the top side and bottom side reflection is negligible. Then and only then interference effects do not influence the measured spectra and a single absorption measurement can be used for the correct determination of α . The measurements of thin films where the polarized light is either reflected or transmitted in the multilayer setup, demands careful application of the Fresnel equations.

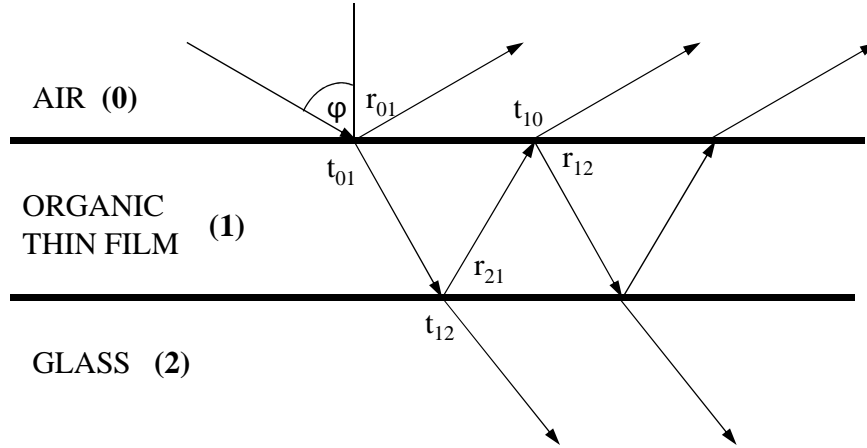


Figure 2.3: Scheme of the possible optical paths in the multilayer configuration

The Figure 2.3 show possible optical paths in the multilayer system, where a thin film is sandwiched between the substrate (such as glass) and the ambient (i.e. air). The transmittances and reflectances in ambient are marked with "0", in the film with "1" and in the substrate with "2". All three layers are assumed to be homogenous and optically isotropic. For thin films, the Fresnel reflectances as well as the phase acquired by multiple passing through the layer, have to be taken into account, demanding the use of equations (eqs. 4.37-4.40 in ref. [47]) involving the acquired phase (φ):

$$r_p = \frac{r_{01p} + r_{12p}e^{-j2\varphi}}{1 + r_{01p}r_{12p}e^{-j2\varphi}} \quad (2.7)$$

$$r_s = \frac{r_{01s} + r_{12s}e^{-j2\varphi}}{1 + r_{01s}r_{12s}e^{-j2\varphi}} \quad (2.8)$$

$$t_p = \frac{t_{01p}r_{12p}e^{-j\varphi}}{1 + r_{01p}r_{12p}e^{-j2\varphi}} \quad (2.9)$$

$$t_s = \frac{t_{01s}r_{12s}e^{-j\varphi}}{1 + r_{01s}r_{12s}e^{-j2\varphi}} \quad (2.10)$$

These equations refer to the optical path length (phase of the field), the complex refractive index of ambient and substrate and the complex refractive index of the thin film.

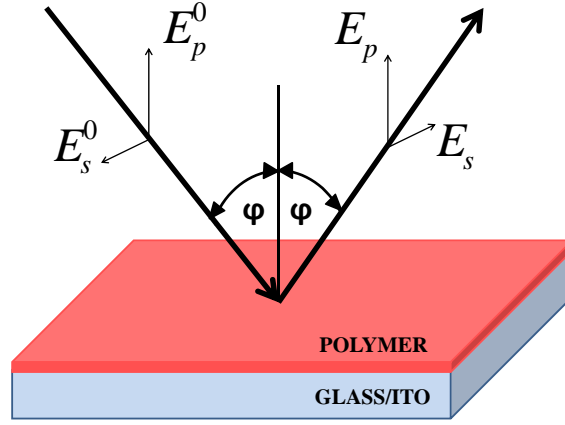


Figure 2.4: Scheme of the spectroscopic ellipsometry showing the principle of operation

To measure the changes of the optical properties of the undoped/doped thin film of the polymer, spectroscopic ellipsometry (SE) measurements was performed. The scheme of spectroscopic ellipsometry is presented in Figure 2.4 Using NIR-Vis-UV and IR SE setups the complex reflectance ratio is determined by [48]

$$\rho = \frac{r_p}{r_s} = \tan\psi e^{i\Delta} \quad (2.11)$$

where ρ is the ratio of the complex reflection coefficients, r_p and r_s are the complex Fresnel reflection coefficients for p- and s- polarized light, respectively. The value ψ represents the absolute value of the ratio and Δ describes the phase difference between p- and s- polarized light.

The measured complex quantity can be converted to a complex pseudo dielectric function $\langle\epsilon(\omega)\rangle$ assuming that the multilayer could be described by a single and uniform dielectric layer, using [48]

$$\langle\epsilon(\omega)\rangle = \epsilon_a \left(\sin^2(\varphi) + \sin^2(\varphi) \tan^2(\varphi) \frac{(1 - \rho)^2}{(1 + \rho)^2} \right) \quad (2.12)$$

where φ is the angle of incidence and ϵ_a the dielectric function of the environment (1 for air). If the sample under study is a single homogeneous material, then the pseudodielectric function is the same as the dielectric function, representing the correct material response. If the sample is not a single homogeneous material, e.g. a thin layer on a substrate, eq. 2.12 as direct inversion can be applied as

2.4 Fourier transform infrared spectroscopy with attenuated total reflection (ATR-FTIR)

well, but then the result is termed pseudodielectric function and indicated by $\langle\epsilon\rangle$. This pseudodielectric function is not an absolute physical quantity, because it consists also of geometrical (and substrate) properties and shows e.g. interference oscillations, which are unphysical, because they occur due to geometry. The dielectric function for the P3HT and PBDTT-c film is obtained by fitting the measured ellipsometric response (ψ and Δ) using a (complex) model dispersion relation. The data were fitted using *WVASETM* software with the known layer thickness, and the assumption of a negligible roughness (i.e. the roughness is small compared to the wavelength) using a generic oscillator. As a result, a preliminary model for the real (ϵ_1) and imaginary (ϵ_2) part of dielectric function was obtained. Then, the fitting was refined by either adding more oscillators, or a point to point fit, and checking the Kramers-Kronig consistency.

2.4 Fourier transform infrared spectroscopy with attenuated total reflection (ATR-FTIR)

The changes in the vibrational structure upon doping were detected using infrared internal reflection spectroscopy. In this technique the characterized material is in contact with the optically denser and transparent substrate. The optical spectrum is recorded by measuring the wavelength dependence of the interface (substrate/material) reflectivity using the light introduced into the denser medium [49]. The infrared spectra were recorded with a FTIR spectrometer (Bruker IFS66S) at room temperature in attenuated total reflection (ATR) mode. In the setup a Mercury-Cadmium-Telluride (MCT) detector cooled with liquid nitrogen prior the measurements was used. For the ATR-FTIR measurements during chemical or photodoping, a ZnSe crystal was used as reflection element. The ZnSe crystals used in the study were pre-cleaned by polishing with diamond paste (1 and 0.25 μm) and rinsing in a reflux system with acetone for approximately 3h.

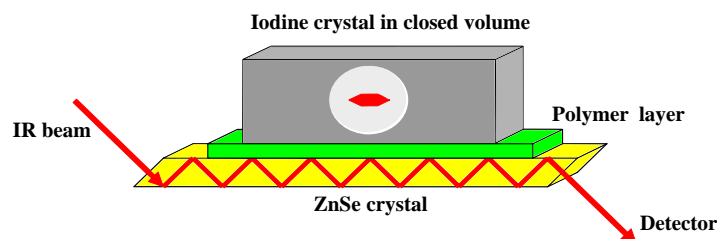


Figure 2.5: Scheme of the ATR-FTIR setup used for the iodine doping

The setup used for chemical doping is presented in Figure 2.5. For the measurement ZnSe ATR together with tightly closed volume was used. During the

measurement, after the 2nd spectrum, a small iodine crystal was dropped in the closed volume. The presence of the I_2 results in the chemical oxidation were incorporation of the I_3^- , compensates the net charge of the oxidized polymer. During doping, ATR-FTIR spectra were recorded consecutively. By defining the first, undoped spectrum as reference spectrum (T_{ref}), and relating the subsequent doped spectra (T_s) to this reference spectrum, specific spectral changes during chemical oxidation by I_2 were obtained. The difference spectra are calculated as

$$\Delta ad \propto -\log\left(\frac{T_s}{T_{ref}}\right) \quad (2.13)$$

For measuring photoinduced absorption (PIA), infrared spectra of the sample in the neutral form, both illuminated and non-illuminated, were recorded.

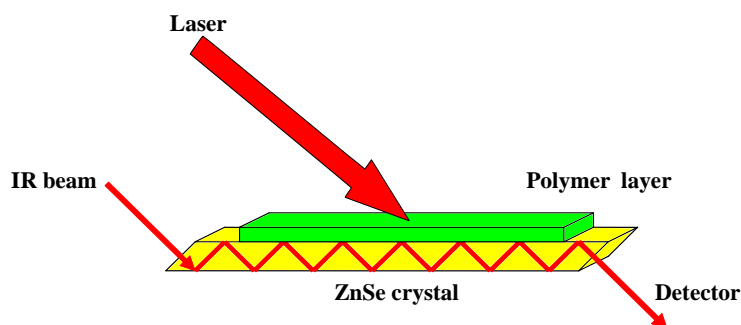


Figure 2.6: Scheme of the ATR-FTIR setup used for photoinduced absorption experiment

A ZnSe crystal with a layer of studied material was illuminated in 45° geometry by 532 or 664 nm diode-laser (45 mW cm^{-2}) (see Figure 2.6). The photoinduced absorption was observed by measuring a sequence of 1000 repetitions of recording 10 single beam spectra in the dark and 10 single beam spectra under illumination. The normalized changes in transmission are then plotted as absorption changes ($-\log(\frac{T_s}{T_{ref}}) \approx \Delta ad$).

2.5 Scanning droplet cell microscopy (SDCM)

The variety of physical and chemical parameters which can be characterized during electrochemical studies led to the development of different in-situ techniques [40, 46, 50–53]. Different spectroscopic methods are used during cyclic voltammetry measurements studying optical, vibrational and electrical changes during oxidation-reduction processes in organic semiconductors. All of them need to be used for understanding the doping effects. Due to this, the need for different sample structures and overall big quantities of material represent

2.5 Scanning droplet cell microscopy (SDCM)

the main challenge. The need to speed up screening of new materials lead to a strong miniaturization of the electrochemical setup which allows for drastically reducing the required amount of chemicals. This can be realized by employing scanning droplet cell microscopy (SDCM) due to its general applicability for all electrochemical methods even including some combined techniques [54–58].

As a part of the PhD study an adaption of the photoelectrochemical scanning droplet cell microscopy for electrochemical characterization of organic semiconductors was done. Photoelectrochemical scanning droplet cell microscopy was applied to measure cyclic voltammetry, electrochemical impedance spectroscopy and photoelectrochemical properties of the studied polymers. The measurement area was down to 3.2 mm^2 allowing multiple characterization on a single sample. The necessary amount of the organic material required for this study was less than 1 mg, and less than 1 ml of electrolyte solution was used. This low consumption of materials together with large amount of reproducible information obtained makes this setup a very promising technique for screening new organic materials.

For all the electrochemical investigations presented in this work using liquid electrolytes, a scanning droplet cell microscope with a 3 electrode configuration was used [59]. Figure 2.7 shows a photograph of the SDCM during an electrochemical measurement.

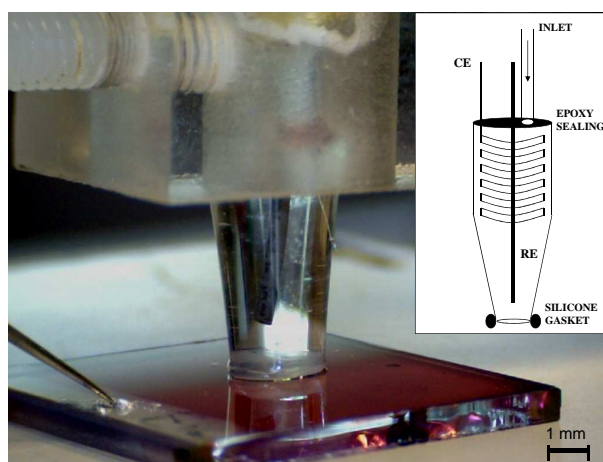


Figure 2.7: Photograph and scheme (inlet) of the tip of scanning droplet cell microscope (SDCM)

A plastic block is used for fixing the cell body to an XYZ translation stage which moves the tip of the cell to various locations on the sample surface. The sample representing the working electrode (WE) is electrically contacted using a tungsten needle pressed on a small Indium (In) droplet placed on the ITO

substrate. This ensures a good stability of the contact over time. The inset of Figure 2.7 shows a schematic representation of the SDCM. The cell was built using a tapered glass capillary (Pasteur pipette) for which a tip diameter of 2 mm was achieved by appropriate grinding. At the top part, an electrolyte inlet is provided by using a 1 mm in diameter teflon tube connected to the inner volume of the cell and isolated from the exterior by using a two component epoxy resin.

An Ag/AgCl micro-quasireference electrode ($\mu - QRE$) was prepared by electrodeposition of AgCl in 1 M HCl on an Ag wire 0.5 mm in diameter according to the recipe given in ref [60]. The silver wire was used as WE electrode was dipped in the 1 M HCl solution. A Pt foil was used as CE and Ag/AgCl as RE electrode. At first, the Ag wire was electrochemically cleaned and roughened during 10 times cycling between 0.1 V vs. SHE and 0.5 V vs. SHE with a scan rate of 10 mVs^{-1} . Next, the silver chloride was then deposited during a potentiostatic measurement at 0.1 V vs. SHE for 120 s and finally at 0.3 V vs. SHE for 600 s. Eventually, the open circuit potential measurement between freshly prepared Ag/AgCl WE and Ag/AgCl reference electrode was performed in order to determine the electrochemical potential of the WE. The potential of the RE was found to be 0.211 V vs. SHE. The AgCl electrodeposition was performed according to ref. [60]. The ($\mu - QRE$) was also inserted into the cell body from the top, keeping a minimum distance to the WE surface (approximately 1 mm) and fixed with epoxy resin.

A gold stripe (Wieland Dentaltechnik 99.999%) (2 mm wide) was used as counter electrode (CE) forming a coil at the top part of the glass capillary, where the inner diameter is still large enough for avoiding electrical contact with the ($\mu - QRE$). The CE was also embedded into the epoxy resin at the top, which in the final stage of the manufacture completely isolated the inner volume of the cell from exterior. A soft silicone gasket was formed on the rim of the SDCM tip by dipping the capillary in liquid silicone followed by drying it under N_2 . The gasket seals the electrolyte inside the cell for avoiding any air contact [27]. This is an important aspect for the electrochemistry of organic materials when non-aqueous electrolytes are used due to the water contamination from the surrounding atmosphere. The reason behind is that non-aqueous electrolytes are preferred due to the large electrochemical window as compared to aqueous electrolytes.

2.5.1 Photoelectrochemical scanning droplet cell microscopy (PE-SDCM)

All photovoltaic investigations presented in this work were performed using a modified version of a SDCM - photoelectrochemical scanning droplet cell micro-

scope (PE-SDCM) adapted for organic based electrolytes [58]. More than 100 measurements were performed on both P3HT/ITO/glass as well as PBDTTT-c/ITO/glass and PBDTTT-c:PCBM/ITO/glass substrates using different cells in order to prevent the film contamination.

A schematic description of a PE-SDCM as well as photograph of the working setup is presented in the Figure 2.8. The PE-SDCM cell was built using 2 mm outer diameter boron-silicate glass capillaries. The tip was pre-formed using a capillary puller (PC-10, Narishige) and afterwards ground using a micro-grinder for achieving the desired tip diameter. Due to the necessity of avoiding the air contact combined with the need for precisely defining the WE area, the PE-SDCM was used in the contact mode [61]. In this way, a high reproducibility of the addressed areas was possible by using a soft silicone gasket [27]. The precisely wetted area on the WE was determined before starting the PE-SDCM experiments. For this purpose, anodic oxides were grown on a Ti thin film using an aqueous electrolyte (acetate buffer) and high resolution optical microscopy with automated pattern recognition was applied for determining the area of the colored spot produced.

The addressed WE area of the cell used with the organic electrolyte without ferrocene was 0.13 mm^2 while the cell used for the electrolyte containing the ferrocene was 0.11 mm^2 . For the possibility of direct comparing the results obtained from both PE-SDCMs, the obtained electrochemical data were normalized to their corresponding area. As reference electrode, an Ag/AgCl micro-quasi-reference electrode was used due to its applicability under non-aqueous conditions. The $\mu - QRE$ wire was inserted into a small glass capillary for mechanical stability, leaving the sensing area exposed outside it. The remaining Ag wire was sealed within the glass capillary for preventing electrolyte contact using two component epoxy resin. As counter electrode, a spiral-shaped 100 μm in diameter high purity Au wire was used (99.999 %, Wieland Dental Technik). The spiral shape of the Au CE was used in order to maximize its total surface area and helps reducing the current density and thus the polarisation. The RE was inserted together with the CE into the 2 mm outer diameter boron-silicate glass capillary. In order to locally illuminate the wetted area, a 270 μm in diameter multi-mode optical fibre was used. The end of the optical fibre and the reference electrode were installed in close proximity to the surface inside the outer body capillary, as presented in Figure 2.8. The electrical contacting of the WE was ensured by using an In droplet connecting both, the ITO film and a W needle. A 500 μm in diameter stainless steel syringe needle installed at the top part of the PE-SDCM was connected to a Teflon tube serving as electrolyte inlet. In a last fabrication step, the top of the droplet cell was sealed with two-component epoxy glue fixing all components. The size of the electrolyte droplet was controlled using a high-precision syringe pump.

2 Materials and experimental setups

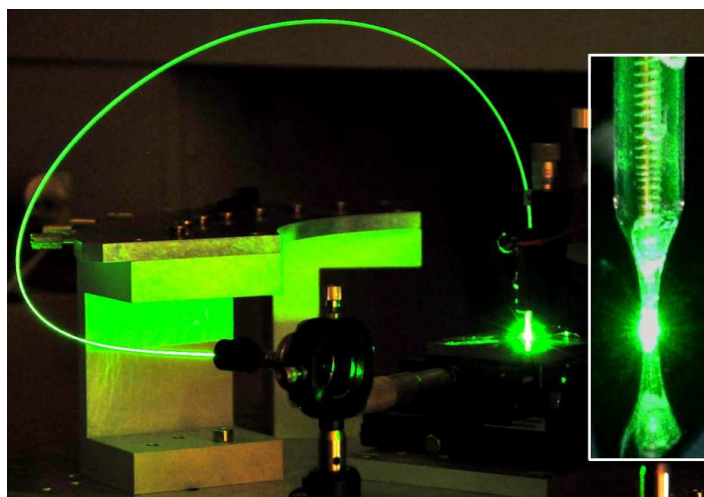
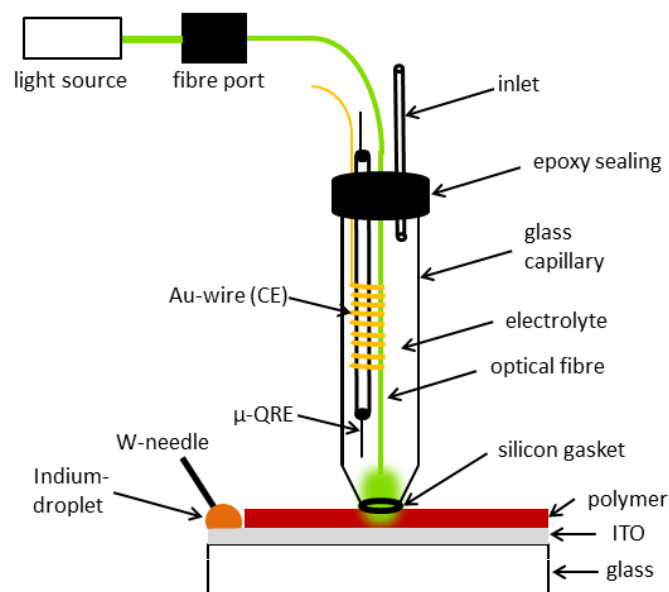


Figure 2.8: In the upper part, the scheme of the photoelectrochemical scanning droplet cell microscope (PE-SDCM) used in all photoelectrochemical characterization is shown. In the lower part a photograph of the operating setup is presented [58].

All photovoltaic measurements presented in this work were performed using a 532 nm (for P3HT) or 633 nm (for PBDTTT-c) diode pumped solid state laser module with auto-power control. The reason of choosing these wavelengths is described later. Due to the high surface photosensitivity, all photovoltaic measurements were done in a specially designed dark room for avoiding radiation contamination of the sample during the experiments. The laser radiation was coupled into the optical fiber using an in-house developed optical fibre port. The

illumination was controlled by a manually operated shutter. In order to measure the optical power on the wetted area, a fully assembled droplet cell was placed on the detection area of an optical power meter (Coherent Lasermate Q, VL54). During photoelectrochemical characterization, samples were additionally measured under the white light with full spectral range. The measured optical power density was approximately 153 mW cm^{-2} for the 532 nm laser, 113 mW cm^{-2} for the 635 nm laser and 56.3 mW cm^{-2} for the white light.

During the photoelectrochemical studies, the photovoltaic properties of the working electrode were investigated using 0.1 M solution of tetrabutylammonium hexafluorophosphate ($TBAPF_6$, $\geq 99\%$, Fluka Analytical), prepared by dissolution in propylene carbonate (PC, 99.7%, Sigma Aldrich). A second substrate was investigated using 0.1 M solution of $TBAPF_6$ in PC, but containing additionally 5.4 mM ferrocene. For the study of PBDTTT-c and PBDTT-c:PCBM only 0.1 M solution of $TBAPF_6$ dissolved in PC was used. The organic electrolytes used in this study were chosen due to their wide electrochemical window. However, extra caution was necessary due to the possible oxygen or water contamination which could have affect the electrochemical measurements and their interpretation.

The tip of the PE-SDCM was positioned on the sample surface using a gantry robot built using three linear stages. For ensuring high reproducibility of the wetted area the applied force was constantly measured and readjusted using a small force sensor (KN 245). All electrochemical experiments were carried out using a CompactStat Potentiostat (Ivium Technologies, The Netherlands) with an integrated frequency response analyzer allowing electrochemical impedance spectroscopy measurements. The full impedance measurements were conducted at frequencies ranging between 10 kHz and 2 Hz. The dynamic changes of the electrical properties were studied in single frequency measurements, where the impedance was detected at 1 kHz. The complete setup was controlled using an in-house developed LabView program.

3 Chemical doping of conjugated polymers

The changes in the optical and electrical properties are described in the following chapter for the P3HT and PBDTTT-c during chemical and photodoping. The doping of the organic semiconductors results in the appearance of new, doping induced, transitions in the band gap, which are normally observed as two new absorptions with maxima in the UV-Vis and MIR region. In this study the doping was performed by exposing the sample to iodine vapor (in a closed glass) for 10 min. The long doping time suppose to increase a doping concentration necessary to measure the ellipsometric signal.

The formation of the polaronic states upon doping leads to appearance of new optical transitions. The higher transitions, for photon energies in the visible range, were measured and discussed using spectroscopic ellipsometry. However beside this new absorption in the visible range, according to the sum rule another transition with energy in the IR region should appear. The spectral response of the thin layer of P3HT and PBDTTT-c after doping was checked in-situ using ATR-FTIR technique. During consecutive measurements, the polymer layer deposited on ZnSe reflection element was contacted with crystal of iodine. The contact with vapors of I_2 leads to a doped polymer which results in changes in the infrared absorption spectra.

For the infrared part of the spectrum, usually after doping a broad transition in the IR, associated with polaron formation and new dipole allowed infrared active vibrations (IRAVs) at lower energies appear. The IRAV bands can be described in different models, e.g. as a coupling between the electronic oscillations and the amplitude oscillation of the single/double bond alternation, introduced in the Amplitude Mode (AM) formalism by Horowitz et al. [62, 63]. Zerbi et al. have pointed out the correlation between IRAV band and totally symmetric Raman modes in the Effective Conjugation Coordinate (ECC) theory [64, 65]. The connection between the doping induced electronic states and spectroscopically detected IRAV bands was formulated by Ehrenfreund and Vardeny [66]. The Girlando-Painelli-Soos (GPS) model describes the electron - phonon coupling [67, 68]. However, all of these models describe the change in the absorption related to equ. 2.6 and therefore require to measure the real and imaginary part of the dielectric function.

3.1 Chemical doping of P3HT

3.1.1 Optical properties of the pristine and chemically doped P3HT investigated by spectroscopic ellipsometry

In order to understand the effect of doping on the optical properties of the polymer, at first films of pristine P3HT and PBDTTT-c were characterized using spectroscopic ellipsometry. The real (plotted in red) and imaginary (plotted in black) part of the dielectric function of the pristine P3HT were determined using SE and are presented in Figure 3.1(a).

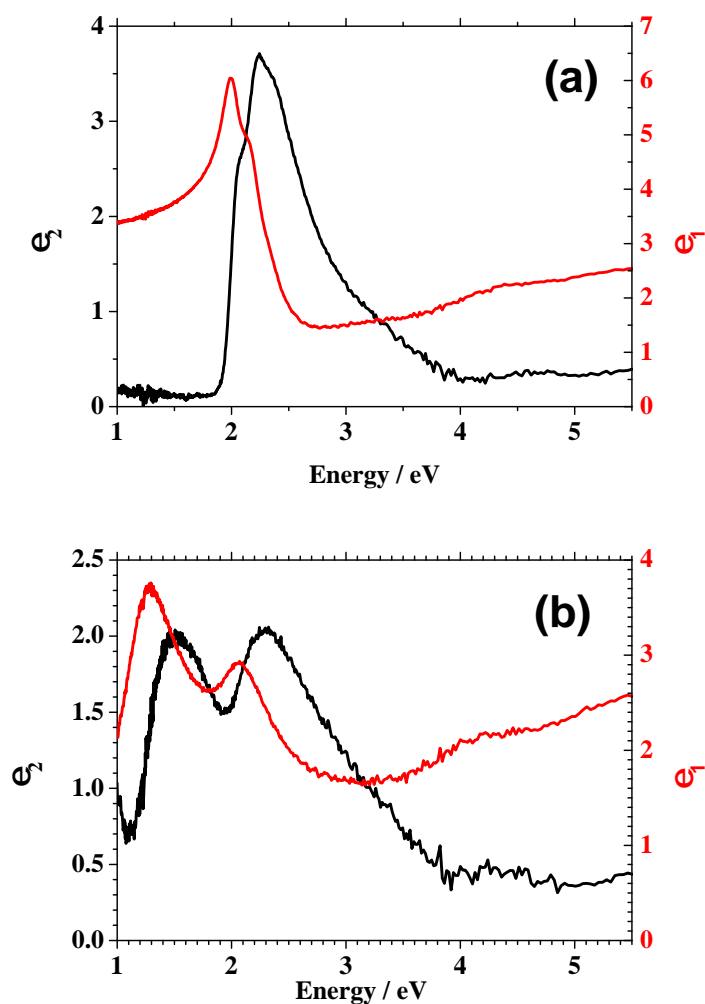


Figure 3.1: Real (ϵ_1) and imaginary (ϵ_2) part of the dielectric function determined for (a) pristine and (b) iodine doped P3HT

For P3HT the imaginary part of the dielectric function shows the presence of two peaks with maxima at 2.1 and 2.3 eV, respectively. The peak with higher energy describes the absorption of the pristine polymer via $\pi \rightarrow \pi^*$ transition. The second peak (2.1 eV) is characteristic for the solid polymer and describes the changes in the polymer structure due to the π/π stacking. The onset of the absorption according to the optical band gap was found to be 1.9 eV. The existing absorptions are reflected in the plot of the real part of the dielectric function. The two absorptions are connected with two oscillators with maxima at 1.95 and 2.1 eV.

For doped P3HT spectroscopic ellipsometry was used after exposing the sample for 600 s in the iodine atmosphere and the resulting (ϵ_1) and (ϵ_2) functions are presented in Figure 3.1(b). In the plot of the imaginary part of the dielectric function, a strong decrease and broadening of the main absorption peak with maximum was found at 2.3 eV. At the same time the appearance of the new peak with maximum at 1.5 eV is observable. The intensity of this new absorption, connected with a formation of polaronic states in-the band gap, is obeying the sum rule.

At higher energies (above 3 eV), the doping does not influence the absorption. A similar behavior can be found in the plot of the real part of the dielectric function. After doping a strong decrease in the oscillator strength connected with the main absorption can be noticed. This decrease is followed by the formation of a new oscillator with maximum at 1.3 eV. At higher energies ($> 3\text{eV}$) also the behavior of (ϵ_1) is independent from doping.

3.1.2 Chemical doping in ATR-FTIR

The formation of the polaron due to the population of the in-the-gap states results in the appearance of new absorption peak in the optical spectroscopy. This clear effect was measured in the visible range of the optical spectrum using spectroscopic ellipsometry. However, according to the sum rule, additional transition should appear in the IR part of the spectrum. To find this polaronic absorption, an ATR-FTIR spectroscopy was used.

The differential spectrum of the doped P3HT is presented in Figure 3.2. The infrared absorption spectra recorded during chemical doping of the polymer show two distinct regions of doping induced bands. The first is a broad absorption band above 1800 cm^{-1} wavenumbers, related to polaron formation which yields to the in-the-gap absorption. The maximum of the broad absorption was found at 2800 cm^{-1} . Additionally, below 1800 cm^{-1} , new doping induced infrared active vibrations appear.

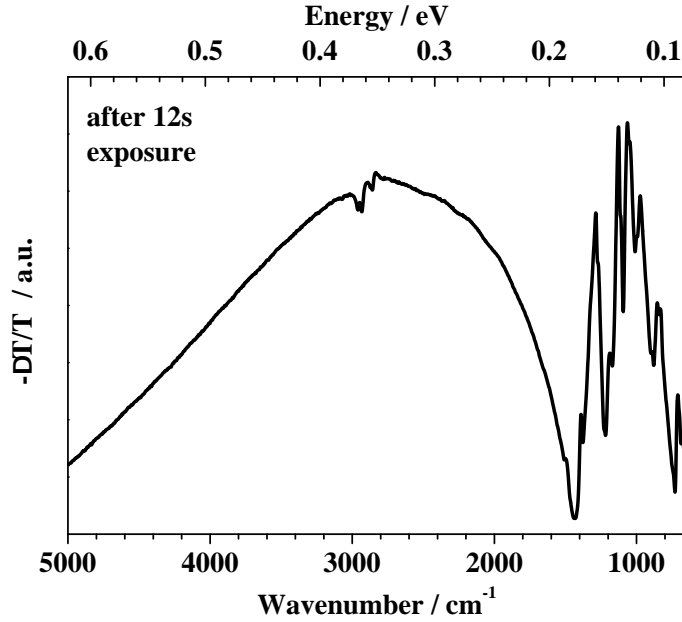


Figure 3.2: ATR-FTIR differential spectra during chemical doping of P3HT in iodine vapors.

The IRAV region is characterized by the existence of the intense and very broad absorption peaks. For P3HT two peaks, one around $1470 - 1240 \text{ cm}^{-1}$ and the second between 1240 and 890 cm^{-1} can be observed. The intensity of the IRAV peak compared to the corresponding polaronic absorption suggests a good electron-phonon coupling.

3.2 Chemical doping of PBDTTT-c

3.2.1 Optical properties of the pristine and chemically doped PBDTTT-c investigated by spectroscopic ellipsometry

As in case of P3HT, the characterization of the optical properties was performed for PBDTTT-c polymer and the resulting plots of (ϵ_1) and (ϵ_2) functions are presented in part (a) of Figure 3.3. Since the polymer was developed to be a low band gap semiconductor, the absorption edge was found at 1.55 eV. In the plot of the imaginary part of the dielectric function, two sharp peaks with maxima at 1.75 and 1.9 eV can be found according to the $\pi \rightarrow \pi^*$ transition. However, at higher energies ($> 2\text{eV}$) additionally three broad absorptions with maxima at 2.6, 3.7 and 5 eV, describing higher transitions are observed. The plot of the real part of the dielectric function show at low energies ($< 2\text{eV}$) the existence of two oscillators with maxima at 1.7 and 1.85 eV related to the main absorption

peaks. Also absorptions related to the higher transitions can be described by three oscillators with maxima at 2.6, 3.4 and 4.75 eV.

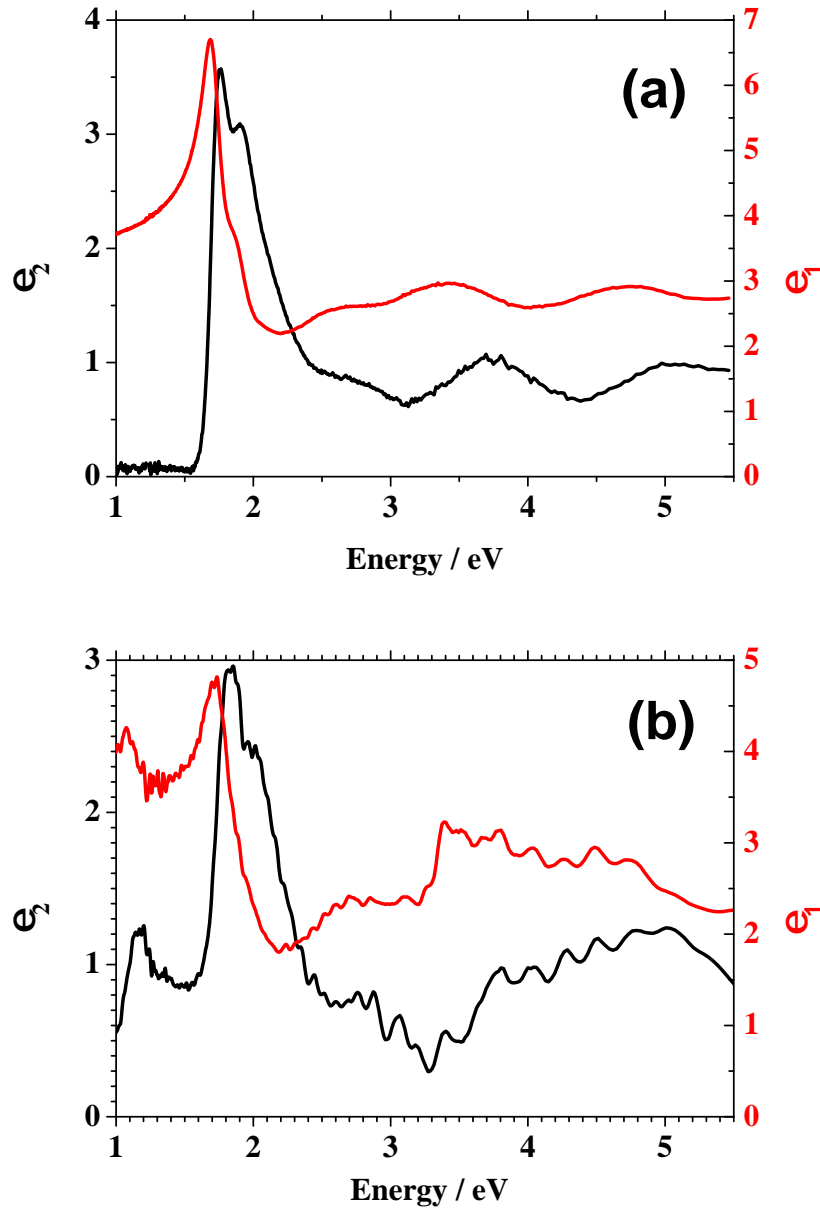


Figure 3.3: Real (ϵ_1) and imaginary (ϵ_2) part of the dielectric function determined for (a) pristine and (b) iodine doped P3HT

The spectroscopic ellipsometry characterization of changes in the optical properties during chemical doping was performed also for PBDTTT-c. The polymer was exposed to iodine vapors for 600 s and immediately after, measured using spectroscopic ellipsometry. The resulting real and imaginary part of the dielec-

tric function is presented in Figure 3.3(b). The behavior of the dielectric function plot obtained for doped PBDTTT-c, as compared to pristine polymer, shows identical behavior of ϵ_1 and ϵ_2 for energies higher than 2.5 eV.

Below this energy, in the plot of the imaginary part of the dielectric function, after exposure to iodine a decrease of the intensity of the main absorption followed by the appearance of a new peak with a maximum at 1.2 eV can be observed. This new absorption is connected with the oscillator which appears in the plot of $\epsilon_1(\omega)$ and has the maximum at 1.1 eV. As in the case of the P3HT, the appearance of IRAV is due to the formation of polaronic states in the gap. Finally, the rather high noise noticeable for both ϵ_1 and ϵ_2 plots, measured for PBDTTT-c, can be explained by a strong instability of the doped polymer layer due to the de-doping process.

3.2.2 Chemical doping in ATR-FTIR

Analogous studies on the changes of the vibrational structure of the polymer using ATR-FTIR were performed for PBDTTT-c. As in the case of P3HT, the layer of PBDTTT-c deposited on ZnSe reflection element was contacted with the iodine vapors and the characteristic changes in the infrared spectrum were recorded. The results are presented in Figure 3.4.

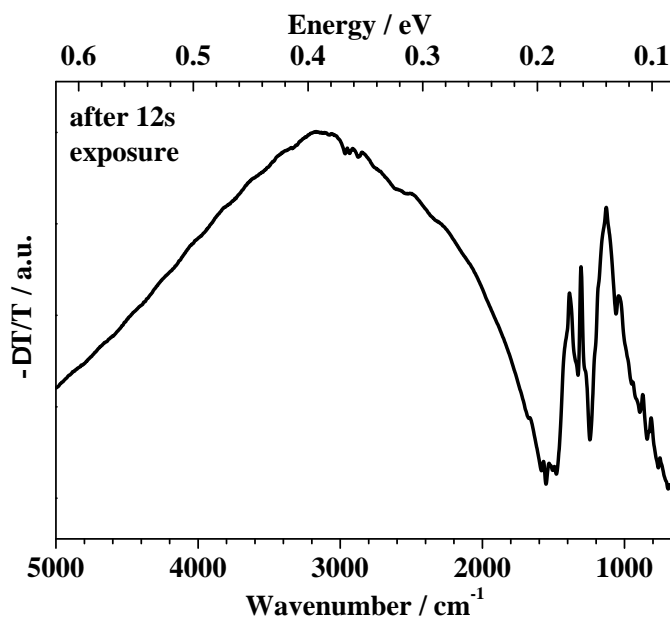


Figure 3.4: ATR-FTIR differential spectra during chemical doping of PBDTTT-c in iodine vapors.

In the differential spectrum, both IRAVs and a broad polaronic absorption can be found. The maximum of the broad absorption, describing polaronic transition was found around 3100 cm^{-1} . Intense and relatively broad IRAV absorption peaks around $1470 - 1240\text{ cm}^{-1}$ and $1240 - 890\text{ cm}^{-1}$ are observed, which indicates a rather high delocalization of charges along the polymer chain. Additionally, two sharp peaks with maximum at 1305 and 1388 cm^{-1} can be observed. The intensity of the IRAV bands compared with the intensity of the maximum of polaronic absorption suggests weaker electron-phonon coupling.

3.3 Electrical conductivity comparison of the pristine/doped P3HT and PBDTTT-c

Since the doping of the polymer affects its optical and electrical properties, conductivity measurement was performed. It is important to verify the origin of this IRAV peaks from the direct measurement of DC conductivity values that depends on the variation of the charge carriers density. Since the increase of the doping level results in the increase and broadening of the IRAV bands and corresponding broad polaronic absorption, their existence can be connected to the increasing of the charge carrier density. The higher charge carrier density is expected to be in the doped polymer. Additionally, it is very important to compare the optical response of the doped polymer to its electrical properties, since it is possible that the polymer, after exposing to oxidizing agent, can show changes in the optical spectrum due to formation of the polaronic states. However, no conductivity can be found. In this case the changes in the polymer after exposing to iodine vapor are due to the oxidation and due to the doping [69]. For P3HT, the measured conductivity of the pristine film was as high as $6\ \mu\text{Scm}^{-1}$. After iodine doping the conductivity increases up to $8.82\ \text{Scm}^{-1}$. In the PBDTTT-C polymer the conductivity of the undoped material measured using four-probe technique in dark was found to be below $1\ \mu\text{Scm}^{-1}$. After exposure to iodine vapor the DC conductivity increases rapidly and reaches equilibrium at $1.3\ \text{Scm}^{-1}$. The increase of the conductivity is consistent with the IRAV peaks measured in the ATR-FTIR. Interestingly, a much higher effect of doping on the conductivity would be expected, but this can be explained by the large side chains in the polymer structure which weaken the interchain transport of the charge carriers and limits the conductivity value.

4 Photodoping of conjugated polymers

As in the case of chemical doping of the p-type organic semiconductors, it is possible to form free positive charge carriers by dissociation of photo-generated excitons. In this study, after illumination of the polymer with light energy higher than the band gap, the exciton is formed. After formation it travels in the p-type semiconductor layer. Dissociation of the exciton existing in a donor polymer after illumination will occur predominantly in the presence of an electron accepting material creating free charges. In the experiment, an n-type semiconductor - PCBM, a soluble derivative of fullerene, was used. In photo-induced vibrational spectroscopy these photo-induced charges can be measured similarly to chemical or electrochemical doping, by the broad polaronic absorption and IRAV bands. To probe this physical behavior, photo-induced infrared spectroscopy (PIA-ATR-FTIR) was performed.

4.1 Photoinduced absorption in ATR-FTIR for P3HT

The PIA-ATR-FTIR results obtained for P3HT are presented in Figure 4.1. A pristine P3HT after illumination with laser shows an IR spectrum characteristic for the doped polymer. The spectrum is plotted in black in the Figure 4.1. As can be seen for wavenumbers below 1500 cm^{-1} a broad IRAV peak containing small sharp peaks can be noticed. Above 1500 cm^{-1} a polaronic absorption can be found. As can be noticed comparing to the Figure 3.2, the feature of the measured IRAV band during PIA experiment is exactly the same as obtained during chemical doping. This suggests the same nature of the vibrational changes during both doping processes. Interestingly, this peak is relatively narrow with a maximum at 1700 cm^{-1} . The formation of free charge carriers in the pristine P3HT is surprising since the material was precleaned to remove the contamination due to the residues from chemical synthesis and no external accepting material, i.e. PCBM was added. After mixing P3HT with PCBM, similar photo-induced absorption measurements using ATR-FTIR were performed.

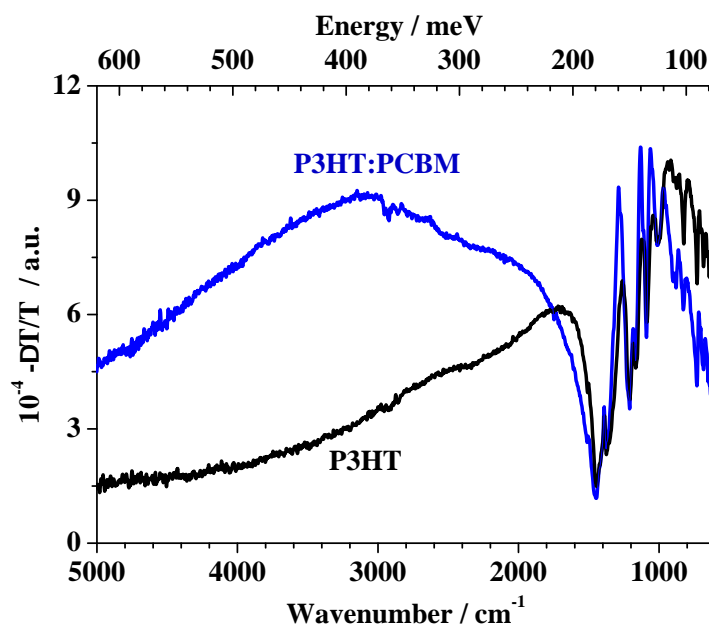


Figure 4.1: ATR-FTIR differential spectra measured during photoinduced absorption of (a) pristine P3HT compared with P3HT:PCBM.

A P3HT:PCBM layer was illuminated with 532 *nm* laser and the spectral response was measured as presented in blue in Figure 4.1. As can be seen photodoped P3HT:PCBM and chemically doped P3HT show similar features in the differential spectra. Both have very broad polaronic absorption and identical IRAV bands. The measured IRAV as well as polaronic absorption show exactly the same feature as obtained during chemical doping.

4.2 Photoinduced absorption in ATR-FTIR for PBDTTT-c

The effect of illumination of the PBDTTT-c and PBDTTT-c:PCBM on the vibrational spectrum was studied using PIA-ATR-FTIR technique. The resulting differential spectra for pristine PBDTTT-c (black) and PBDTTT-c:PCBM (blue) films deposited on ZnSe crystals are presented in Figure 4.2. The pristine polymer shows no spectral changes (polaronic absorption or IRAV bands), arising from the photogenerated charge carriers under illumination. This result is expected since no accepting material is present. In a bulk heterojunction blend of PBDTTT-c with the organic acceptor PCBM, strong photo-induced absorption bands in the IR region are observed. As a result of photoexcitation new IR spectrum was measured.

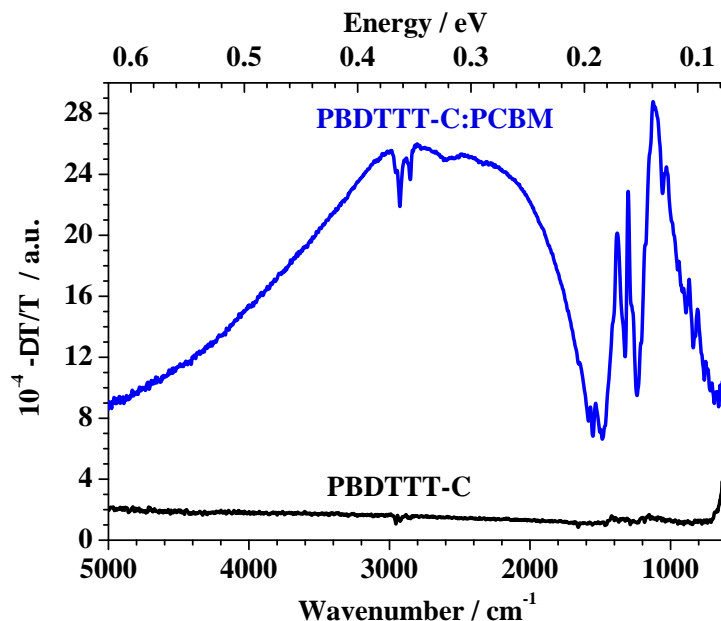


Figure 4.2: ATR-FTIR differential spectra measured during photoinduced absorption of (a) pristine PBDTTT-c compared with PBDTTT-c:PCBM.

The IRAV features are very similar to the ones measured for chemically doped polymer. Additionally, very broad electronic absorption connected with polaron formation between $0.15\text{ eV} - 0.6\text{ eV}$ with maximum around 0.35 eV was detected. As in the case of chemical doping, new enhanced peaks related to the IRAV bands are observed. Their broadness can again be described by high delocalization of the charge in the polymer chain. This delocalization of charge carriers is advantageous for construction of high efficiency organic solar cells.

4.3 Air stability influence on the P3HT and PBDTTT-c spectroscopic response

Comparing the spectral results detected during photoinduced and chemically doping of polymers in the FTIR some important differences can be found. For P3HT and PBDTTT-c polymers it is noticeable that both types of doping have the same IRAV bands which suggest the similar vibrational coupling of phonons to the electronic charges upon the doping process. However, differences can be observed in polaronic absorption bands. Iodine doped PBDTTT-c has much broader absorption peak with maximum around 3175 cm^{-1} which is shifted according to photo-doped PBDTTT-c:PCBM. For photo-induced absorption this maximum is around 2700 cm^{-1} . Additionally shifting toward higher energies

and the broadening of the polaronic absorption is observed. The effect of doping in PBDTTT-c was compared to those obtained for P3HT. As can be seen chemically doped P3HT and photodoped P3HT:PCBM show similar features. Both of them have very broad polaronic absorption and identical IRAV bands. The change in the position of the polaronic absorptions, as observed for the different doping techniques, cannot be easily understood and described by using the existing theories of FTIR spectroscopy.

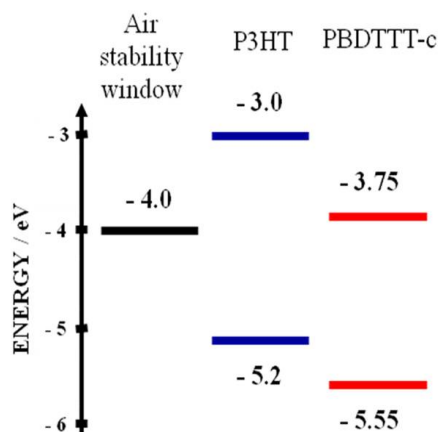


Figure 4.3: Comparison of the HOMO/LUMO levels of the studied polymers with air stability window.

The higher DC conductivity value in iodine doped sample obviously show the presence of a larger number of delocalized charge carriers as corroborated in the shift of the polaronic absorption in FTIR data. This suggests that the doping either chemically or photoinduced (in presence of PCBM) is following exactly the same process. An interesting situation can be observed for photodoping of P3HT. Although IRAV bands show the same features like those obtained for chemical doping of P3HT and photodoping of P3HT:PCBM, the strong difference can be observed in the position of the polaronic absorption. A possible explanation of such behavior might be an air stability of the polymer. Possible influence of air on the electrical performance of organic semiconductors was shown in the study of organic solar cell [70, 71] or organic field effect transistor performance [72–75]. The Figure 4.3 show comparison of the HOMO/LUMO levels of P3HT and PBDTTT-c compared to the air stability level. According to this in P3HT after illumination, exciton is diffusing in the polymer layer and then dissociate at the interface with air (i.e. O_2 or H_2O) creating radicals. These existing radicals with very low concentration, in the polymer matrix allow local exciton dissociation and formation of low-energy polaronic states.

5 Electrochemical doping of conjugated polymers

5.1 Electrochemical oxidation of P3HT

In order to understand the doping effect on the polymer in the controlled environment, electrochemical characterization was performed. Even though P3HT was successfully applied as donor material in the organic electronics, no detailed electrochemical characterization was done. In this chapter an electrochemical oxidation was characterized using scanning droplet cell microscopy. The kinetics of the doping process is described by various electrochemical measurements. In this term, the dynamic characterization using cyclic voltammetry as a function of the scan rate and as a function of the final applied reversible potential was performed. These results were compared with the potentiostatic measurement, where current transients at specific and constant applied potential in the electrochemical process were detected. Using these results, various calculations were done and the information about the amount of charge involved in the electrochemical process was obtained. Finally the behaviour of the film resistance and capacitance variation during electrochemical oxidation were studied using electrochemical impedance spectroscopy. From this experiment detailed information about the electrical properties of the polymer in comparison with the electrochemical processes were obtained.

5.1.1 Cyclic voltammetry

At first, for understanding the changes in the material upon doping, a dynamic characterization using cyclic voltammetry was performed. In this method, a current flowing through the electrochemical cell at a certain potential is measured. The electrochemical processes observed at certain applied potentials result in drastic changes in current flow. Figure 5.1 shows a series of cyclic voltammograms measured using $TBAPF_6$ electrolyte dissolved in propylene carbonate, with a rate of potential increase of 0.01 V s^{-1} . The maximum achievable potential was increased in 0.05 V steps up to 1.5 V for carefully probing the oxidation and the reduction potentials of the polymer. Two distinct and reversible ox-

idation potentials were found. The maximum of the first oxidation peak was measured at 0.52 V and the maximum of the second oxidation peak was found at 0.93 V.

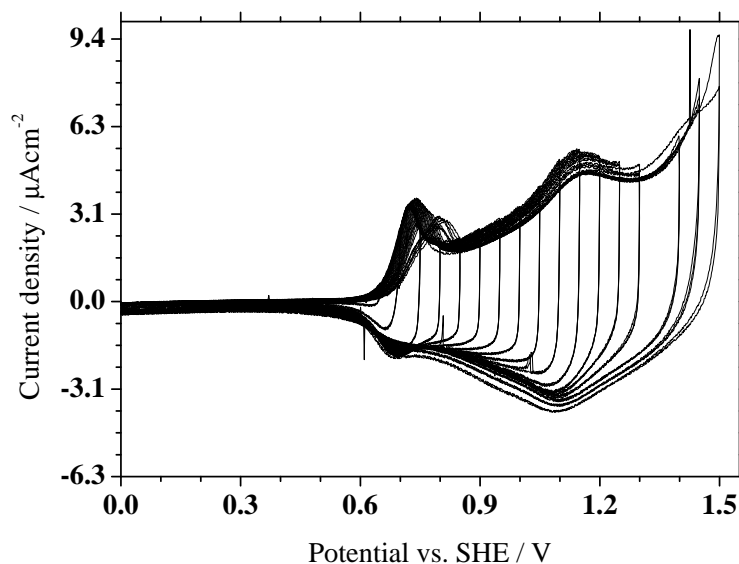


Figure 5.1: Cyclic voltammogram of P3HT measured as a function of maximum achievable potential. The measurement was performed with scan rate of 10 mV s^{-1} .

The reproducibility and stability of the oxidation potentials can be directly analyzed from the CVs shown in Figure 5.1. It was found that the first oxidation potential is shifting by 0.1 V during the entire series of investigation. For the second oxidation potential, only a slight shift smaller than 0.1 V was noticed. A constant shift might be explained by a non fully reversible oxidation, resulting in a continuous growth of the oxidized polymer layer. In addition, the current density corresponding to the first oxidation peak decreases with approximately 20 % during the entire study suggesting a possible decrease of the effective area. This can be attributed to a degradation process of the electrochemical cell.

In order to study the electrochemical reaction kinetics, cyclic voltammetry with variable scanning rates were used. The SDCM tip was moved to a new location on the surface of the P3HT film and scan rates of 1, 3, 10, 30 and 100 mV s^{-1} were successively applied. In Figure 5.2 these cycles are presented together and a direct comparison between them becomes possible. For each measurement, the current was divided by the used scanning rate. The obtained values of dQ/dE as a function of the applied potential in the electrochemical process are presented in Figure 5.2. With the increase of the potential scan rate up to 10 mV s^{-1} , the oxidation peaks positions are invariable. For the first three curves, the oxida-

tion peaks are found at 0.52 V and 0.93 V, which are identical with the result obtained previously from Figure 5.1.

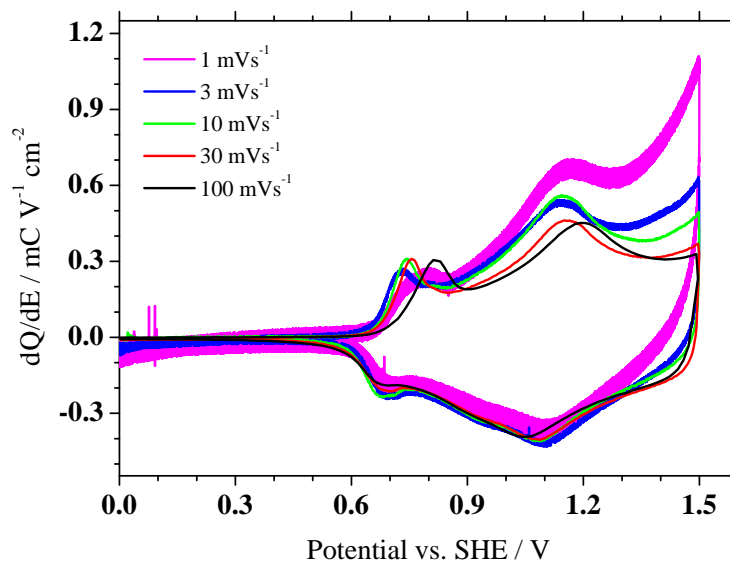


Figure 5.2: Scan rate dependent normalized cyclic voltammogram of P3HT with identical final potential.

Also, the reduction peaks are found in the same position as before. When further increasing the potential scan rate, the oxidation and reduction peak positions are found to be shifted towards higher respectively lower potentials. The maximum shifts of the oxidation peaks were measured as 0.07 V and 0.05 V corresponding to the first and second peak, respectively. This scan rate dependent measurement offers an insight into the kinetics of the underlying processes. The stronger shift of the first peak with increasing scan rate indicates a stronger kinetic hindrance for this process. An initial decreased conductivity in the fully reduced state does not allow a direct charge penetration whereas this effect is significantly lower for the second peak.

5.1.2 Potentiostatic characterization

In addition to cyclic voltammetry, a sequence of potentiostatic experiments was conducted in which the constant potential was increased stepwise in an attempt to determine the oxidation potentials. For the entire measurement series, the layer of P3HT was kept for 10 s at the corresponding potential while the transient current response was measured. These results are presented in the 3D graph of Fig 5.3.

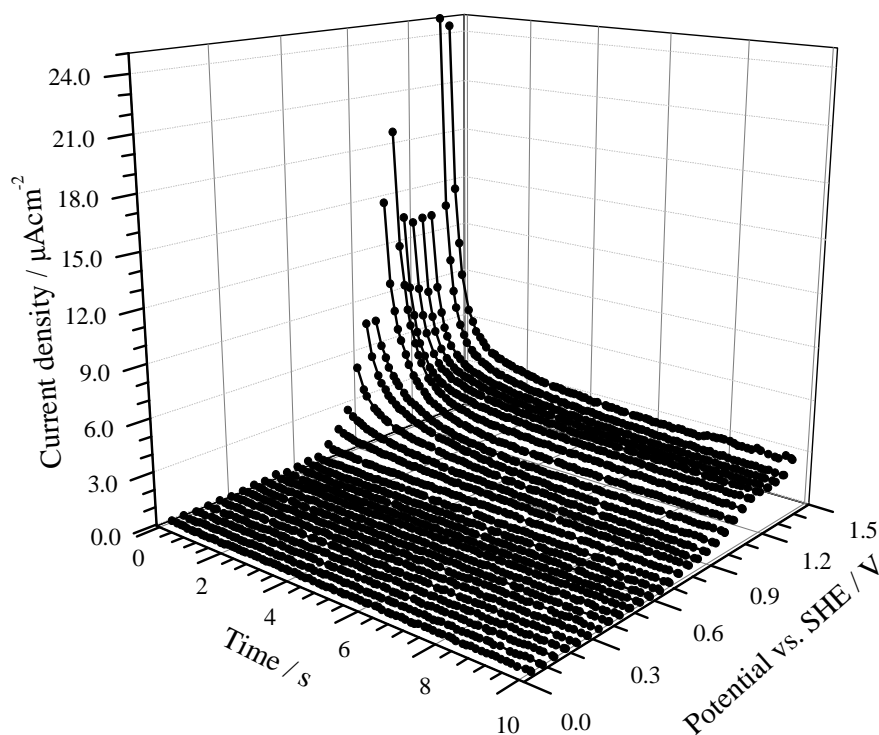


Figure 5.3: Time dependent potentiostatic characteristic during oxidation of P3HT.

Differences in the electrochemical processes can be better determined in such series of potentiostatic experiments by an increase in the current, especially when a sufficiently small step of the constant potential is used. For this purpose, a potential increase of 50 mV was found to be suitable. For low potentials, only a background current in the order of $10^{-8} \text{ A cm}^{-2}$ could be measured. During the 10 s timeframe for the measurements, this current remains constant. At potentials higher than 0.6 V, the beginning of the current transients shows much higher values than the background level. These values are increasing with the potential from one curve to the next within the series. During the first two seconds, a decrease of the current can be seen. This decrease characterizes the oxidation process of P3HT. Later on, the current stabilizes in plateaus describing the set-in of the electrochemical equilibrium. The values of the current plateaus are higher than the initial background current and increase with the applied potential. This effect might be attributed to an increase in the P3HT conductivity.

The measured current densities after the potentiostatic 10 s pulse can be used for the characterization of the electrochemical processes. All these values are summarized in Figure 5.4 for the entire series of potentiostatic experiments.

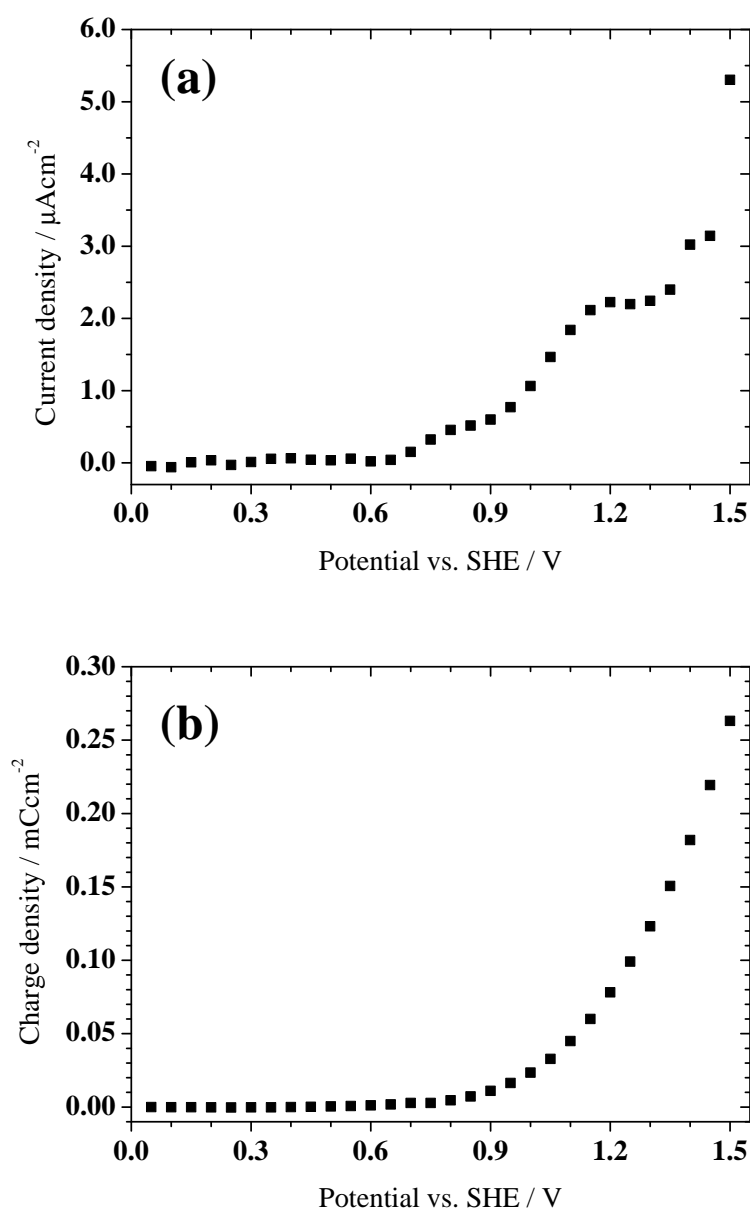


Figure 5.4: Analysis of potentiostatic measurement during oxidation of P3HT - the current density (a) and charge density (b)

Up to 0.65 V, a constant current density can be observed with a low value in the range of $10^{-8} \text{ A cm}^{-2}$. This value is directly describing the background current of the electrochemical system. Starting from 0.65 V, a first small increase of the current density can be observed, which settles in a first plateau at $4.5 \cdot 10^{-7} \text{ A cm}^{-2}$. The potential range of this current increase matches the first oxidation peak measured in the CVs from Figure 5.1. The first plateau describes the transitional potential range between the first and the second oxi-

duction peaks. Above 0.95 V, a second current increase can be observed and the presence of a second current density plateau is revealed starting with 1.2 V. These results fit very well the CVs data presented in Figure 5.1. The second current increase characterizes the second oxidation peak, while the second current plateau ends at high potentials where the stability of the system already changes due to various possible degradation processes in the electrolyte, P3HT, ITO or a combination of these factors.

The integration of the potentiostatic transients presented in Figure 5.3 combined with their summation allow a description of the total charge consumed up to each potential step during the electrochemical process. In Figure 5.4 together with the current densities, the total charge is plotted as a function of the potential. At low potentials up to 0.65 V, the charge level is low, just slightly increasing due to the capacitive charging. Above this potential, a stronger increase of the consumed charge can be observed indicating the start of the oxidation process of the P3HT.

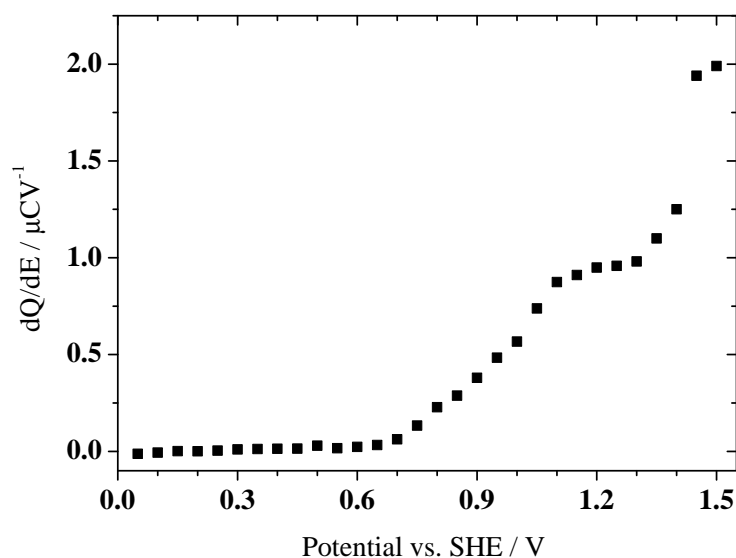


Figure 5.5: Charge variation dependence on the applied potential for the P3HT.

Additionally, more detailed study on the oxidation processes can be done by integrating the potentiostatic currents and subsequently plotting the resulting charge as dQ/dE vs. E for each potential step. Since the charge value is calculated for each potential step after equilibrium is attained, this plot will describe the infinitesimal changes in the electrochemical system. Therefore, it can be interpreted as infinitesimally slow cyclic voltammetry also referred to as quasi stationary measurements. The dQ/dE plot vs. E is presented in Figure 5.5. At low potentials up to 0.65 V the amount of charge which consumed in the elec-

trochemical process is low. This is due to the capacitive charging which occurs in the cell. Above 0.65 V, an increase in the charge is noticeable since the electrochemical oxidation starts. The slope of the increase can be fitted with two linear functions which describe a double step oxidation process. Above 1.1 V, the values of the dQ/dE reach a plateau which is characterizing the fully oxidized form of the P3HT. Above 1.3 V a further charge increase can be observed. This slope is then representing the degradation processes of various components in the electrochemical cell. In principle the same information would be expected from a CV and a series of potentiostatic current transients. However, the problem with CV can be that a slower process is apparently shifted towards higher potentials and may overlap with a faster process that thermodynamically starts only at higher potentials. In such a case not only an overlap of these two processes would be observed but also a shift in the peak position may be found since the second process might then start from a different initial state. A series of potentiostatic pulse experiments in which the final states are plotted against the potential does not show this restriction.

5.1.3 Electrochemical impedance spectroscopy

Electrochemical impedance spectroscopy was applied for investigation of the P3HT impedance as a function of the frequency at various potentials. All the measurements were done during the potentiostatic experiment presented in Figure 5.3. After each potentiostatic 10 s pulse, necessary for establishing an equilibrium state of the electrochemical process at a given potential, a full impedance spectrum, rather than a single frequency measurement, was recorded. For each measurement, a bias equal to the constant potential previously used in the potentiostatic experiment was applied. During the entire EIS, the SDCM addressed a single measurement spot. The Bode plots of the impedance spectroscopy on P3HT are presented in Figure 5.6. The impedance plotted as a function of the frequency presented in part (a) of Figure 5.6 shows a strong dependence on the applied potential. Increasing the bias of the electrochemical process (indicated by the arrow in Figure 5.6 (a)) resulted in a decrease of the low frequency impedance. This is a direct result of the doping process of P3HT during the electrochemical oxidation which changes the electrical conductivity of the polymer film [23].

The phase shift measured in the EIS experiment is presented in part (b) of Figure 5.6. The potential increase is again indicated by an arrow and is strongly affecting the measured phase. At low biases, a phase shift of approximately -75° can be observed at frequencies below 1 kHz. Increasing the potential, the phase shift is approaching -10° even at higher frequencies. This behavior can be used for best choosing the necessary equivalent circuit for fitting all EIS data.

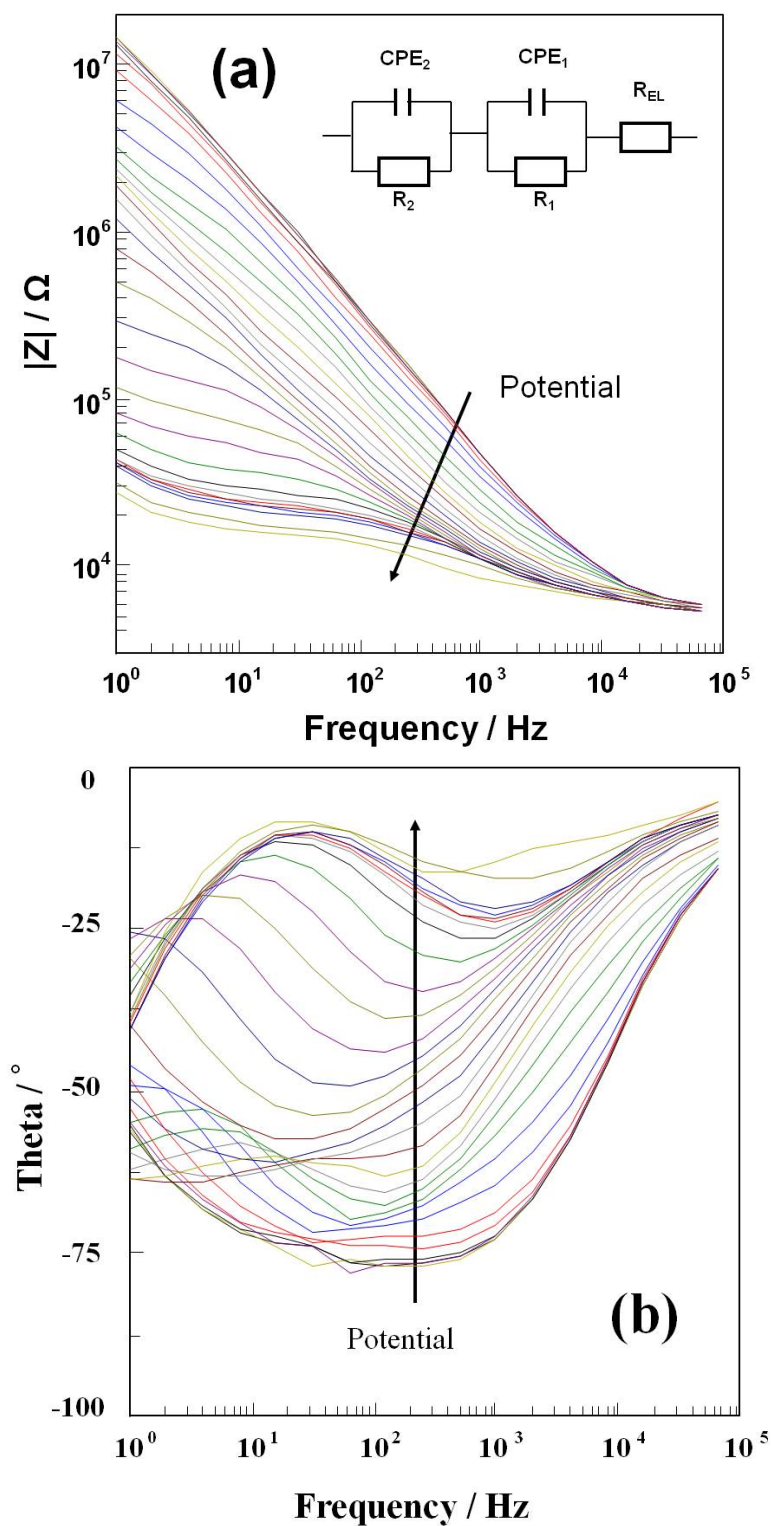


Figure 5.6: Bode plots from Electrochemical Impedance Spectroscopy measured in Mott-Schottky regime. The measurements were done for potentials between 0 and 1.5 V vs. SHE

The inset of Figure 5.6 (a) is depicting the proposed equivalent circuit. For EIS on organic materials, many equivalent circuits were used up to date. All of them contain many resistance and capacitance elements. [76–80]. In this work the use of a simple equivalent circuit was sufficient. The electrolyte is characterized by a series resistance R_{EL} . This is consistent with all models describing electrochemical processes in conducting electrolytes. The interface between the P3HT film and the bulk electrolyte is characterized by a constant phase element CPE_1 in a parallel configuration with a resistor R_1 . This describes the diffuse double layer which forms at the contact between the polymer surface and the electrolyte due to the dipole alignment of adsorbed electrolyte molecules. The CPE_1 simulates a capacitor that is formed by the dipoles, while the R_1 simulates the charge transfer from the electrolyte to the organic layer. The P3HT layer is described by a second parallel circuit formed from another constant phase element CPE_2 and its resistance R_2 . The oxidation of the polymer will have as a result the formation of $P3HT^+$ cations which are stabilized by the PF_6^- anions from the electrolyte. This process will influence both values of the R-CPE model used here.

Using the equivalent circuit presented in the inset of Figure 5.6(a) all the measured impedance spectra were fitted using a specialized software (ZView - Scribner Associates Inc.). In this way, the influence of the separate components of the electrochemical system can be independently analyzed. During the electrochemical process, the value of the electrolyte resistance was found to be constant with a value of 5.3 k Ω . A particular attention was given to the values of interface and P3HT layer resistances (R_1 and R_2 , respectively). These values are presented in Figure 5.7 as a function of the applied potential during the electrochemical process. The interface resistance shows an initial decay starting from approximately 2.5 M Ω . This happens during the bias increase up to 0.1 V and the process can be attributed to the dipole alignment of adsorbed electrolyte molecules at the interface. At higher potentials, the interface resistance stabilizes around 400 k Ω slightly fluctuating during the entire potentiostatic analysis up to 1.5 V. The values of the P3HT resistance (R_2) as calculated from the impedance spectra together with the conductivity values are presented in the lower graph from Figure 5.7.

The change of the polymer layer resistance due to the electrochemical doping is presented as a function of the applied bias. Three distinct regions can be identified. Below 0.65 V a small decrease of the P3HT resistance can be noticed according to the doping of the polymer in contact with electrolyte. This idea is supported by the CVs and the potentiostatic measurements where only background currents were measured. This large film resistance is equivalent with very low film conductivity in the range of $mS\ cm^{-1}$. This is expected for undoped or very low doped materials. For higher bias values up to 1.2 V a strong decay by two orders of magnitude of the film resistance are observed. In this potential

range both oxidation peaks were found during the cyclic voltammetry (Figure 5.2). This region describes a transition to the conducting form of the P3HT and directly characterizes the electrochemical doping of the polymer film. Also, these results can be very well correlated to the current density increase found in the potentiostatic experiments (Figure 5.4 (b)) due to the first and second oxidation peaks. In this region the values of conductivity increase by three orders of magnitude reaching 8.4 S cm^{-1} .

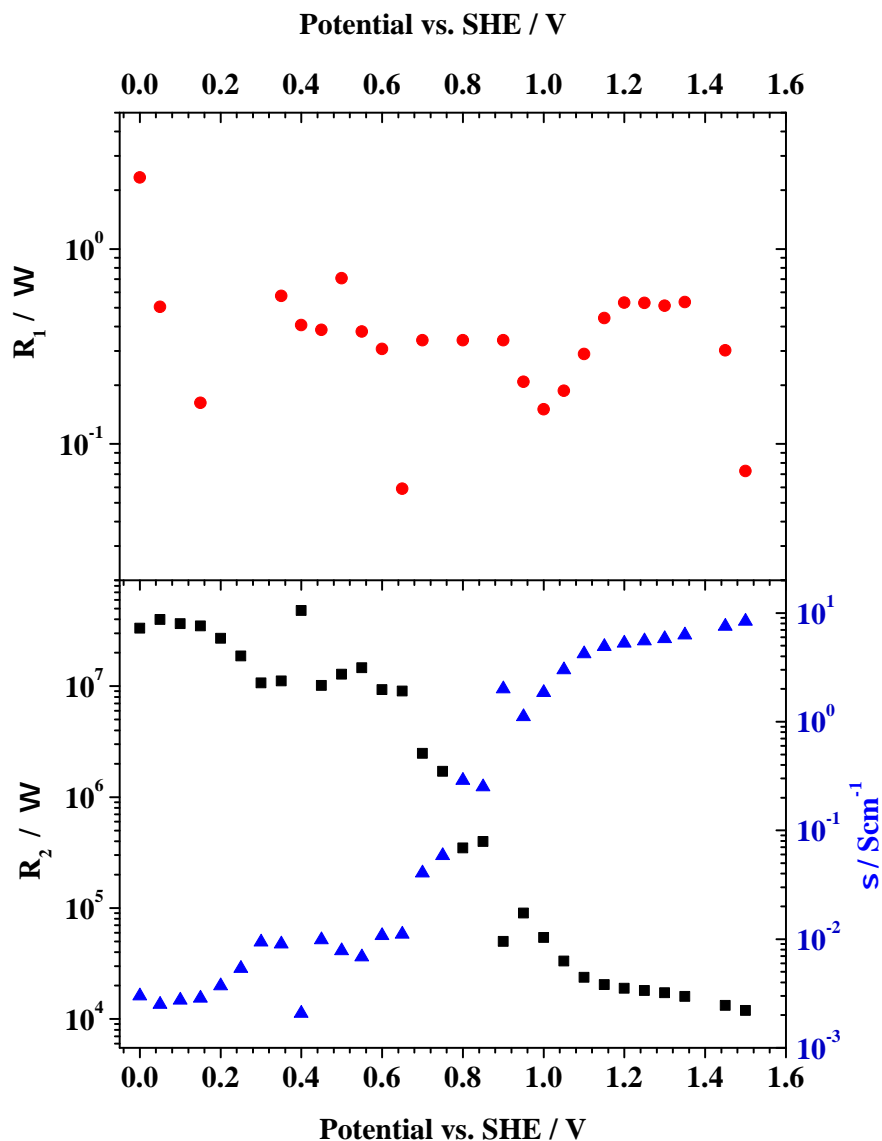


Figure 5.7: Comparison of resistances calculated from EIS spectra

This value is in full agreement with the previously reported conductivity measurements of the P3HT film after chemical doping in iodine vapors [81]. For potentials higher than 1.2 V, the P3HT film resistance showed only a slight de-

crease indicating the presence of a fully doped state. This result indicates that the final current density increase found during the potentiostatic investigations (Figure 5.4 (b)) at potentials above 1.2 V might not be attributed only to an electrochemical doping of the P3HT. This statement can be also proven by conductivity calculations where a plateau is observed for potentials above 1.2 V. This would rather describe a degradation process of the electrolyte and/or the metallic electrodes.

5.1.4 Mott-Schottky analysis

For analyzing the semiconducting properties of the P3HT film, Mott-Schottky analysis was conducted during the electrochemical impedance spectroscopy. According to this theory, the inverse square capacitance of a semiconducting layer is proportional to the applied potential [82, 83]. In the current study, the conductivity change due to an increase in the doping level is directly reflected in a capacitance change. Therefore, the doping level can be studied qualitatively and quantitatively using this method. The capacitance values of the polymer were determined from CPE_2 measured in the impedance spectra (see Figure 5.6) using the equivalent circuit described before. The inverse square capacitance dependence on the applied bias can be followed in Figure 5.8.

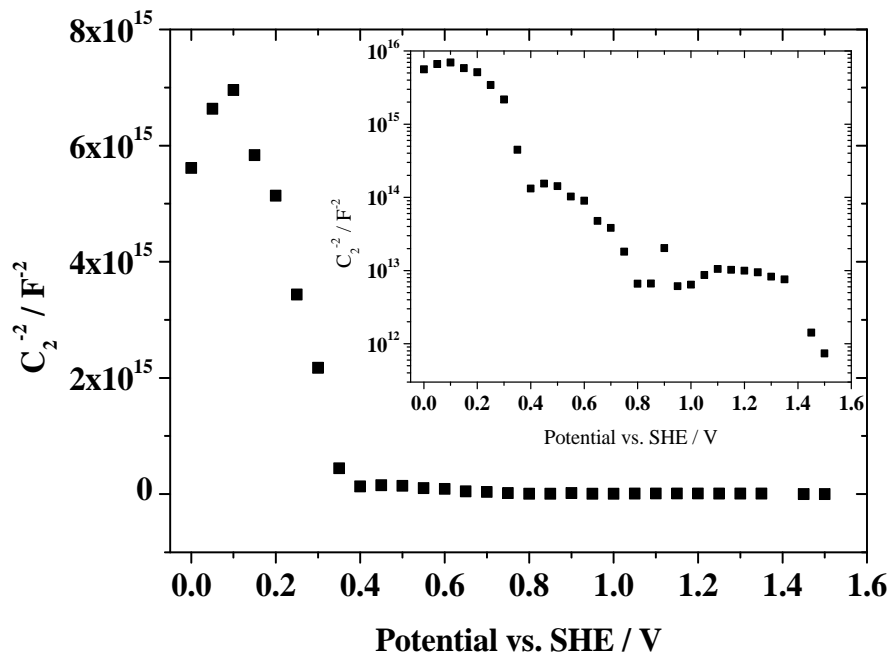


Figure 5.8: Mott-Schottky characteristic of P3HT electrochemical doping. The results plotted in the logarithmic scale are presented in the inset.

In this figure a drop in the value of the inversed capacitance can be observed above 0.2 V. Since in all experiments no oxidation processes could be measured up to 0.4 V, this slope describes the semiconducting behavior of the P3HT substrates prior to the electrochemical doping. In this region P3HT has a very low conductivity and still can be described as semiconductor. Using the equation

$$C_A^{-2} = 2 \frac{E - E_{fb} - kT/e}{e\epsilon\epsilon_0 N_D} \quad (5.1)$$

where C_A^{-2} is the area normalized inverse square capacitance at certain potential, e is the elementary charge, ϵ is the P3HT permittivity (in this study 3.5), ϵ_0 is the vacuum permittivity, E is the applied potential, E_{fb} is the flat band potential and a donor concentration (N_D) of $1.3 \cdot 10^{18} \text{ cm}^{-3}$ was calculated. This high charge carrier concentration is connected with the air induced doping [84, 85] as well as self-doping of the polymer in contact with electrolyte leading to cation formation. Above 0.4 V the existence of another slope can be noticed as presented in the logarithmic scale in the inset of Figure 5.8. However, since they describe a polymer in the oxidized form which can be treated already as metal, the Mott-Schottky analysis is no longer valid.

5.2 Electrochemical oxidation of PBDTTT-c

5.2.1 Cyclic voltammetry

The electrochemical oxidation of PBDTTT-c was studied in a series of cyclic voltammograms measured with increased achievable final potential and the results are presented in Figure 5.9. During the experiment, the maximum potential was increased from 0 V vs. SHE in steps of 0.05 V up to 1.50 V vs. SHE in order to probe the effect of doping of the polymer. For each measurement, two consecutive cycles were performed for probing the reproducibility of the oxidation process. As it can be observed, above 0.95 V vs. SHE an increase in the current, due to the beginning of the electrochemical oxidation process, was detected. This increase is fully reversible and is followed by a reduction process in the cathodic scan. The minimum of this reduction process is found at 1.15 V vs. SHE. Since the polymer was developed to serve as donor in organic photovoltaic devices, the reversibility of the electrochemical oxidation process suggests a possible hole transporting property of this material. Further increasing the potential above 0.95 V vs. SHE, an almost linear increase in the maximum measured current is noticeable up to 1.4 V vs. SHE. Above this potential, a sudden decrease of the maximum current achieved due to the degradation process is observed. This process is related to the dissolution of the oxidized PBDTTT-c layer in PC as well as to a possible incipient degradation of the electrolyte or substrate.

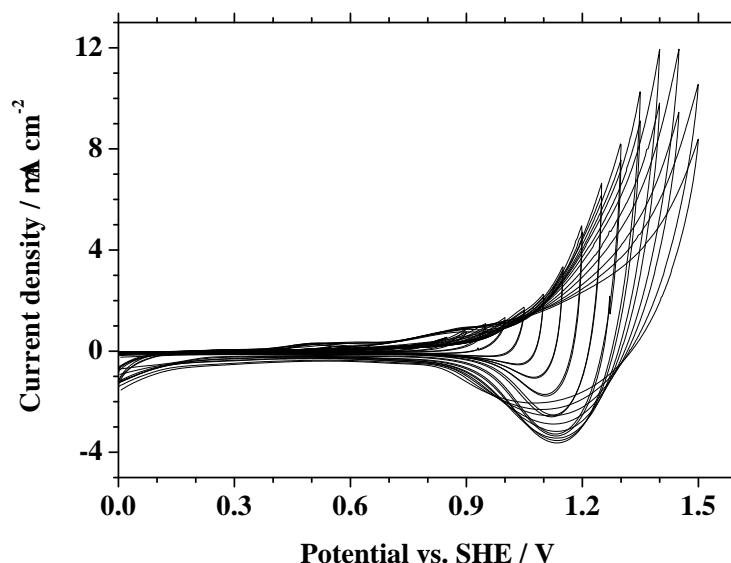


Figure 5.9: Cyclic voltammetry as a function of the maximum achievable potential measured during oxidation of PBDTTT-c polymer

Additionally, above 1.3 V vs. SHE a strong difference between the first and the second scan is found. This difference increases with the increase in the applied potential. This behaviour, suggesting an irreversibility of the oxidation process, may be due to the degradation of the PBDTTT-c which starts to be dominant at high potentials. At the same time, the reduction process changes due to the same reason. A decrease in the peak minimum followed by a broadening of this peak is noticeable. This can be attributed to a degradation of the polymer layer. Interestingly, for this type of polymer no distinct oxidation peak was observed, but rather a continuous current increase until the maximum potential is reached.

5.2.2 Potentiostatic characterization

For better understanding the electrochemical doping, time dependent potentiostatic experiments with different maximum achieved potentials were performed. The potential was increased step-wise from 0.0 V vs. SHE up to 1.5 V vs. SHE in 0.05 V steps for a precise determination of the oxidation potential. For the entire measurement series, the layer of PBDTTT-c was kept for 10 s at the corresponding constant potential and the transient current response was measured. A data acquisition rate of 10 Hz corresponding to a time resolution of 100 ms was used. The changes of the current in the transients as a function of the applied potential during the electrochemical oxidation process of PBDTTT-c are presented in Figure 5.10 as a 3D plot.

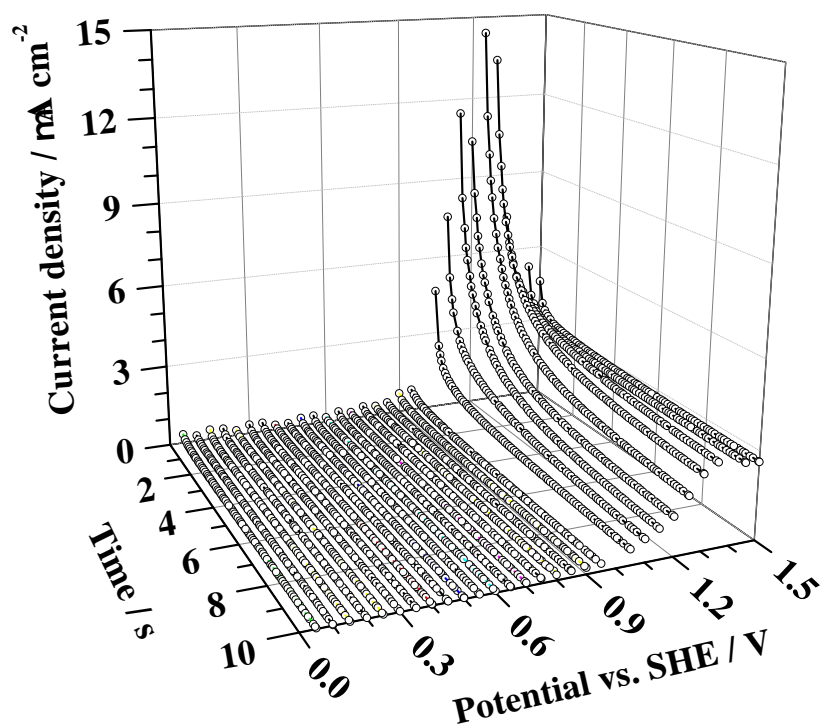


Figure 5.10: Time dependent potentiostatic characterization during oxidation of PBDTTT-c. Analysis of potentiostatic measurement during oxidation process

For potentials below 1.0 V vs. SHE only background currents in the range of $10^{-8} - 10^{-7} \text{ A cm}^{-2}$ can be observed. Above this potential, the first values of the recorded current transients are much higher than the background level. These values increase according to the increase of the potential driving the oxidation process. The highest transient current measured after the first 100 ms was found at 1.3 V vs. SHE. Above this potential, a strong decrease of these first values is noticeable. This may be correlated with the results obtained from the cyclic voltammograms presented in Figure 5.9. Starting from a potential of approximately 1.3 V vs. SHE, the maximum achievable current at the end of each CV sweep was decreasing. Additionally, the shift between the two subsequently recorded sweeps for each measurement was the highest. Combined with the results obtained from the potentiostatic experiments, this suggests that above 1.30 V vs. SHE a degradation process of the polymer film starts.

In order to better describe the electrochemical oxidation of PBDTTT-c, the current densities at the end of the potentiostatic experiments (after 10 s of applying the constant potential) are presented in Figure 5.11 as a function of the potential.

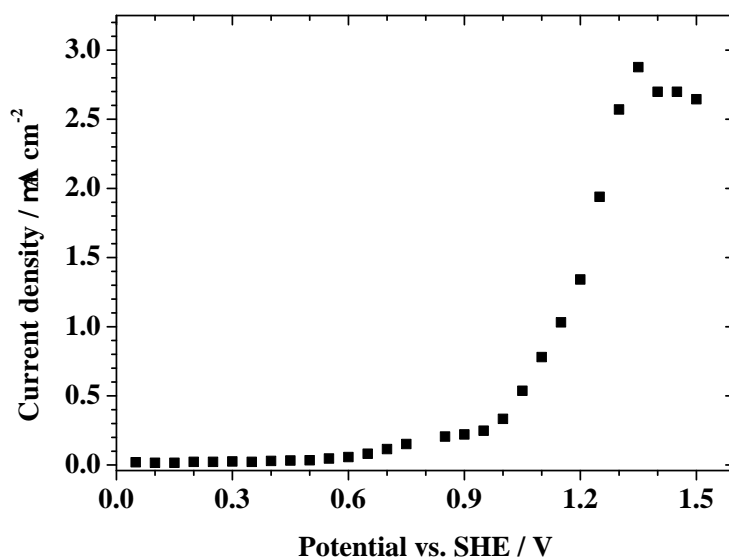


Figure 5.11: Analysis of potentiostatic measurement during oxidation process - current density

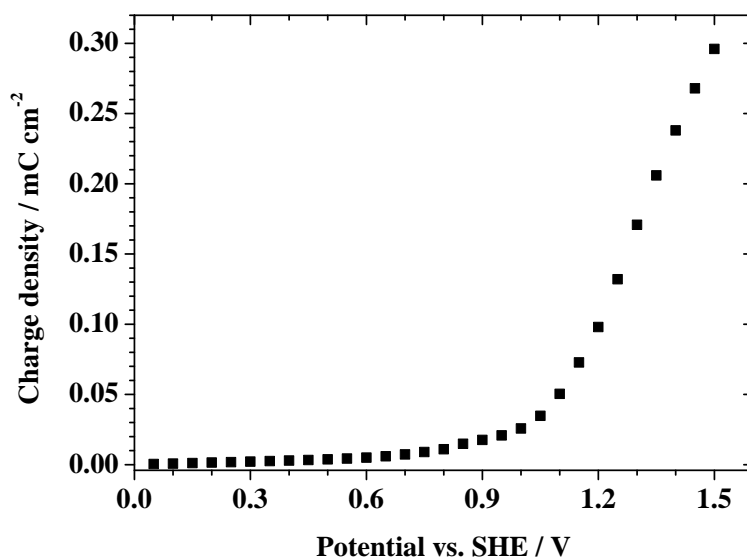


Figure 5.12: Analysis of potentiostatic measurement during oxidation process - charge density

As it can be noticed, up to 1.0 V vs. SHE only a small increase of the current densities can be measured. These values are describing the background current

flowing through the electrochemical cell. Starting from 1.0 V vs. SHE a continuous increase in the value of the current density can be observed. This may be attributed to a continuous increase in the PBDTTT-c conductivity due to the oxidation process which will have as a result an increase in the background current, as previously also observed in Figure 5.10. Above 1.3 V vs. SHE, a small decrease in the current density can be observed at the end of the potentiostatic experiments. The same trend was previously found in the cyclic voltammograms from Figure 5.9 and together may be attributed to a potential driven degradation process in the PBDTTT-c.

The integration of the individual potentiostatic transients gives information about the charge consumed at each potential step during the electrochemical oxidation process. The total charge can then be calculated by summation of all individually measured charges consumed at each potentiostatic step. The total charge dependence on the maximum applied potential is plotted in Figure 5.12. Similarly to the current density behaviour, only a small change in the total charge taking part in the electrochemical transfer can be found for potentials up to 1.0 V vs. SHE. However, above 1.0 V vs. SHE a strong increase of the total charge is observed. This is related to the electrochemical oxidation process in the PBDTTT-c. Additionally, a linear behaviour was found for the charge density dependence on the applied potential above 1.0 V vs. SHE. No charge saturation is observed in this plot. This fact is similar to the previously analyzed behaviour during the cyclic voltammetry (Figure 5.9). The intercept of the linear fit presented in Figure 5.12 shows a value of 1.05 V vs. SHE which can be considered the starting potential of the oxidation process.

The amount of charge consumed in the electrochemical process for each equidistant applied potential can be directly probed by plotting dQ/dE as a function of the potential. Since the charge value is calculated after equilibrium is attained, for each potential step this plot will describe the infinitesimal changes in the electrochemical system. The results are presented in Figure 5.13. The amount of charge consumed in the electrochemical process for each equidistant applied potential can be directly probed by plotting dQ/dE as a function of the potential. Since the charge value is calculated after equilibrium is attained, for each potential step this plot will describe the infinitesimal changes in the electrochemical system. The results are presented in Figure 5.13. The plot reveals that for potentials below 1.0 V vs. SHE no significant changes occur, suggesting an oxidation of the PBDTTT-c at higher potentials.

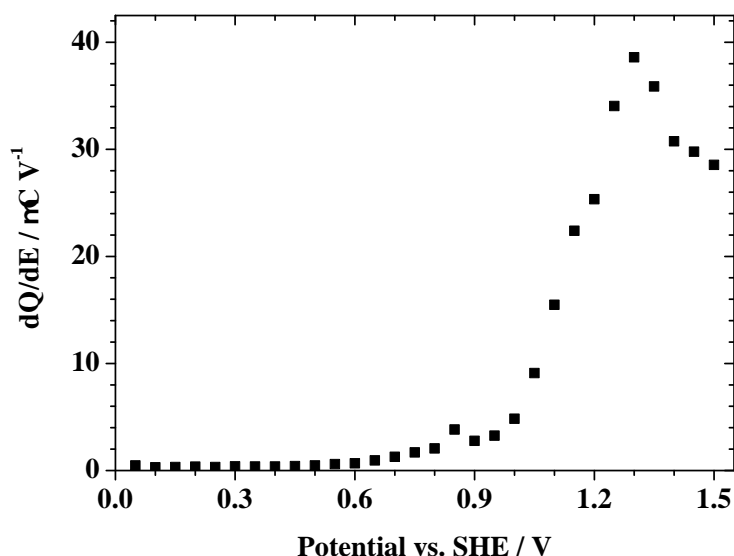


Figure 5.13: Analysis of potentiostatic measurement during oxidation process - charge variation

Above 1.0 V vs. SHE an increase in the charge consumed by the electrochemical system at each potential step was found describing one more time the oxidation process of the polymer. A peak with maximum at 1.3 V vs. SHE could be identified marking the beginning of the potential range where the polymer degradation starts. By polymer degradation one should understand the dissolution of the oxidized form in the electrolyte.

5.2.3 Electrochemical impedance spectroscopy

The electrical properties during electrochemical doping of the PBDTTT-c were investigated using electrochemical impedance spectroscopy. During this study, the changes of the resistance and capacitance of the oxidized polymer can be detected. In the present study all the measurements were done immediately after each potentiostatic experiment which was previously discussed in Figures 5.10 - 5.13. Every potentiostatic pulse of 10 s duration, necessary for establishing an equilibrium state of the electrochemical process at a given potential, was followed by an impedance measurement in a broad frequency range. For each impedance step, a bias equal to the constant potential previously used in the potentiostatic experiment was applied. Between switching from the potentiostatic measurements to the impedance, the electrochemical cell was always under constant potential control referenced to the SHE. During the entire EIS, the SDCM addressed a single measurement spot and the frequency response analyzer recorded

the real and imaginary parts of the impedance. Further, the impedance modulus and the phase shift are calculated by transforming the cartesian into a polar coordinate system according to the Bode representation. The Bode plots of the impedance spectroscopy on PBDTTT-c are presented in Figure 5.14.

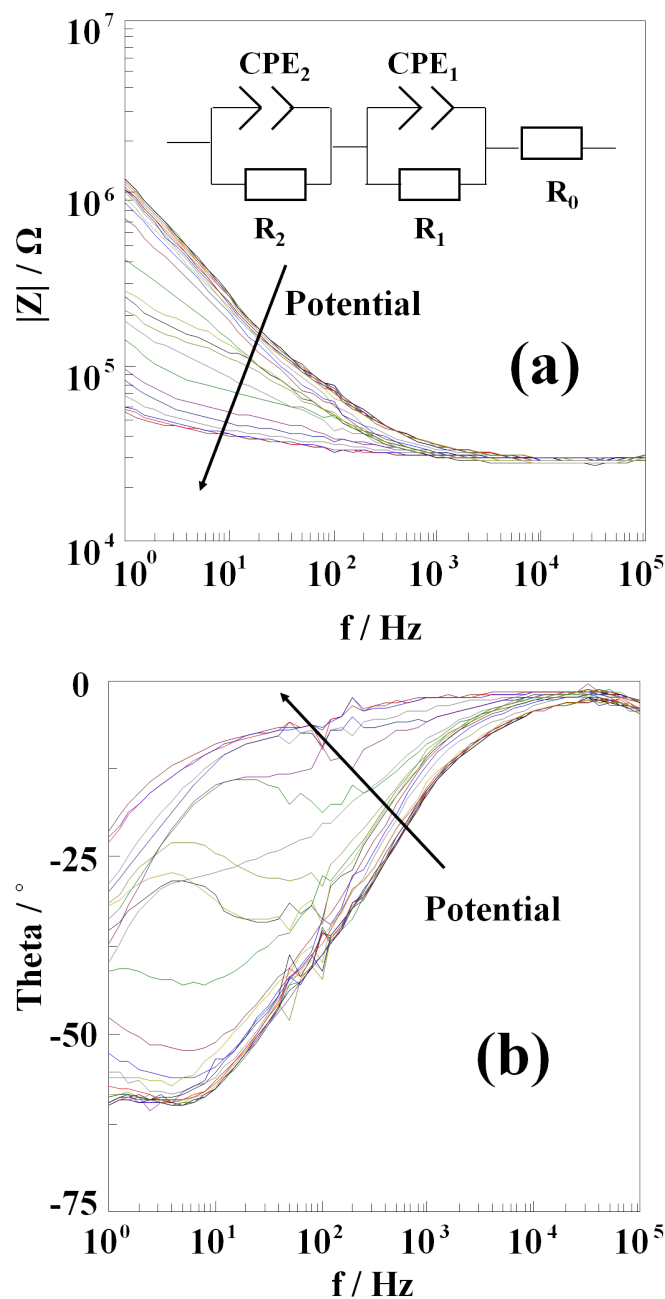


Figure 5.14: Bode plots of impedance magnitude (a) and phase (b) as a function of frequency measured during electrochemical oxidation. The measurement was done between 0 and 1.5 V vs. SHE

In the part (a) of Figure 5.14 the impedance is plotted as a function of the frequency for the entire analyzed spectrum. All measurements obtained at different biases immediately after the potentiostatic treatment are presented together. The arrow indicates the direction of the potential increase. At low biases up to 0.9 V vs. SHE, only a small change in the impedance can be observed. Above this threshold the impedance starts to decrease due to the progressive oxidation of the PBDTTT-c layer. Eventually, at applied biases as high as 1.3 V vs. SHE, the impedance value reaches a minimum limited by the electrolyte resistance of approximately $20k\Omega$ which can be directly observed at high frequency. The part (b) of Figure 5.14 shows the associated phase shift measured during the electrochemical impedance spectroscopy. Similar to the previous case, the arrow describes the direction of the potential increase. At low biases, the phase shift has an invariant behaviour up to 0.90 V vs. SHE, which is consistent with the data obtained from the impedance spectra. A capacitive behaviour can be identified due to the phase shifting towards negative values. Above this potential, the phase shift starts to increase during the oxidation process of PBDTTT-c suggesting a progressive increase in the layer conductivity due to the doping effect. For organic materials, this can be attributed to an insulator/metal transition which in the present case will weaken the dominant capacitive behaviour. One possible interpretation of the shapes of phase shifts can be related to the use of a two-time constant equivalent circuit, which is best observed in the potential range corresponding to the oxidation process. The equivalent circuit describing the electrochemical system used is presented as an inset in Figure 5.14 a. Two constant phase elements (CPE) in parallel with resistances are connected in series with the electrolyte resistance. The two R-CPE elements (1 and 2) are describing the electrolyte/polymer interface and the PBDTTT-c layer, respectively.

Using the previously defined equivalent circuit, the full impedance spectra were fitted using ZView software (Scribner Associated) in order to obtain the electrical properties of the undoped and electrochemically doped PBDTTT-c layer. The constant phase elements fit had errors of maximum 3 % for the capacitances. The CPE_1 describing the PBDTTT-c layer showed an exponent of minimum 0.85 suggesting a behaviour consistent to that of a real capacitor. The impedance measurements done at various applied biases define a Mott-Schottky type of analysis usually involved in the semiconductor properties studies.

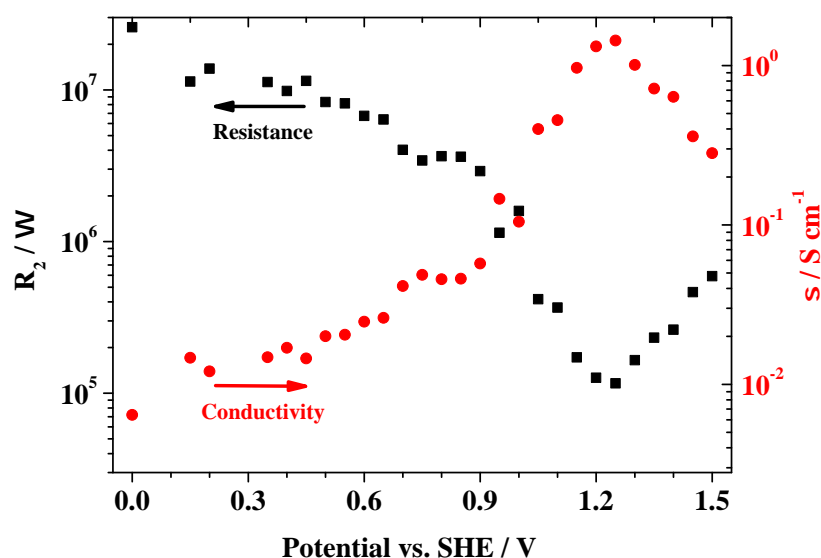


Figure 5.15: Resolved electrical parameters from EIS study - resistance values of PBDTTT-c layer plotted together with corresponding conductivity values

In Figure 5.15 these results are summarized. At low biases up to 0.90 vs. SHE only a small changing in the film resistance can be observed. These values obtained from electrochemical impedance spectroscopy are in the range of tens of $M\Omega$. The changes in the film resistance can be related to a slow doping of the polymer in contact with the electrolyte. This effect was observed in the previously described cyclic voltammetry and potentiostatic measurements as a background current. Above this potential a strong decrease of the polymer resistance down to approximately $100\text{ k}\Omega$ can be measured. This is due to the electrochemical oxidation of the PBDTTT-c. The process of the layer oxidation is dominant for potentials up to 1.25 V vs. SHE, above which an increase in the resistance can be noticed. Similar to the case of cyclic voltammetry and potentiostatic measurements, this growth of the resistance value can be attributed to the degradation (dissolution) of the PBDTTT-c layer. Since the material was developed to work as a conducting polymer in organic electronics, in addition to the resistance values, the conductivity values (σ) measured during the electrochemical process are given as normalized to the film thickness. The results are presented in the Figure 5.15. For low applied potentials, the large measured film resistance is equivalent to the low film conductivity in the range of $mS\text{ cm}^{-1}$. Since the conductivity of the undoped polymer should be in the range of $\mu S\text{ cm}^{-1}$, this conductivity value is surprisingly high [23]. However, this could be explained by considering that a certain doping takes place through spontaneous ion diffusion due to the direct contact between polymer and elec-

trolyte. After initiation of the oxidation process at 0.90 V vs. SHE, a strong increase in conductivity is found up to 1.25 V vs. SHE. In this region, the value of conductivity increases by two orders of magnitude reaching a maximum of 1.4 S cm^{-1} . Considering the high photovoltaic performance achieved in a solar cell containing PBDTTT-c, this relatively low value of the conductivity measured after doping is surprising when compared to other conducting polymers such as P3HT [81]. For biases higher than 1.25 V vs. SHE, a decrease in the conductivity is observed according to the dissolution of the PBDTTT-c.

5.2.4 Mott-Schottky analysis

The semiconducting properties of PBDTTT-c were characterized using Mott-Schottky analysis. According to the Mott-Schottky theory [82, 83] the capacitance values determined from CPE_2 measured during the impedance spectroscopy were first normalized to the investigated area. Furthermore, the obtained normalized capacitance was inverse squared and the resulting values are presented in Figure 5.16 as a function of the applied potential.

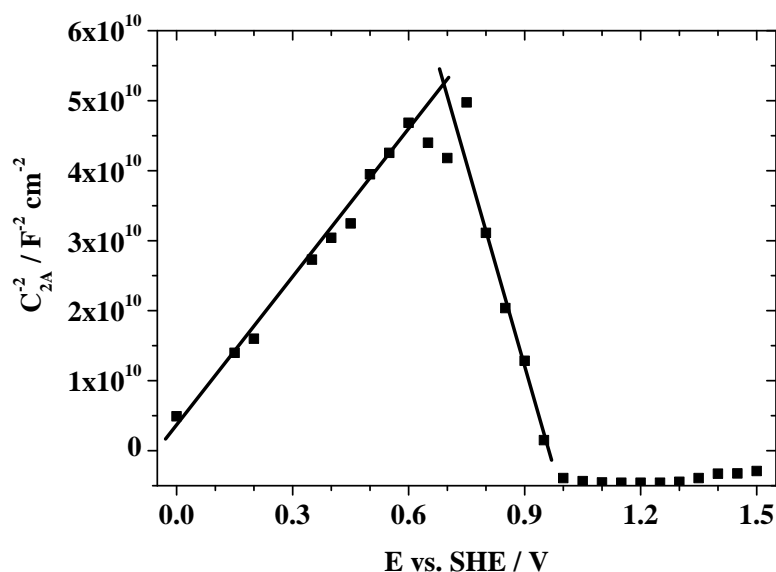


Figure 5.16: Resolved electrical parameters from EIS study - Mott-Schottky plot of the conductivity

For bias values of up to 0.75 V vs. SHE, the value of the inversed square capacitance increases. This behaviour can be attributed to the formation of an inversion layer leading to an apparent n-type conductivity. The inversion layer can be formed as soon as the Fermi level at electrolyte/polymer interface ap-

proaches the band edge of the mobile minority charge carriers. It results in the increase of the potential drop across the depletion layer. Due to this, minority charge carriers are accumulated in the inversion layer and at a specific potential the interfacial properties of the apparent semiconductor behaviour can change from the n- to p-type [86]. Between 0.75 and 1.00 V vs. SHE a slope describing the semiconducting properties of the PBDTTT-c due to the electrochemical oxidation can be observed. In this region, the PBDTTT-c layer has still a very low conductivity and the polymer can still be described as a semiconductor using the Mott-Schottky formulation (equ.5.1). For biases below 0.60 V, where the inversion layer describing the n-type conductivity can be found, an electron concentration of $5.6 \cdot 10^{20} \text{ cm}^{-3}$ was calculated using a linear fitting of the experimental points presented in Figure 5.16. In this case a flat band potential of -0.10 V vs. SHE was calculated. For the p-type conduction region above 0.75 V vs. SHE, a donor concentration of $2.3 \cdot 10^{20} \text{ cm}^{-3}$ was found. Additionally, a flat band potential of 0.95 V vs. SHE was calculated taking into account the thermal contribution from kT/e of 25.8 mV. For biases above 1.00 V vs. SHE an electrochemically doped PBDTTT-c cannot be considered anymore as a semiconductor but rather as a metal.

6 Photoelectrochemical characterization of conjugated polymers

Due to its high localization capability, the use of scanning droplet cell microscopy is expected to improve the understanding and predict possible applications in the field of organic electronics, especially for application in photovoltaics. Usually, characterization of the photovoltaic effect is done using measurements of the pristine photoactive material as well as its mixture with an acceptor material in a bulk heterojunction (BHJ) solar cell. In both cases an exciton is formed after illumination with photon energy higher than the band gap of the photoactive material. As soon as the photoactive material or BHJ is confined between two electrodes, or in the case of an electrochemical cell between the electrode and electrolyte, an effective migration of the exciton formed in the photoactive material becomes possible upon field application. At the interface with the electrode/electrolyte or an accepting material (from BHJ) it separates into free carriers which are transported in opposite directions according to their charge. During device construction material mixtures forming BHJs are preferred due to their stronger output photocurrent.

At first, the study about the influence of the electrolyte formulation on the photoelectrochemical cell containing P3HT as a photoactive material was performed. Furthermore, the photovoltaic effect in pristine polymer and bulk heterojunction was done using scanning droplet cell microscopy, where as a model compound PBDTTT-c polymer as well as its mixture with PCBM were used. All photoelectrochemical processes described in this chapter are referenced to Ag/AgCl $\mu - QRE$.

6.1 Photoelectrochemical characterization of P3HT

6.1.1 Dark/illumination current transients

The effect of illumination on the P3HT covered WE in contact with both, pure electrolyte or electrolyte containing ferrocene is sequentially presented in the Figure 6.1. In the part (a) of Figure 6.1 the results obtained from contacting the WE with the pure electrolyte (0.1 M TBAPF₆ in PC) are shown. After contacting the surface, the current transients corresponding to an applied potential of 0 V vs. Ag/AgCl were measured for alternating dark and illuminated conditions. According to previous studies, at this potential no electrochemical process occurs (see Chapter 4.1). All changes detected during this experiment result from the interaction between the 532 nm laser radiation and WE. As mentioned before, the chosen wavelength fits to the maximum absorption of P3HT as previously evidenced by the ellipsometric study (Figure ??). At first, the PE-SDCM was kept for 10 s in the dark and a background current density (dark current) of approximately $0.2 \mu\text{Acm}^{-2}$ was measured. After this time period the shutter was opened allowing the laser radiation to illuminate the addressed surface also for 10 s. This sequence of 10 s current density measurements in dark followed by measurements under illumination conditions was repeated for a total time of 90 s.

During the first illumination period a strong current density peak reaching $-20 \mu\text{Acm}^{-2}$ is noticeable immediately after opening the shutter. This negative peak decays rapidly during the first second under illumination conditions and later on the current density stabilizes at a value of $-4.5 \mu\text{Acm}^{-2}$ at the end of the predefined time period. This behavior can be attributed to a photo-doping (charging) effect. After illumination of the P3HT, a transition from the highest occupied molecular orbital (HOMO) to the lowest unoccupied molecular orbital (LUMO) (or $\pi \rightarrow \pi^*$ transition) occurs. The absorption of light leads to the formation of an exciton which at the polymer/electrolyte interface splits into elementary mobile charges (electrons and holes). Ideally, the holes should be transported through the P3HT layer to the ITO electrode, while the electrons should be finally transported to the CE using the electrolyte path via ionic transfer. However, in the real system, some of the charges present at the P3HT/electrolyte interface, are heavily localized by electrolyte anions (PF_6^-) attachment creating a doped form of polythiophene ($\text{P3HT}^+\text{PF}_6^-$). This doped polythiophene interfacial layer should have a much higher conductivity as compared to the P3HT film. At the same time, after doping, new energetic states are created in the bandgap leading to its decrease. This effect was already presented in Figure 3.1 where, after doping, the main absorption peak decreases

and a new absorption peak appears at lower energies.

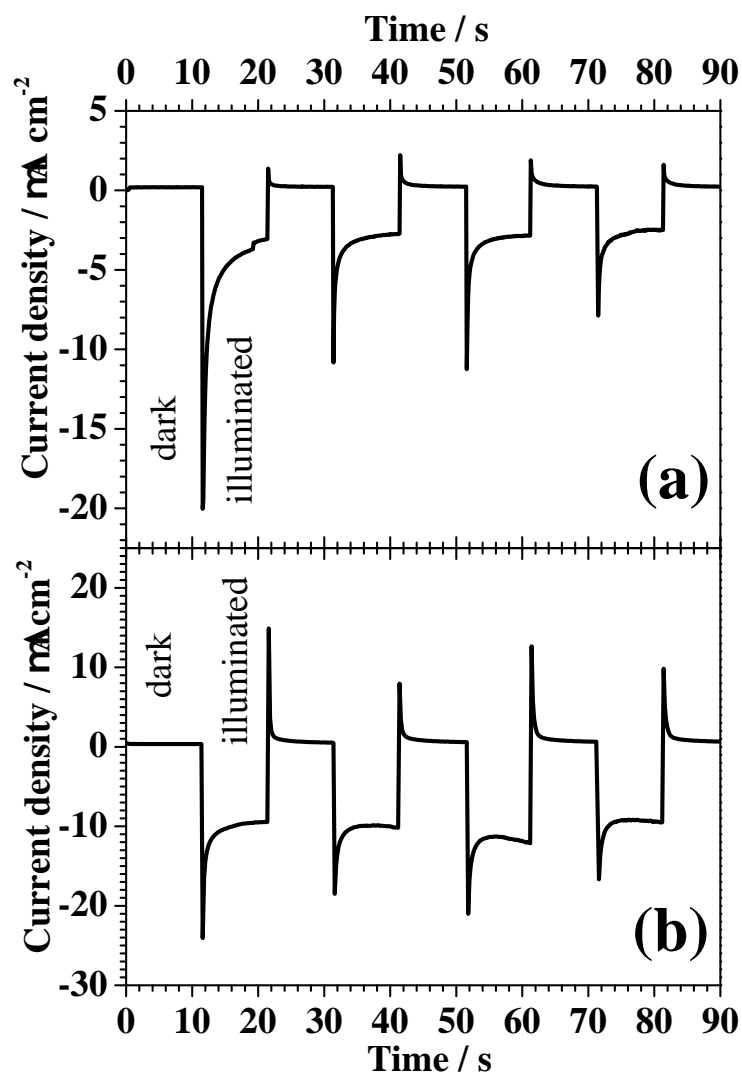


Figure 6.1: Current transients measured in the dark and during illumination with the laser light. The results of the measurement were done in presence of (a) the pure 0.1M TBAPF₆ in PC and (b) 5.4 mM Fc/Fc^+ redox couple dissolved together with 0.1M TBAPF₆ electrolyte in PC

As soon as the first illumination period was finished, the shutter was closed and the current transient was measured in the dark. As can be noticed from Figure 6.1 (a) within the first second of the measurement, a strong increase in the positive current density was recorded. This can be attributed to a de-doping process triggered by discharging of polymer/electrolyte interface. The absolute height of the de-doping current density peak is much smaller as compared to the doping peak. Afterwards, a strong decrease in the current density is observable

down to the background value. Further alternating measurements in the dark and under illumination reveal the same behavior as described above, suggesting a good reproducibility and stability of the photovoltaic effect evidenced here.

Similar measurements were performed using a second PE-SDCM filled with electrolyte containing 5.4 mM ferrocene. These results are presented in Figure 6.1 (b). As in the case of using pure electrolyte, the current transient was at first measured in the dark for 10 s. The background level of the current density was slightly higher as compared to the pure electrolyte case, a stable value of $0.6 \mu A cm^{-2}$ being identified. This increase of the dark current density can be due to a different formulation of the electrolyte, which in this case is expected to have a slightly higher conductivity. After opening the shutter during the first illumination period, the measured photocurrent shows a strong negative peak. The value of the photocurrent density peak reaches $-24 \mu A cm^{-2}$ and rapidly increases to $-11 \mu A cm^{-2}$ where it stabilizes. Similar to the case of pure electrolyte, the strong change in the current flow during laser irradiation is due to P3HT excitation and charge separation at the polymer/electrolyte interface. Interestingly, the value of the photocurrent density plateau is tripled as compared to the experiment where pure electrolyte was used. This increase can be explained by a slightly modified charge transport. The presence of the redox couple Fc/Fc^+ in the electrolyte solution will modify its redox energetic level. Holding the applied potential at a constant value (0 V vs. Ag/AgCl) will result in an alignment between the ITO Fermi level and the new redox level of the electrolyte which increases the bending of the P3HT HOMO-LUMO levels improving the charge transfer.

As soon as the first illumination period was finished, the next dark period was triggered by closing the shutter. The resulting current density shows from its beginning a strong positive peak with maximum at $16 \mu A cm^{-2}$. Similar to previous situations, this peak can be attributed to a discharge of P3HT/electrolyte interface taking place in the first second of the measurement. At this point, comparing with the experiment using pure electrolyte, it can be observed that addition of ferrocene results in a better reversibility of the charging process. This is suggested by the current density peak heights measured within the first second during illumination and in the dark, which are very similar. This is in contrast to the case when pure electrolyte was used, where the difference between the peak heights is substantially larger (Figure 6.1 (a)). This effect of reversibility when the cell containing electrolyte with dissolved ferrocene was used is reproducible for all measured light/dark cycles up to 90 s.

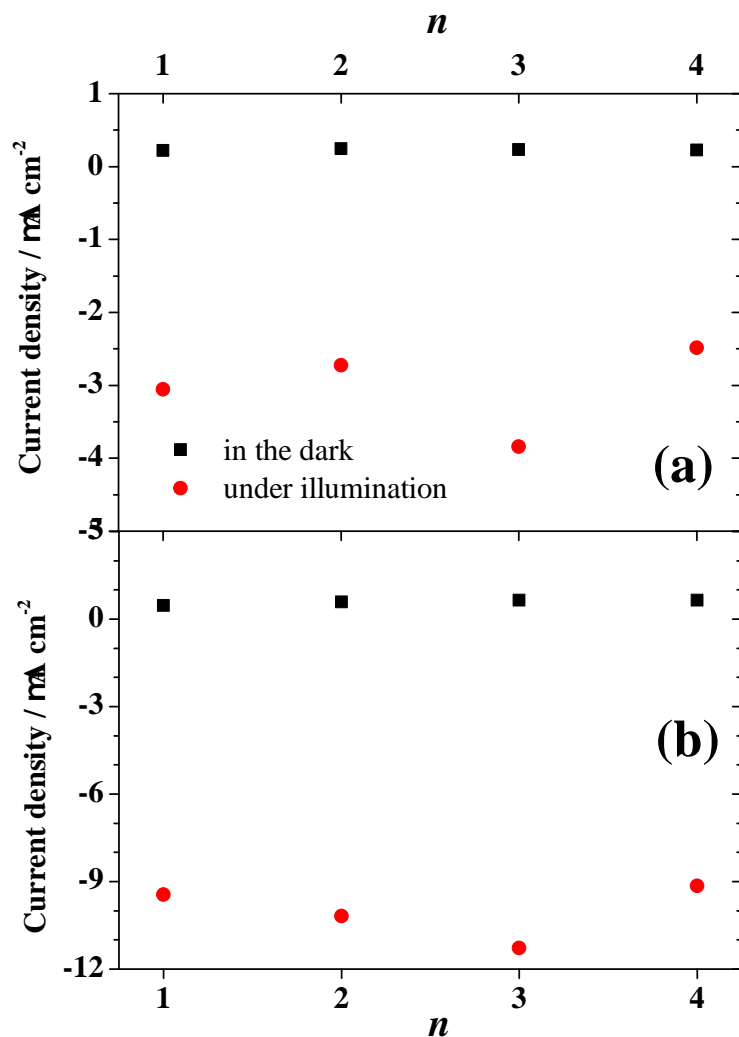


Figure 6.2: The measured short circuit current from current transients measured in the dark and during illumination with the laser light of 532 nm for (a) pure electrolyte and (b) electrolyte with dissolved 5.4 mM Fc/Fc^+ redox couple

The values of the current density plateaus measured under illumination and dark conditions in each cycle (n) using pure electrolyte are presented in Figure 6.2(a). Every time during illumination within the time frame of each cycle, the current density settles in a plateau level oscillating between -3 and -4 $\mu A cm^{-2}$. Within all four cycles, the photocurrent is reproducible suggesting a good stability of the polymer in contact with pure electrolyte. When the shutter is closed and dark conditions are established, the plateau values of the current densities increase, slightly oscillating in the range of 0.2 - 0.4 $\mu A cm^{-2}$. These values are comparable to the initial current measured before the first cycle describing the electrochemical dark current. The difference between the photocurrent and the

dark current plateaus is directly related to the photoinduced charge formation during radiation absorption. A similar characterization of the P3HT/electrolyte system was performed using the ferrocene containing electrolyte and the results are presented in Figure 6.2 (b). Under illumination, the photocurrent density plateaus observed in each cycle show values ranging between 9.5 and 11 μAcm^{-2} . These values are approximately three times higher than those obtained using the pure electrolyte. This effect is due to the presence of the Fc/Fc^+ redox couple which is modifying the flat band potential of the system, as previously discussed.

In order to study in more detail the effect of charging/discharging of the system under illumination and in the dark, the charge taking part in both processes was calculated from each transient by integrating the current densities presented in Figure 6.1. For the transients measured under illumination, each negative current density peak was integrated using as reference line the photocurrent plateau, while for the positive current density peaks obtained after actuating the shutter, the integration reference line used was defined by the dark current level. All four charging/discharging pair of peaks observable in Figure 6.1 for both electrolytes/cells were analyzed in this manner and the obtained surface normalized charge was used for further discussions. The results obtained when using pure electrolyte are presented in the Figure 6.3 (a). It can be observed that under illumination the amount of normalized charge taking part in the photoelectrochemical process is for the first cycle approximately 50 μCcm^{-2} , while the first dark measurement shows that only 0.45 μCcm^{-2} is responsible for the de-doping process. Starting with the second cycle, the situation changes and the charge balance becomes reproducible. The charge density levels responsible for the doping process under irradiation conditions settle to a lower value of 20 μCcm^{-2} while the de-doping process is defined by a slightly increased charge consumption of approximately 0.8 μCcm^{-2} as compared to the first cycle. Therefore, the use of pure electrolyte in the PE-SDCM resulted in an almost 25 times stronger charging process as compared to the discharging in the dark. This leads to an accumulation of PF_6^- doped $P3HT^+$ at the polymer/electrolyte interface decreasing the effective absorbance of the WE.

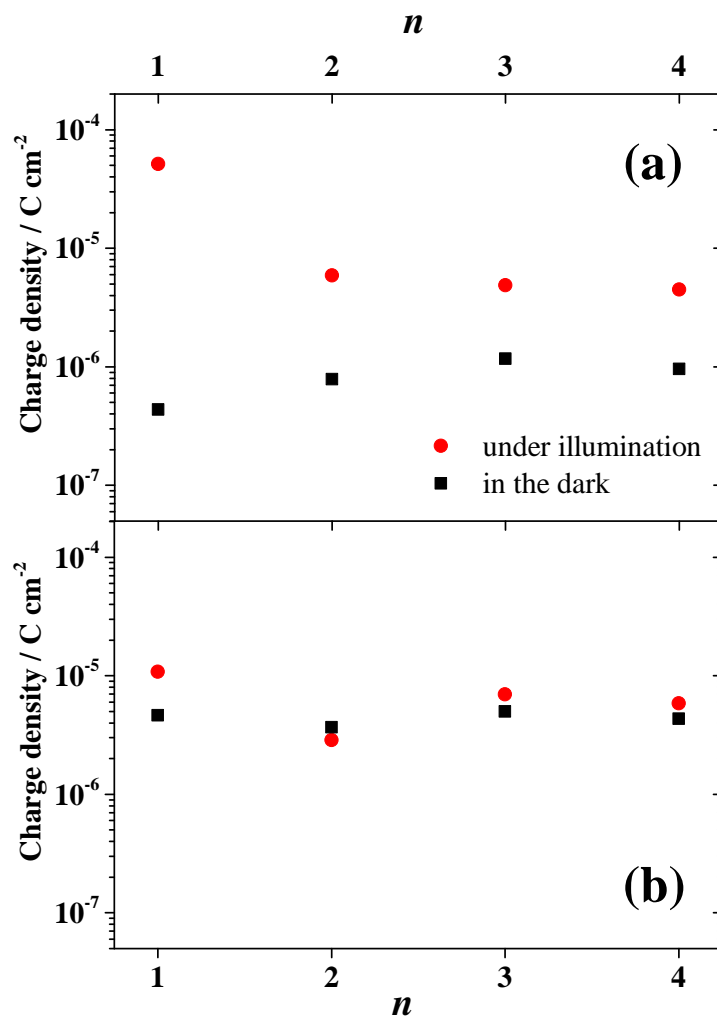


Figure 6.3: Charge density calculated from current transients measured in the dark (black square) and under illumination (red circle) with the laser light of 635 nm for (a) pure electrolyte and (b) electrolyte with dissolved 5.4 mM Fc/Fc^+ redox couple

Similar evaluations were conducted for the results obtained using the electrolyte containing 5.4 mM ferrocene. Charge densities calculated from current transients measured in the dark and under illumination are presented in the Figure 6.3 (b). In this case, the amount of charges accumulated during charging and released during discharging are almost identical in each cycle. This equilibrated charge balance provides better system stability. Furthermore, only small variations of the charge densities (between 3 and 10 μCcm^{-2}) were found between different cycles. Comparing the behavior of the charge/discharge processes for both electrolytes used it can be observed that the P3HT in contact with pure electrolyte has a very unbalanced charge transport, the differential charge density value

being almost one order of magnitude higher in the absence of ferrocene. This is most likely caused by an accentuated charge accumulation at the interface due to a lower electrolyte conductivity resulting in the formation of a stable salt upon neutralization by ions. The situation is different in the case of the ferrocene containing electrolyte where the electrochemical reduction of Fc^+ to the neutral Fc takes actively part in the charging/discharging processes.

6.1.2 Photocurrent stability

The stability of the photocurrents evidenced during the on/off illumination cycling presented so far, was furthermore studied using longer terms illumination. In this experiment the sample was kept under constant illumination for 600 s while continuously recording the photocurrents. For both cells/electrolytes used, new spots were addressed on the surface of the WE for this purpose. As done previously, both PE-SDCMs were first used to measure the dark current flowing through the cell for 10 s. In order to check the dark currents reproducibility after the 600 s of radiation exposure, the shutter was closed and the current densities in the dark were again observed. The resulting current transients are presented in Figure 6.4. When the glass/ITO/P3HT electrode is in contact with pure electrolyte (black line), after opening the shutter a negative peak with a minimum at $-3 \mu Acm^{-2}$ is observed. Afterwards, within the first second, the current increases to $-1.8 \mu Acm^{-2}$ and later on slowly decreases until a new minimum of $-2.8 \mu Acm^{-2}$ is reached after 20 s of illumination (30 s from beginning the experiment). As soon as the second current density minimum is surpassed, the current increases to $-1 \mu Acm^{-2}$ during the next 130 s (160 s from the experiment beginning) and remains constant until the end of the measurement.

A similar trend can be noticed for the electrolyte containing ferrocene (red line) also presented in Figure 6.4. After opening the shutter, a much stronger negative peak with a minimum at $-37 \mu Acm^{-2}$ was recorded, and the current density increases within the first 10 s up to $-10 \mu Acm^{-2}$. Also in this case, a second negative peak of the current density with a minimum at $-15 \mu Acm^{-2}$ can be observed at 60 s after opening the shutter (70 s since the experiment started). The increase toward a stable photocurrent level is much slower when using ferrocene. Approximately 300 s are necessary for establishing a photocurrent plateau level at $-4 \mu Acm^{-2}$, which remains constant until the end of the exposure.

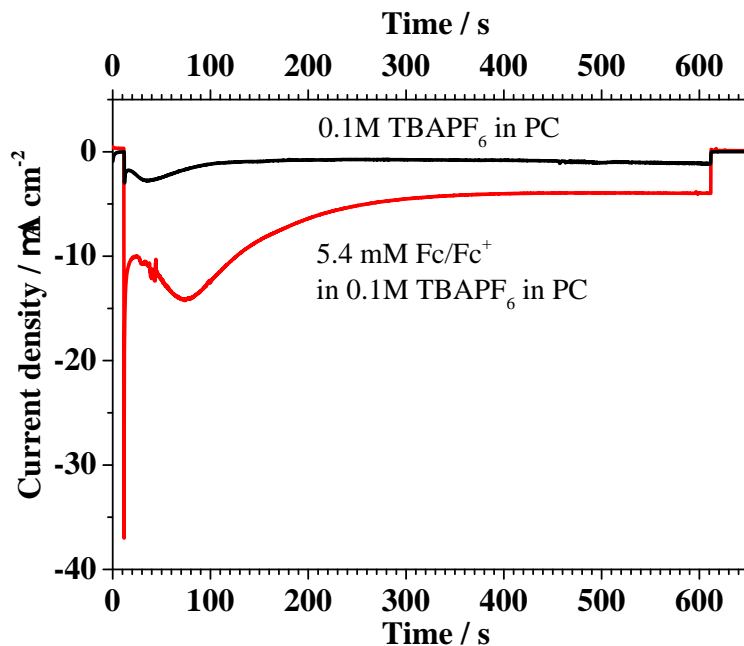


Figure 6.4: The current transients measured within 600 s during illumination of P3HT layer with the laser light in contact with pure electrolyte (black line) and electrolyte with dissolved 5.4 mM Fc/Fc^+ redox couple (red line)

The photocurrent densities measured in the photoelectrochemical cell are influenced by the cell geometry and the materials properties. Thus a longer radiation exposure will describe the cell/material stability. When comparing the behavior of the glass/ITO/P3HT working electrode contacted with either type of electrolyte solutions (without and with ferrocene), very similar shapes of the current density transients can be noticed. The first sharp negative peak of the current density present for both investigated electrolytes (Figure 6.4) can be attributed to charging of the P3HT/electrolyte interface. This occurs after photoexcitation of the P3HT layer and the same process was observed during the cyclic measurements presented in Figure 6.1. The different peak current density values can be correlated to the different nature of the electrochemical double layer when using different electrolytes. As soon as the interface charging process is completed, a second negative current peak is present for both types of electrolyte. The second peak measured using pure electrolyte becomes visible faster than the one measured using electrolyte containing the redox couple. Since the photocurrent depends on both, light absorption and electrical conductivity of the P3HT film, any change of the current value must be attributed to a modification of both parameters. Their change is caused by the photooxidation of the sample leading to a decrease in the optical absorption (see Figure 3.1) and a strong increase in the electrical conductivity. Even though the photodoping of the P3HT film triggers a decrease of the amount of photogenerated charges due to the absorption

decrease, the charge transport is at the same time much improved due to higher film conductivity. Both effects are competing and a dominance of the increased conductivity is responsible for the second photocurrent peak observed in Figure 6.4. Later on, equilibrium is attained which is described by the presence of the photocurrent plateaus.

In the case of the pure electrolyte, the position of the second peak is reached faster than in the case of the electrolyte containing redox couple. This is again due to a difference in the electrical conductivity, this time of the electrolyte. An increase in the conductivity of the electrolyte containing the redox couple is due to the easier charge transport through the system even for a decreased amount of carriers. The addition of new charge transporting material results also in a longer time necessary for attaining the equilibrium. The decay of the photocurrent toward the plateaus is due to the strong decrease of the amount of photogenerated charges, a point being reached where no photooxidation can occur anymore.

6.1.3 Photoelectrochemical impedance spectroscopy

Electrochemical impedance spectroscopy was used for characterization of the electrical properties of P3HT in both analyzed cases with pure and ferrocene containing electrolytes. All measurements were performed at the same applied potential of 0 V vs. Ag/AgCl, allowing the detection of changes in the electrochemical system due to the interaction with radiation. During the EIS investigations a single measurement spot was addressed by the PE-SDCM for each electrolyte in order to directly compare the effect of the doping/de-doping process on the impedance when the illumination conditions change. The resulting Bode plots of the full impedance spectra obtained from the P3HT are presented in Figure 6.5 for the case of using pure electrolyte (Figure 6.5(a)) and electrolyte containing the redox couple (Figure 6.5(b)).

Both electrolytes/cells were used in two different situations and results are shown in Figure 6.5. The impedance behavior was analyzed in the absence of light (plotted in black) and upon reaching the equilibrium photocurrent after 600 s of illumination (plotted in blue). The frequency dependent impedance is presented in the upper part of Figure 6.5, while the corresponding phase shift is plotted in the lower part. A substantial difference between the spectra measured in the dark and under illumination conditions can be observed for both electrolytes. At high frequencies the impedances have almost the same value (around $10\text{ k}\Omega$), while the low frequency impedances decrease upon irradiation with almost one order of magnitude, affecting in turn the slope of the curves. The reason for this behavior is connected to the increase of the charge density due to the charge photogeneration under illumination conditions. The frequency dependent phase

analysis shows a phase shift exceeding -80° (-85° when ferrocene is used) when the measurements are done in the absence of radiation. A phase shift to -60° is observed after the equilibrium is reached at 600 s of light exposure.

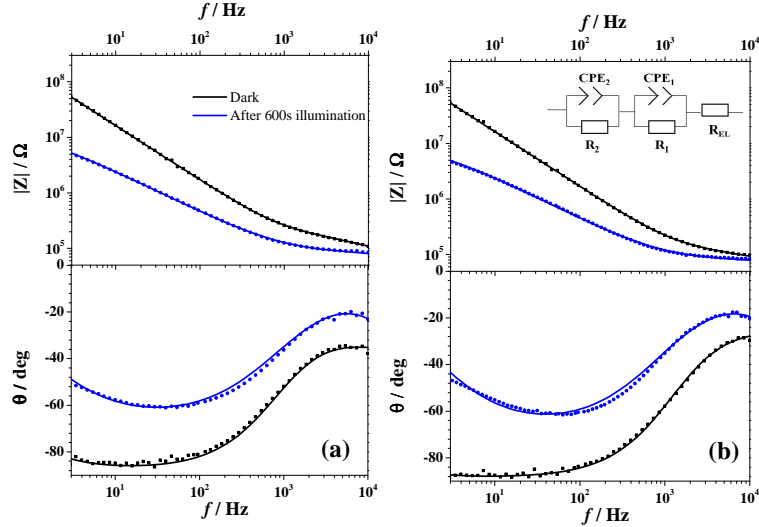


Figure 6.5: The results of the electrochemical impedance spectroscopy study measured for P3HT in contact with pure electrolyte (a) and electrolyte with dissolved 5.4 mM Fc/Fc^+ redox couple (b) in the dark (black spots) and after 600 s (blue spots). The fitting of the measured data are presented as solid lines.

In order to quantify the electrical circuit elements responsible for the impedance behavior, all measured impedance spectra were fitted using an equivalent model presented in the inset of the Figure 6.5 (a). The presence of the redox couple in the electrolyte did not affect significantly the impedance spectra, small differences between the results shown in Figure 6.5 (a) and Figure 6.5 (b) being observed only upon fitting. In the model, R_{EL} characterizes the electrolyte. The interface between the P3HT and electrolyte is described by the resistance (R_1) connected in parallel with a constant phase element (CPE_1) describing the interface capacitance relevant during the charging process. In this way, the diffuse double layer which forms at the contact between the polymer surface and the electrolyte due to dipoles alignment of the adsorbed electrolyte molecules is described. Additionally, the changes of the double layer which occur upon charge generation after laser illumination are also considered by the model. The P3HT film is described by a resistance (R_2) connected in parallel to a second constant phase element (CPE_2). This part of the equivalent circuit describes all changes in the P3HT layer as a function of illumination.

Sample		R_1 / Ω	C_1 / F	R_2 / Ω	C_2 / F
0.1M TBAPF ₆	Dark	148310	$4.38 \cdot 10^{-9}$	$8.27 \cdot 10^8$	$1.10 \cdot 10^{-9}$
	After 600s illumination	62511	$9.50 \cdot 10^{-11}$	$1.49 \cdot 10^7$	$1.72 \cdot 10^{-8}$
0.1M TBAPF ₆ +5.4mM Fc/Fc ⁺	Dark	119070	$1.92 \cdot 10^{-8}$	$2.12 \cdot 10^9$	$1.04 \cdot 10^{-9}$
	After 600s illumination	61521	$7.6 \cdot 10^{-11}$	$1.04 \cdot 10^7$	$1.55 \cdot 10^{-8}$

Figure 6.6: The calculated values for the circuit elements used for fitting the EIS spectra. The data were obtained using the Gaussian distribution of activation energy (GDAE) algorithm.

Using the equivalent circuit presented in the inset of Figure 6.5 (a), all the measured impedance spectra were fitted using specialized software (ZView - Scribner Associates Inc.). The values obtained from the fitting procedure are listed in Figure 6.6. The value of the electrolyte resistance (R_{EL}) was found to be approximately 25 k Ω in the case of pure electrolyte and in the second case it decreased to 17 k Ω due to the presence of dissolved ferrocene. The resistance of P3HT/pure electrolyte interface in the dark was calculated and a value of 148 k Ω was found. After 600 s of illumination the value of the interface resistance (R_1) decreased to 62.5 k Ω indicating the doping process which results in an increased electrical conductivity. The interface changes are also reflected in the behavior of the area normalized capacitance. As compared to the measurements in the dark, the interface capacitance (C_{1A}) decreased by two orders of magnitude reaching $10^{-8} F cm^{-2}$ after 600 s of illumination. This decrease can be related to a change in the effective dielectric constant (previously observed in Figure 3.1) triggered by the photodoping process reaching stationary conditions as indicated by the presence of the photocurrent plateaus (Figure 6.1). In the case of P3HT layer, after illumination the resistance of the film drops by almost two orders of magnitude while the film capacitance increases with more than one order of magnitude. This behavior is due to an increased charge density in the bulk of the P3HT caused by photoexcitation.

When using the electrolyte containing the redox couple, the values of the circuit elements obtained from the EIS measurements upon fitting closely follow the same trend as described for pure electrolyte. Overall, small differences between the obtained values can be observed. The stronger difference was found in the case of measurements in the dark, where the presence of ferrocene decreased the interface resistance while slightly increasing its capacitance. This change can be explained by a different dipole formation mechanism at the P3HT/electrolyte:ferrocene interface in the presence of Fc^+ ions. A study of

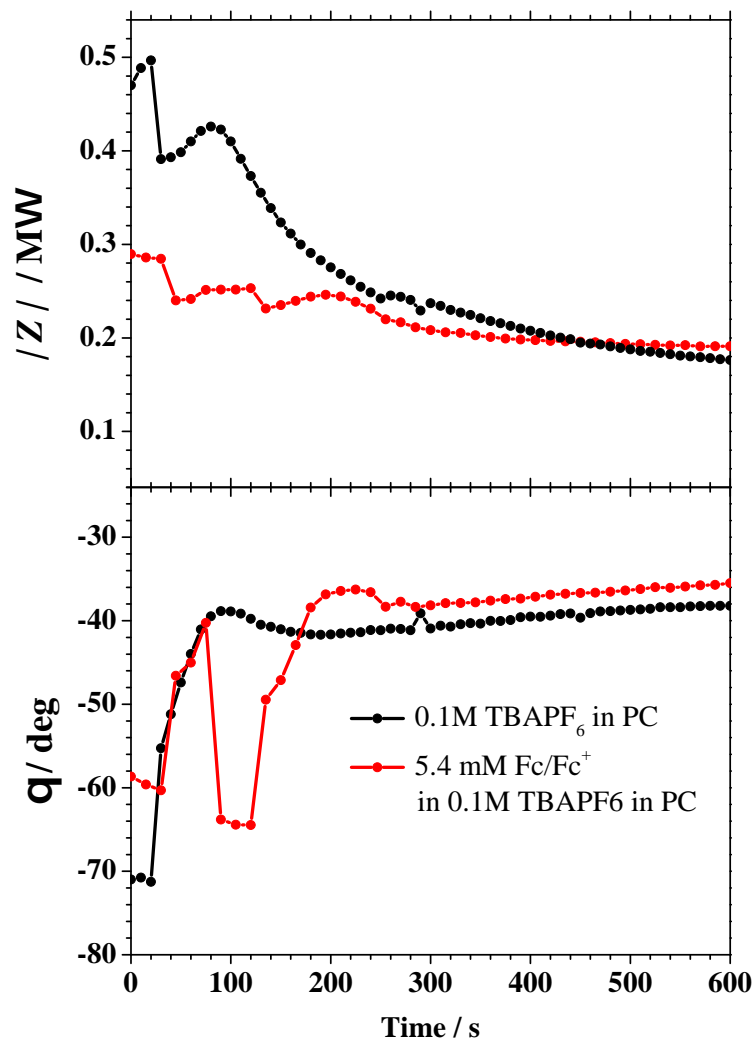


Figure 6.7: The time evolution of the impedance modulus (a) and phase shift (b) measured at a fixed frequency of 1 kHz.

the dynamic changes taking place in the P3HT/electrolyte system during the radiation exposure was performed using single frequency impedance transients (1 kHz). This was necessary since the time used for acquiring a full impedance spectrum is larger than the time needed for reaching equilibrium conditions under irradiation. In Figure 6.7 the results obtained are presented as a function of time. The part (a) of Figure 6.7 shows the modulus of the 1 kHz impedance while part (b) presents the corresponding phase shifts, measured in both analyzed cases of using electrolytes with or without ferrocene. After a short time in the dark (30 s), the shutter was opened allowing a constant radiation exposure of the P3HT up to 600 s while continuously measuring the impedance.

For both electrolytes the dark impedance show an almost constant level, a difference of approximately 200 k Ω observable in Figure 6.7 (a) being consistent with

the previously shown full impedance spectra from Figure 6.5. The beginning of the irradiation exposure coincides with an impedance drop for both electrolytes. During the previously observed (see Figure 6.4) time necessary for reaching the photocurrent plateau when using pure electrolyte (100 s) the impedance shows a small peak which later on decays toward a value of approximately 175 k Ω . This slow decay of the impedance suggests a time dependent photodegradation of the system containing pure electrolyte. The presence of the redox couple modifies the overall behavior of the impedance. During the longer system equilibration time (300 s) needed in this case (see Figure 6.4), variations of the impedance can be observed defining a transitional regime towards the stable photocurrent plateau. The time evolution of the impedance is more constant when the redox couple is present since it triggers a faster discharging of the film, promoting a better stability of the system.

The time evolution of the associated phase shifts is similar to the impedance behavior. After the illumination startup both phase shifts increase to values close to -40° . The equilibration times needed for each electrolyte are visible also in this case. Using the pure electrolyte, after 100 s the phase appears almost stable, slightly increasing in time. Strong phase variations were detected due to the presence of ferrocene. These can be attributed to the dynamic processes taking place during the equilibration time of 300 s. After this time, the phase fluctuations are diminished and further evolution follows the same pattern as the phase corresponding to the pure electrolyte. A constant difference in time between both phases is also observed and it can be correlated to the constant difference between the photocurrent plateaus previously discussed (Figure 6.4).

6.2 Photoelectrochemical characterization of PBDTTT-c and PBDTTT-c:PCBM

6.2.1 Current transients behavior as a function of the electrolyte composition

For investigating the photoconductivity of the PBDTTT-c, at first the effect of the electrolyte composition on the photocurrent was studied. Since for the P3HT a strong increase in the photocurrent after dissolving 5.4 mM of ferrocene in the 0.1 M TBAPF₆, a similar experiment was performed for PBDTTT-c. The results are presented in Figure 6.8. In Figure 6.8 the dark/illumination sequences as measured using a laser radiation matching the absorption of the polymer (635 nm - see Figure??) are plotted. As previously discussed, the presence of the redox couple Fc/Fc^+ in the electrolyte solution should modify its redox energetic level and therefore improve the charge photogeneration and transport.

As can be noticed, the composition of the electrolyte does not influence the photocurrent. This phenomenon can be explained by the electrochemical stability of the polymer.

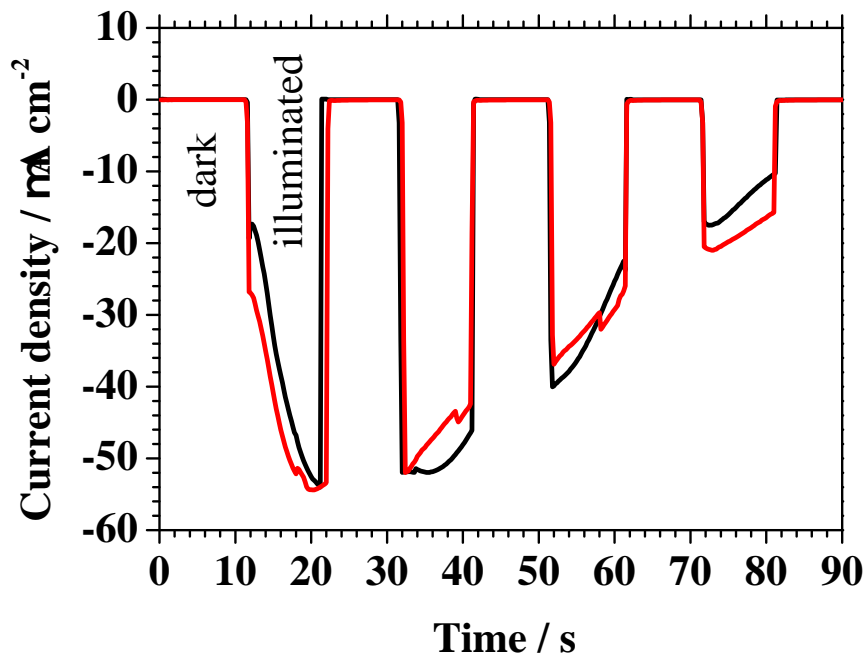


Figure 6.8: Photocurrent transients measured during illumination with the laser light (633 nm). The results of the measurement were done in the 3 electrode mode, on pristine PBDTTT-c. The photocurrent was measured in contact with pure electrolyte (black line) and electrolyte containing 5.4 mM ferrocene/ferrocenium redox couple (red line)

It was shown in the photoinduced absorption experiment (see Chapter 3.2.3) that PBDTTT-c is stable during the doping in the presence of air. This stability should prevent the doping in the presence of the ions dissolved in the electrolyte. Additionally, the charged polymer does not form the stable radical.

6.2.2 Dark/illumination current transients

For investigating the effect of the illumination on the PBDTTT-c and PBDTTT-c:PCBM films in contact with 0.1 M TBAPF₆ dissolved in PC, sequential dark/illumination photocurrent measurements were performed. To better understand the influence of the illumination on the photoelectrochemical process, the measurements were done using both, single wavelength (matching the polymer ab-

sorption maximum) and white light with full spectral range. The applied potential was set at 0 V vs. Ag/AgCl and the current transients were measured for alternating dark and illuminated conditions. Since at this potential no electrochemical process occurs (See Chapter 4) the measured change in the current can be related only to light induced processes. The resulting current transients are presented in Figure 6.9.

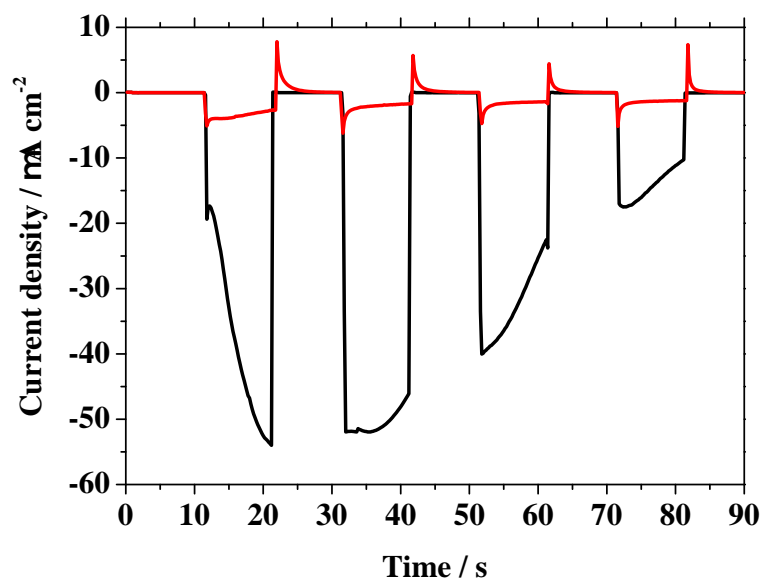


Figure 6.9: Photocurrent transients measured during illumination with the laser light. The results of the measurement were done in the 3 electrode mode, on pristine PBDTTT-c (black line) and PBDTTT-c:PCBM (red line)

In the case of PBDTTT-c (plotted in black), during the first 10 s in the dark only the electrochemical background current can be observed. After opening the shutter allowing the radiation to flow through the optical fiber embedded in the SCDM, a strong decrease in the current can be observed. This resulted in a sharp peak with the minimum at $-20 \mu A cm^{-2}$ recorded within the first second of illumination. This sharp peak is followed by a continuous decrease of the measured photocurrent down to $-55 \mu A cm^{-2}$. After 10 s of illumination the shutter was closed and the dark conditions were restored. As a result, the measured current immediately approaches the electrochemical background current level where it remains constant for the next 10 s. After opening the shutter a second time, the current level drops to the value where it was last observed during the first illumination period ($-55 \mu A cm^{-2}$). After 5 s of radiation exposure, an increase in the photocurrent can be observed. During the third and fourth sequence of illumination with laser light only a smooth increase of the current

can be observed. The photocurrent transient measured using the PE-SDCM for the PBDTTT-c:PCBM is presented in Figure 6.9 in red.

For the first 10 s of the experiment only a background current, similar to the one obtain for the pristine polymer, can be seen. After opening the shutter, an interesting situation can be observed when comparing the behavior of pure polymer under laser illumination with the BHJ. Due to mixing the PBDTTT-c with an accepting unit, an increase of the exciton separation probability (and therefore of the overall charge density) is expected, resulting in a high photocurrent. Surprisingly, the value of the current measured under illumination for the BHJ is much lower as compared to the one measured for the pristine polymer. Also, the shape of the current transient is different. Within the first second of illumination a peak with a minimum at approximately $-6 \mu A cm^{-2}$ can be noticed. Afterwards the current increases and stabilizes at a level of about $-4 \mu A cm^{-2}$. Interestingly, upon closing the shutter during the first dark sequence, a positive peak is observed which can be attributed to discharging of the WE/electrolyte interface. The existence of both peaks observed under illumination and in the following dark measurement can be explained by a photodegradation of the BHJ. This process can be associated with charging (under illumination) and discharging (in the dark) of the film. Since the measurement was performed on the film containing PCBM, by comparing to the measurement performed on the pristine material it can be concluded that the effect of charging/discharging directly describes the charge trapping in the acceptor. The shape of the discharging and the current flow direction measured in the dark suggests that the flow of the negative charges is directed toward the working electrode. The next illumination/dark sequences follow the same trend with a slight increase of the photocurrent plateau suggesting a continuation of the degradation process.

Opposite to the expected behavior of a bulk heterojunction solar cell [87] in the present photoelectrochemical investigation of the PBDTTT-c:PCBM the electrochemical instability of the acceptor strongly hinders the cell performance. The PCBM electrochemical stability plays a crucial role in the charge transport process. While in most of the solid state devices using BHJ containing PCBM the photocurrent is strongly enhanced due to the improved charge extraction [88, 89], in the photoelectrochemical process the acceptor traps most of the charges. Since in most of the BHJ systems after film formation a phase separation occurs, the interface between the electrolyte and the BHJ can be described as either PCBM/electrolyte or PBDTTT-c/electrolyte. In this situation, a large surface coverage of the PCBM islands [90] would lead to a strong decrease of the photocurrent. Due to this fact, the use of PCBM in contact with 0.1 M TBAPF₆ in a photoelectrochemical cell is disadvantageous, as opposed to the experience according to the common knowledge in the field of organic solar cell [88, 89].

Due to the fact that the polymer was primarily developed to serve as donor material in organic solar cells, the photoelectrochemical properties of PBDTTT-c were also assessed under full-spectral light illumination. In a manner similar to the laser irradiation experiment, the effect of full-spectral illumination is reported as a sequence of dark/illumination periods and the resulting photocurrent transients are presented in Figure 6.10.

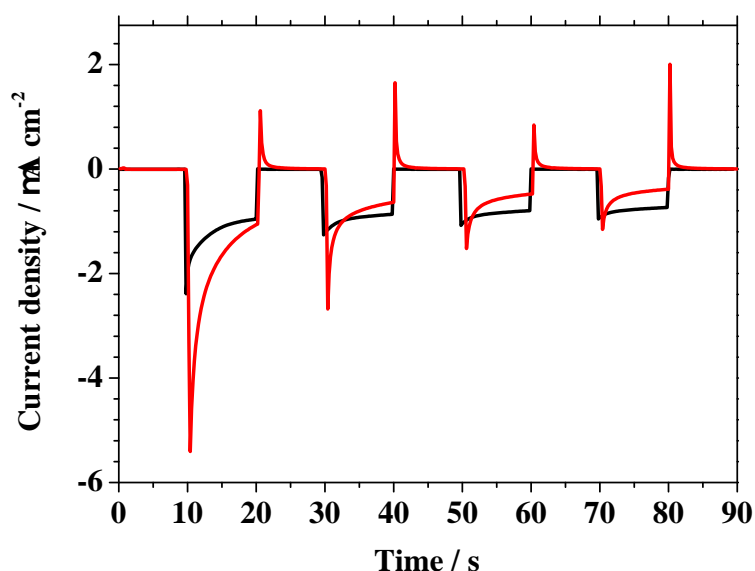


Figure 6.10: Photocurrent transients measured during white light illumination. The results of the measurement were done in the 3 electrode mode, on pristine PBDTTT-c (black line) and PBDTTT-c:PCBM (red line)

Illumination with full-spectral light results in a decrease of the overall photocurrent measured for the pristine PBDTTT-c (plotted in black) as compared with the single wavelength case (Figure 6.10). The measured photocurrent is almost 30 times lowered as compared to the one measured during laser illumination. One reason for this change is the radiation source power density which in the case of the full-spectral light is lowered by a factor of 2. However, is not likely that this alone would cause such a strong photocurrent decrease. The shape of the current transients also change as compared to the case of laser illumination. This time an increase of the photocurrent during the first illumination is observed until a plateau is reached. The plateau level is reproduced in next illumination sequence. During laser illumination only the main transition of the polymer is activated (first oxidation step). In this situation, the high instability of the photodoped form of the polymer promotes charge trapping rather than charge transfer leading to the suppression of the photodegradation pro-

cess. However, during illumination of the polymer with full-spectral light not only the main transition is triggered but also higher transitions (higher oxidations) can occur. Most likely the stability of these transitions is higher leading to formation of a blocking layer which prevents photogenerated current flow as suggested by the shape of the current transients from Figure 6.10. Since the charge separation of the exciton can occur only at the polymer/electrolyte interface, the photodegradation dominates the current flow process when the pristine PBDTTT-c in contact with 0.1 M TBAPF₆ dissolved in PC is used.

For analysis of the BHJ where PBDTTT-c is mixed with PCBM, the photocurrent transients measured during full-spectral illumination are plotted in red in Figure 6.10. They show a similar behavior as compared with the case of single wavelength irradiation. Both, the value and the shape of the current transients for each sequence are weakly dependent on the used irradiation source. The only observed effect of using full-spectral light is evidenced by a slow increase of the photocurrent plateau levels during the light/dark sequences. Different from the case of pristine material, in the BHJ the exciton separation occurs in the bulk instead of electrolyte interface. This is the reason for the observed weak photocurrent dependence on the light source.

Photocurrent measurements using two electrode configuration of the PE-SDCM were performed in order to characterize the photoactive material under typical operation conditions of optoelectronic devices. In these devices the current is measured while a constant potential difference of 0 V is applied between the WE and CE [91]. In the three electrode configuration, the potential applied during the photoelectrochemical experiment was set at 0 V in respect to the Ag/AgCl ($\mu - QRE$). However, the effective potential which is applied between WE and CE in the phototelectrochemical cell is influenced by the work function of the CE and is also affected by the potential drop in the electrolyte. In order to overcome this problem, measurements using two electrode configuration are preferred. Even though the information about the electrochemical processes is not correct in this configuration, the WE-CE polarization can be precisely set at 0 V as in the case of an operating photovoltaic device.

The photocurrents using PBDTTT-c and PBDTTT-c:PCBM systems were measured during illumination with single wavelength as well as under full-spectral irradiation. The photocurrent transients measured using the laser light were studied and the results are shown in Figure 6.11.

As compared to the photocurrents measured using the three electrode configuration, the pristine polymer (plotted in black) shows similar shapes of the photocurrent transients. For the first 10 s of the experiment only background current was detected. During the first second of illumination a strong peak with a minimum at $-10 \mu Acm^{-2}$ can be observed. Its nature can be related to the PBDTTT-c/electrolyte interface charging. Afterwards, an increase in the

photocurrent can be observed followed by a decrease in the current down to $-9 \mu\text{Acm}^{-2}$. For the next illumination periods, the behavior of the photocurrent is similar to the one described in the Figure 6.9 where a three electrode configuration was used. Although the values of the photocurrents measured in the two electrode configuration are six times smaller, the photocurrent transient shapes are identical to those measured in the three electrode configuration. This demonstrates that the absence of the ($\mu - QRE$) in the setup influences only the photocurrent flowing through the electrochemical cell, due to the different potential, but does not influence the electrochemical processes occurring under illumination. In this case the significance of the applied potential can be evidenced.

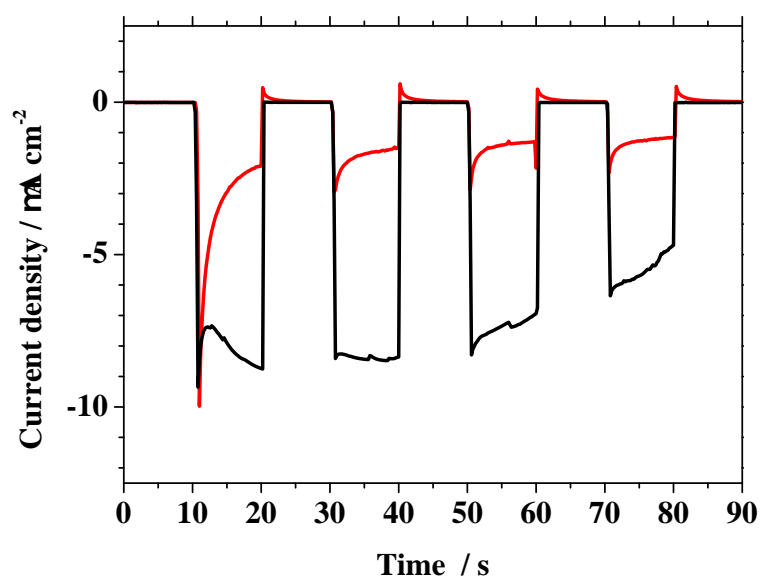


Figure 6.11: Photocurrent transients measured during illumination with the laser light. The results of the measurement were done in the 2 electrode mode, on pristine PBDTTT-c (black line) and PBDTTT-c:PCBM (red line)

The behavior of the PBDTTT-c:PCBM bulk heterojunction was studied using two electrode configuration in the dark and under laser illumination. The resulting photocurrent transients are plotted in red in Figure 6.11. It can be noticed that the shape and the value of photocurrent transients are similar to the ones measured in the three electrode configuration. After starting the illumination, a strong negative peak with a minimum at $-10 \mu\text{Acm}^{-2}$ followed by an increase up to $-2.5 \mu\text{Acm}^{-2}$ can be observed. As mentioned before, this behavior can be explained by the electrochemical instability of PCBM. Interestingly, in the following dark sequence, only a small peak due to the discharging

of the BHJ/electrolyte interface can be observed in comparison with the three electrode configuration. Within the next illumination sequences the degradation can be again observed resulting in the smaller detected photocurrent. This can be explained considering the energetic levels alignment. In the cell having three electrodes, the effective WE-CE potential present during the photoelectrochemical characterization can be drastically different from the one measured between the WE and CE when the potentiostat is using $\mu - QRE$.

The photocurrent observed with the two electrode configuration using laser illumination was compared with the one measured under full-spectral irradiation. The measured photocurrent transients of the pristine PBDTTT-c (plotted in black) and PBDTTT-c:PCBM mixture (plotted in red) is presented in Figure 6.12.

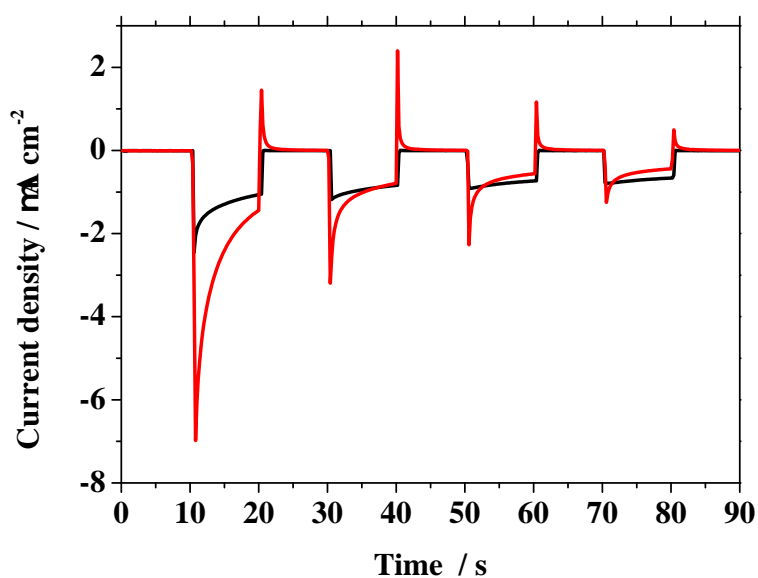


Figure 6.12: Photocurrent transients measured during illumination with white light. The results of the measurement were done in the 2 electrode mode, on pristine PBDTTT-c (black line) and PBDTTT-c:PCBM (red line)

In both cases, the full-spectral light irradiation of the pristine polymer and its mixture with the acceptor only slightly influences the photoelectrochemical response. Although the shape of the photocurrent transients is identical to the one obtained in the three electrode configuration, a small difference can be observed in the value of the measured photocurrent. The pristine polymer photocurrent reach values close to $-2 \mu Acm^{-2}$ (later increasing) while for the PBDTTT-c:PCBM mixture the measured photocurrent was as low as μAcm^{-2} . The reason of this behavior can again be related to the energetic levels align-

ment.

6.2.3 Photocurrent stability

The stability of the photovoltaic effect for both PBDTTT-c and PBDTTT-c:PCBM was studied during longer photoelectrochemical measurements using the PE-SDCM. In this experiment, both materials contacted with 0.1 M TBAPF₆ dissolved in PC were illuminated either with a single wavelength laser or with full-spectral light. During irradiation, 600 s photocurrent transients were measured. For a correct electrochemical characterization, the measurements were performed using the three electrode configuration of PE-SDCM.

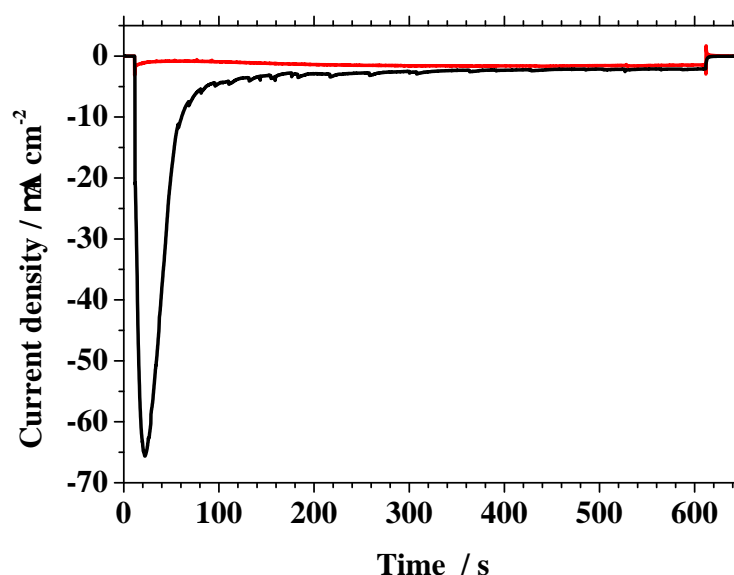


Figure 6.13: The current transients measured within 600 s during illumination with the laser light. The results of the measurement were done in the 3 electrode mode, on pristine PBDTTT-c (black line) and PBDTTT-c:PCBM (red line).

In Figure 6.13 the effect of 600 s irradiation with laser light is presented. During the first 10 s of the experiment the PBDTTT-c (plotted in black) was kept in the dark and only the background current was measured. After opening the shutter for radiation exposure a peak in the photocurrent can be observed within the next 100 s. The value and the shape of the photocurrent transient follows the behavior of the photocurrent transients presented in Figure 6.9. The photocurrent peak value reaches $-65 \mu A cm^{-2}$ after approximately 25 s. This matches the previous results of the experiment where dark/illumination sequences were

used if one visualizes the envelope of the curves presented in Figure 6.9. After another 100 s a photocurrent increase is observed due to the degradation process and finally a photocurrent plateau at $-6 \mu A cm^{-2}$ is reached. A similar characterization was performed for the BHJ. The resulting photocurrent transient measured during 600 s of irradiation with single wavelength is plotted in red in Figure 6.13. The value and the shape of the photocurrent measured for BHJ in contact with electrolyte also visualizes the envelope of the corresponding curves presented in Figure 6.9. A photocurrent decrease in the first second is observed which is followed by a continuous increase up to a plateau positioned at $-1.4 \mu A cm^{-2}$. This behavior of the photocurrent can also be attributed to the photodegradation of the PCBM.

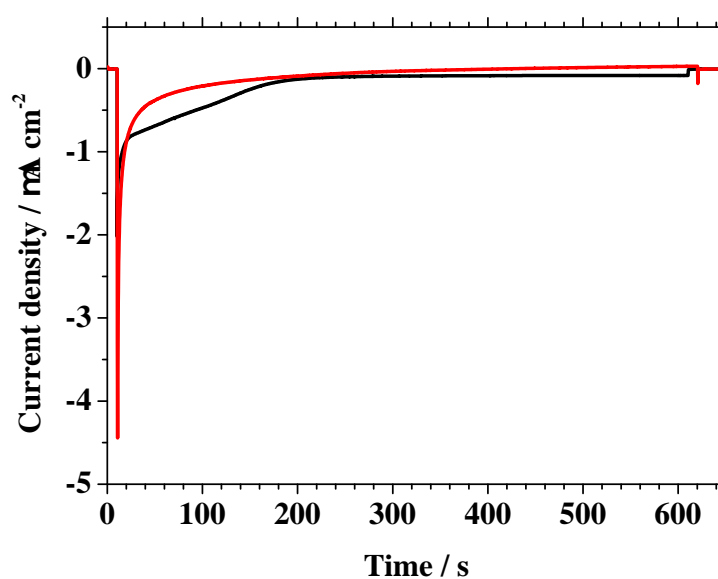


Figure 6.14: The current transients measured within 600 s during illumination with the white light. The results of the measurement were done in the 3 electrode mode, on pristine PBDTTT-c (black line) and PBDTTT-c:PCBM (red line).

The photocurrent stability measurements under laser irradiation performed for PBDTTT-c and PBDTTT-c:PCBM using the three electrode configuration for the PE-SDCM are compared with the corresponding curves detected when full-spectral light was used. The resulting photocurrent transients are plotted in Figure 6.14. The photo-response of the pristine PBDTTT-c is plotted in black. Similar to the previous case of laser illumination, the photocurrent transients under full-spectral irradiation follow the envelope of the corresponding photocurrent transients presented in black in Figure 6.10. The photocurrent value obtained has a minimum of $-3 \mu A cm^{-2}$ and increases reaching a plateau at -

$0.5 \mu A cm^{-2}$ after 300 s. An identical situation can be observed for the case of PBDTTT-c:PCBM. The irradiation with full spectral light results in a peak with a value of $-4.5 \mu A cm^{-2}$ which increases within the first 100 s of the experiment. The final photocurrent measured after 600 s of irradiation is very low and can be considered as background.

6.2.4 Photopotential characterization

Beside the information about the current generated under illumination, the usual photovoltaic characterization also describes the position of the energetic levels alignment. In the solar cells, the open circuit potential is especially important since it describes the maximum potential generated when no current is flowing. The value of the open circuit potential is affected by all materials building the cell. The influence of the irradiation as well as measurement configuration on the open circuit potential of PBDTTT-c and PBDTTT-c:PCBM is studied. The resulting potential transients are presented in Figure 6.15.

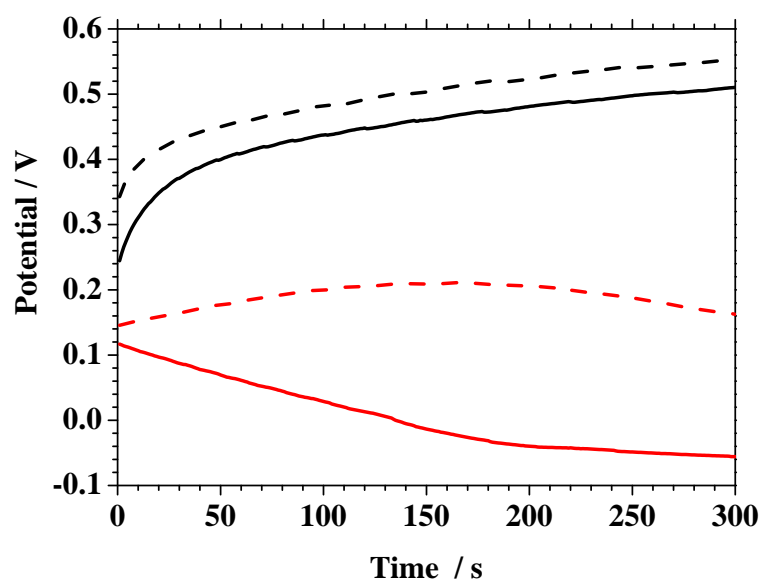


Figure 6.15: The potential transients measured within 300 s during illumination with the laser light. The results of the measurement were done in the 3 electrode mode (solid line) and 2 electrode mode (dashed line) for pristine PBDTTT-c (black line) and PBDTTT-c:PCBM (red line)

The photovoltages measured in the three electrode configuration of the PE-SDCM for the pristine PBDTTT-c is plotted in black while those obtained for

the BHJ are shown in red. The corresponding transients measured in the two electrode configuration are plotted using dashed lines.

The photovoltage measured during irradiation with laser light is presented in Figure 6.15. For pristine PBDTTT-c (plotted in solid, black) at first a potential of 0.24 V vs. Ag/AgCl was measured. A continuous increase in the potential can be observed as a function of time. This increase can be explained by the continuous charging of the PBDTTT-c layer. After 300 s of laser illumination, the photovoltage reaches 0.51 V vs. Ag/AgCl. A similar experiment was performed in the two electrode configuration (plotted dashed, black). The shape of the photovoltage transient in this case is identical to that obtained during the measurement in the three-electrode configuration. However, the values are higher for each measured point by approximately 50 mV. In this way, the effective potential between the WE and CE is directly probed and its increase can be related to the potential drop in the electrolyte and the work function of the CE.

Using laser light irradiation the photovoltage transients were also measured for PBDTTT-c:PCBM and the results are plotted in red in Figure 6.15. The measurements were again performed in two (dashed line) or three (solid line) electrode configuration. As can be noticed for the PBDTTT-c:PCBM, a strong difference in the photovoltage transients can be observed depending on the configuration used. In the three electrode configuration (where the photovoltage is referred to the $(\mu - QRE)$) a photovoltage decrease with time can be observed. After starting the radiation exposure, the measured photovoltage was 0.12 V vs. Ag/AgCl and 300 s later decreased to -0.04 V vs. Ag/AgCl. This change in the value of the photovoltage can be related to the charging of the PCBM. The photovoltage of PBDTTT-c:PCBM measured in the two electrode configuration shows opposite behavior. After opening the shutter, the value of the photovoltage was found to be 0.15 V, similar to the one obtained in the three electrode configuration. During the 300 s illumination sequence this value slightly increases. As previously discussed, the measured photovoltage is strongly dependent from the effective potential between the WE and CE.

Finally the effect of illumination on the photovoltage transients in PBDTTT-c (plotted in black) and PBDTTT-c:PCBM (plotted in red) were characterized under full spectral irradiation in the two (dashed line) or three electrode (full line) configuration. The resulting photovoltage transients are presented in Figure 6.16.

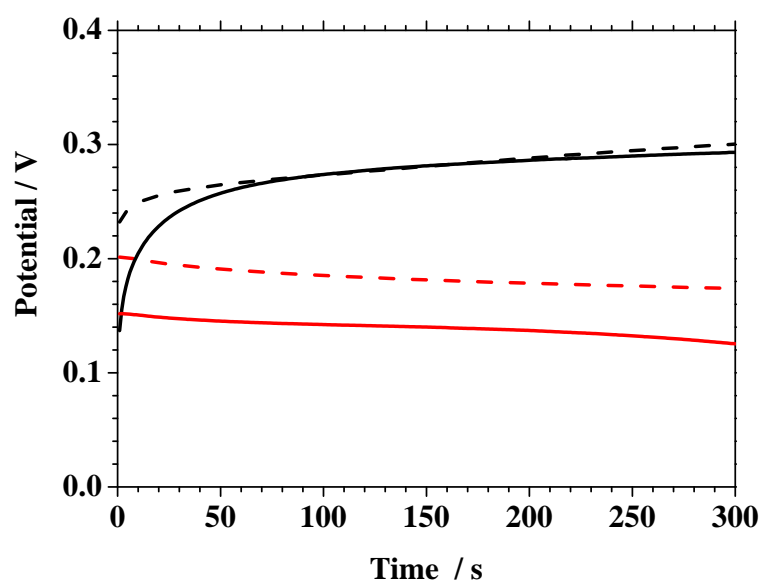


Figure 6.16: The potential transients measured within 300 s during illumination with the white light. The results of the measurement were done in the 3 electrode mode (solid line) and 2 electrode mode (dashed line) for pristine PBDTTT-c (black line) and PBDTTT-c:PCBM (red line)

The photovoltage measured for the pristine PBDTTT-c in the three electrode configuration shows similar behavior to those obtained during laser illumination. After opening the shutter, the value of the photovoltage was measured as 0.14 V vs. Ag/AgCl and increased during the measurement period up to almost 0.3 V vs. Ag/AgCl. As previously described, this increase can be explained by photocharging of the PBDTTT-c layer. Similarly to the previously described photocurrent behavior, the value of the photovoltage is much smaller during illumination with full spectral light than those obtained during laser illumination. Since in the electrochemical cell the photovoltage describes the difference between the oxidation potential of the material and the redox potential of the electrolyte, the change in the potential can be related to a decrease of the band position in the gap. This effect can be seen, since during illumination of the PBDTTT-c with a white light all absorption energies are probed, while during illumination with the laser only the lowest one is excited. When comparing, the results of the photovoltage measured in the two electrode configuration (dashed line) to three electrode configuration (solid line), it can be noticed that, although the shape of the curve is similar, within the first 80 s a difference in the values can be seen. The photovoltage measured in the two-electrode configuration just after starting the illumination, is higher by 80 mV and this difference decreases in time. Using white light irradiation the photovoltage transients were addition-

ally measured for PBDTTT-*c*:PCBM and the results are plotted in red in Figure 6.16. In the three electrode setup (solid lines) a potential of 0.15 V vs. Ag/AgCl was measured. Within 300 s a slight decrease in the potential can be observed as a function of time. A similar experiment was performed in the two electrode configuration (plotted dashed, red). The shape of the photovoltage transient is identical to that obtained during measurement in the three-electrode configuration with the values higher by 50 mV at each measurement point.

7 Summary

The optical properties (dielectric function) of the undoped/doped P3HT as well as PBDTTT-c were determined using ellipsometric spectroscopy, a powerful method for unambiguous data determination. The optical properties - real and imaginary part of the dielectric function related to the electronic transitions have been determined by spectroscopic ellipsometry in the range of 1 - 6.5 eV. As a major result of the polymer doping study, the quantification of the optical properties of new electronic transitions at lower energy due to the in-the-gap transitions was possible with SE. It was found that the absorption peaks in the dielectric function are strongly dependent on doping. Additionally, the low band gap, block co-polymer PBDTTT-c was characterized using infrared spectroscopy and the specific infrared response was compared to the one obtained for P3HT. The materials were studied under chemical doping (in iodine vapor) and photo-induced conditions and the characteristic changes - polaronic absorption and associated new vibrations were detected for both polymers. The resulting curves were compared to those obtained in the SE showing a fulfillment of the sum rule. For PBDTTT-c the photoinduced absorption experiment shows no changes in the IR region but after mixing with an acceptor (PCBM) strong changes in FTIR spectra were recorded. The IRAV bands from photoinduced absorption experiment were compared with those obtained during chemical doping, showing a full agreement in the IRAV region and polaronic absorption maximum. Opposite to the PBDTTT-c, pristine P3HT shows a photo-induced absorption which was later enhanced by adding PCBM. Interestingly the photodoping of P3HT yields completely different polaronic absorption lines compared to the chemical doping of this polymer and photo-doping of P3HT:PCBM. The polaronic absorptions as well as IRAV bands are clearly observed. The DC conductivity values agree very well with IRAV response in both chemically and photodoped samples.

The electrochemical redox cycles on thin films of P3HT and PBDTTT-c were locally investigated using a modified version of a scanning droplet cell microscope adapted to organic electrolytes. The possibility of addressing small areas on the surface of the working electrode combined with the advantage of using low electrolyte volumes (<1 ml) have been exploited in this study. For P3HT, the existence of two oxidation peaks during the cyclic voltammetry was found and confirmed by further experiments. The electrical behavior of the polymer was characterized in-situ by electrochemical impedance spectroscopy. A two

7 Summary

time constants model was used for fitting the impedance data. An improvement in the electrical conductivity by at least three orders of magnitude was experimentally found. Additionally, Mott-Schottky analysis was employed for determination of the doping level of P3HT. For PBDTTT-c no distinct oxidation peak was observed, but rather a continuous current increase until the maximum applied potential is reached. This result was confirmed by potentiostatic measurements. From the current transients and the calculated charge consumed in the electrochemical process as function of applied potential, the existence of an oxidation peak with a maximum at 1.30 V vs. SHE was confirmed. The electrical characterization of the polymer was performed by electrochemical impedance spectroscopic measurements. The results were fitted using a two time constant equivalent model describing the behaviour of the polymer layer during electrochemical processes. As expected during the doping process, an increase in the electrical conductivity was determined showing the insulator/semiconductor/metal transitions. For characterization of the doping level in the semiconducting state, a Mott-Schottky analysis was applied and a hole conduction mechanism was evidenced.

The photoelectrochemical properties of the P3HT were studied using PE-SDCM. The behavior of the photocurrent generated under illumination light having a wavelength of 532 nm, was characterized when P3HT was in contact with pure electrolyte as well as in contact with electrolyte containing 5.4 mM ferrocene/ferrocenium redox couple. The photoelectrochemical characterization revealed a strong non-reversible photodegradation of the P3HT when the measurement was done in the pure electrolyte, due to stability of the created radicals. Addition of the ferrocene/ferrocenium redox couple results in better charge transfer within the electrochemical cell. The stability of the photocurrents evidenced during the dark/illumination sequences, was furthermore studied using longer terms illumination. Finally, photoelectrochemical impedance spectroscopy was performed showing the changes in the resistance after illumination due to the photogenerated charge carriers. Similar studies were performed for PBDTTT-c. In this case the effect of the radiation used for photogeneration was studied. The PBDTTT-c as well as PBDTTT-c:PCBM was illuminated with single wavelength light (635 nm) matching to the maximum absorption of the polymer and compared with results obtained during illumination with full spectrum light. The behavior of the photocurrent was characterized using dark/illumination sequences and compared with the longer term illumination. It was found that an addition of the PCBM strongly decreases the photocurrent due to the photoelectrochemical degradation of the acceptor.

8 Outlook

Based on the results of this work, some further experiments could be proposed:

1. Ellipsometric spectroelectrochemistry

Spectroscopic ellipsometry was found to be a powerful technique for characterization of optical properties of pristine/doped organic materials. The work was performed during chemical doping. As a continuation, application of ellipsometric spectroscopy in electrochemistry could be proposed. In this study the information about the changes in the dielectric function, as a function of doping level, should be obtained.

2. Theory of the spectroscopic response of doped polymer

Application of the spectroscopic ellipsometry, presented in this work, for the first time gave a broad view in the optical properties of organic materials in wide spectral range. The information about the changes in the complex dielectric function/complex refractive index should be used to confirm/modify the assumptions of the existing theories describing the physical effects from the spectroscopic response. In this terms, especially the existing theories describing IRAV bands and polaronic absorption should be revised.

3. Scanning Droplet Cell Microscopy

In this work scanning droplet cell microscopy was presented as a very useful method for electrochemical and photoelectrochemical characterization of small amounts of organic materials. From the construction point of view, this method can be easily connected with any existing method used in the field of electrochemistry. As a future work, the application of PE-SDCM in spectroelectrochemistry and CO_2 reduction can be proposed.

4. Photoelectrochemistry on organic semiconductors

Recent interest in the use of organic semiconductors in the photoelectrochemical reduction of CO_2 or H_2O need a detailed study on the organic semiconductors behavior during photoelectrochemical processes. In this matter, the possibility of using PE-SDCM in multiple electrochemical characterizations on a single substrate gives an opportunity for detailed and comparative discussions about the photoelectrochemical properties of organic semiconductors.

Bibliography

- [1] H. Hoppe, N. S. Sariciftci, Organic solar cells: An overview, *J. Mater. Res.* **19** (2004) 1924–1945.
- [2] S. H. Park, A. Roy, S. Beaupré, S. Cho, N. Coates, J. S. Moon, D. Moses, M. Leclerc, K. Lee, A. J. Heeger, Bulk heterojunction solar cells with internal quantum efficiency approaching 100%, *Nat. Photon.* **3** (2009) 297–302.
- [3] M. Irimia-Vladu, E. D. Głowacki, P. A. Troshin, G. Schwabegger, L. Leonat, D. K. Susarova, O. Krystal, M. Ullah, Y. Kanbur, M. A. Bodea, V. F. Razumov, H. Sitter, S. Bauer, N. S. Sariciftci, Indigo - a natural pigment for high performance ambipolar organic field effect transistors and circuits, *Adv. Mater.* **24** (2012) 375–380.
- [4] E. Wang, L. Hou, Z. Wang, S. Hellström, F. Zhang, O. Inganäs, M. R. Andersson, An easily synthesized blue polymer for high-performance polymer solar cells, *Adv. Mater.* **22** (2010) 5240–5244.
- [5] M. Kaltenbrunner, M. S. White, E. D. Głowacki, T. Sekitani, T. Someya, N. S. Sariciftci, S. Bauer, Ultrathin and lightweight organic solar cells with high flexibility, *Nat. Comm.* **3** (2012) 770.
- [6] M. S. White, M. Kaltenbrunner, E. D. Głowacki, K. Gutnichenko, G. Kettlgruber, I. Graz, S. Aazou, C. Ulbricht, D. A. M. Egbe, M. C. Miron, Z. Major, M. C. Scharber, T. Sekitani, T. Someya, S. Bauer, N. S. Sariciftci, Ultrathin, highly flexible and stretchable p-LEDs, *Nat. Photon.* doi:10.1038/nphoton.2013.188.
- [7] Y.-J. Cheng, S.-H. Yang, C.-S. Hsu, Synthesis of conjugated polymers for organic solar cell applications, *Chem. Rev.* **109** (2009) 5868–5923.
- [8] M. Nicho, M. Medrano-Baca, U. León-Silva, J. Escalante, G. González-Rodríguez, M. Güizado-Rodríguez, I. Linzaga-Elizalde, Effect of adhesion promoter in corrosion protection of 1018 mild steel by using poly(3-hexylthiophene) coatings in 0.5 M H₂SO₄ solution, *Corrosion* **67** (2011) 105002–105002–12.
- [9] P. Vanlaeke, A. Swinnen, I. Haeldermans, G. Vanhoyland, T. Aernouts, D. Cheyens, C. Deibel, J. D’Haen, P. Heremans, J. Poortmans, J. Manca,

- P3ht/pcbm bulk heterojunction solar cells: Relation between morphology and electro-optical characteristics, *Sol. En. Mater. Sol. Cells* **90** (14) (2006) 2150–2158.
- [10] S. K. Hau, H.-L. Yip, H. Ma, A. K.-Y. Jen, High performance ambient processed inverted polymer solar cells through interfacial modification with a fullerene self-assembled monolayer, *Appl. Phys. Lett.* **93** (2008) 233304.
- [11] J.-Y. Chun, J.-W. Han, T.-W. Kim, D.-S. Seo, Enhancement of organic light-emitting diodes efficiency using carbon nanotube doped hole-injection layer on the al-doped zno anode, *ECS Sol. State Lett.* **1** (2012) R13–R15.
- [12] S. Cho, K. Lee, J. Yuen, G. Wang, D. Moses, A. J. Heeger, M. Surin, R. Lazzaroni, Thermal annealing-induced enhancement of the field-effect mobility of regioregular poly(3-hexylthiophene) films, *J. Appl. Phys.* **100** (2006) 114503.
- [13] R. F. Service, Outlook brightens for plastic solar cells, *Science* **332** (2011) 293.
- [14] D. Abou-Ras, D. Cahen, R. Noufi, T. Unold, M. A. Green, K. Emery, Y. Hishikawa, W. Warta, E. D. Dunlop, Solar cell efficiency tables (version 40), *Prog. Photovolt. Res. Appl.* **20** (2012) 606–614.
- [15] H.-Y. Chen, J. Hou, S. Zhang, Y. Liang, G. Yang, Y. Yang, L. Yu, Y. Wu, G. Li, Polymer solar cells with enhanced open-circuit voltage and efficiency, *Nat. Photon.* **3** (2009) 649–653.
- [16] J. Hou, H.-Y. Chen, S. Zhang, R. I. Chen, Y. Yang, Y. Wu, G. Li, Synthesis of a low band gap polymer and its application in highly efficient polymer solar cells, *J. Am. Chem. Soc.* **131** (2009) 15586–15587.
- [17] L. Huo, S. Zhang, X. Guo, F. Xu, Y. Li, J. Hou, Replacing alkoxy groups with alkylthienyl groups: A feasible approach to improve the properties of photovoltaic polymers, *Angew. Chem. Int. Ed.* **50** (2011) 9697–9702.
- [18] Y. He, C. Chen, E. Richard, L. Dou, Y. Wu, G. Li, Y. Yang, Novel fullerene acceptors: synthesis and application in low band gap polymer solar cells, *J. Mater. Chem.* **22** (2012) 13391.
- [19] Z.-G. Zhang, H. Li, Z. Qi, Z. Jin, G. Liu, J. Hou, Y. Li, J. Wang, Poly(ethylene glycol) modified [60]fullerene as electron buffer layer for high-performance polymer solar cells, *Appl. Phys. Lett.* **102** (2013) 143902.
- [20] T. E. Kang, H.-H. Cho, C.-H. Cho, K.-H. Kim, H. Kang, M. Lee, S. Lee, B. Kim, C. Im, B. J. Kim, Photoinduced charge transfer in donor–acceptor (da) copolymer: Fullerene bis-adduct polymer solar cells, *ACS Appl. Mater.*

- Interfaces* **5** (2013) 861–868.
- [21] H. Ohkita, S. Ito, Transient absorption spectroscopy of polymer-based thin-film solar cells, *Polym.* **52** (2011) 4397–4417.
- [22] T. Kyu An, C. Eon Park, D. Sung Chung, Polymer–nanocrystal hybrid photodetectors with planar heterojunctions designed strategically to yield a high photoconductive gain, *Appl. Phys. Lett.* **102** (2013) 193306.
- [23] A. J. Heeger, N. S. Sariciftci, E. B. Namdas, Semiconducting and metallic polymers, Oxford graduate texts, Oxford University Press, Oxford and New York, 2010.
- [24] M. Geoghegan, G. Hadziioannou, Polymer electronics, Vol. **22** of Oxford master series in physics, Oxford University Press, Oxford, 2013.
- [25] H. Shirakawa, E. J. Louis, A. G. MacDiarmid, C. K. Chiang, A. J. Heeger, Synthesis of electrically conducting organic polymers: halogen derivatives of polyacetylene, (ch)_x, *J. Chem. Soc. Chem. Comm.* (**16**) (1977) 578.
- [26] A. Hassel, M. Lohrengel, Preparation and properties of ultra thin anodic valve metal oxide films, *Mater. Sci. Forum* **185-188** (1995) 581–590.
- [27] A. I. Mardare, A. W. Hassel, Quantitative optical recognition of highly reproducible ultrathin oxide films in microelectrochemical anodization, *Rev. Sci. Instrum.* **80** (2009) 046106.
- [28] A. I. Mardare, A. P. Yadav, A. D. Wieck, M. Stratmann, A. W. Hassel, Combinatorial electrochemistry on al–fe alloys, *Sci. Tech. Adv. Mater.* **9** (2008) 035009.
- [29] A. I. Mardare, A. Ludwig, A. Savan, A. D. Wieck, A. W. Hassel, Combinatorial investigation of hf–ta thin films and their anodic oxides, *Electrochim. Acta* **55** (2010) 7884–7891.
- [30] M. T. Woldemedhin, D. Raabe, A. W. Hassel, Grain boundary electrochemistry of b-type nb-ti alloy using a scanning droplet cell, *Phys. Stat. Sol. (a)* **208** (2011) 1246–1251.
- [31] A. I. Mardare, A. D. Wieck, A. W. Hassel, Microelectrochemical lithography: A method for direct writing of surface oxides, *Electrochim. Acta* **52** (2007) 7865–7869.
- [32] A. I. Mardare, M. Kaltenbrunner, N. S. Sariciftci, S. Bauer, A. W. Hassel, Ultra-thin anodic alumina capacitor films for plastic electronics, *Phys. Stat. Sol. (a)* **209** (2012) 813–818.
- [33] R.-H. Xie, G. W. Bryant, G. Sun, M. C. Nicklaus, D. Heringer, T. Frauen-

- heim, M. R. Manaa, V. H. Smith, Y. Araki, O. Ito, Excitations, optical absorption spectra, and optical excitonic gaps of heterofullerenes - c_{60} , $c_{59}n^+$ and $c_{48}n_{12}$: Theory and experiment, *J. Chem. Phys.* **120** (2004) 5133.
- [34] I. van Severen, M. Breselge, S. Fourier, P. Adriaensens, J. Manca, L. Lutsen, T. J. Cleij, D. Vanderzande, 2,5-substituted ppv-derivatives with different polarities: The effect of side chain polarity on solubility, optical and electronic properties, *Macromol. Chem. Phys.* **208** (2007) 196–206.
- [35] A. Rivaton, S. Chambon, M. Manceau, J.-L. Gardette, M. Firon, N. Leaitre, S. Guillerez, S. Cros (Eds.), Photonics Europe: Impact of light on organic solar cells: evolution of the chemical structure, morphology, and photophysical properties of the active layer, *SPIE Proceedings*, SPIE, 2008.
- [36] T. Yohannes, H. Neugebauer, G. Farinola, C. Winder, F. Babudri, A. Cardone, F. Naso, N. Sariciftci, Vibrational spectroscopic study of a push-pull substituted fluorinated poly(p-phenylenevinylene) copolymer, *Synth. Met.* **152** (2005) 149–152.
- [37] H. Neugebauer, C. Kvarnstrom, C. Brabec, N. S. Sariciftci, R. Kiebooms, F. Wudl, S. Luzzati, Infrared spectroelectrochemical investigations on the doping of soluble poly(isothianaphthene methine) (pim), *J. Chem. Phys.* **110** (1999) 12108.
- [38] O. Khatib, J. D. Yuen, J. Wilson, R. Kumar, M. Di Ventra, A. J. Heeger, D. N. Basov, Infrared spectroscopy of narrow gap donor-acceptor polymer-based ambipolar transistors, *Phys. Rev. B* **86**.
- [39] T. F. Otero, M. Bengoechea, Uv–visible spectroelectrochemistry of conducting polymers. energy linked to conformational changes, *Langmuir* **15** (1999) 1323–1327.
- [40] T. Yohannes, S. Lattante, H. Neugebauer, N. S. Sariciftci, M. Andersson, In situ ftir spectroelectrochemical characterization of n- and p-dopable phenyl-substituted polythiophenes, *Phys. Chem. Chem. Phys.* **11** (2009) 6283.
- [41] L. F. Chazaro-Ruiz, A. Kellenberger, L. Dunsch, In situ esr/uv–vis–nir and atr-ftir spectroelectrochemical studies on the p-doping of copolymers of 3-methylthiophene and 3-hexylthiophene, *J. Phys. Chem. B* **113** (2009) 2310–2316.
- [42] J. Brédas, J. Scott, K. Yakushi, G. Street, Polarons and bipolarons in polypyrrole: Evolution of the band structure and optical spectrum upon doing, *Phys. Rev. B* **30** (1984) 1023–1025.
- [43] A. O. Patil, A. J. Heeger, F. Wudl, Optical properties of conducting polymers, *Chem. Rev.* **88** (1988) 183–200.

- [44] A. Moliton, R. C. Hiorns, Review of electronic and optical properties of semiconductingp-conjugated polymers: applications in optoelectronics, *Polym. Int.* **53** (2004) 1397–1412.
- [45] H. Neugebauer, Infrared signatures of positive and negative charge carriers in conjugated polymers with low band gaps, *J. Electroanal. Chem.* **563** (2004) 153–159.
- [46] L. Dunsch, Recent advances in in situ multi-spectroelectrochemistry, *J. Sol. State Electrochem.* **15** (2011) 1631–1646.
- [47] Azzam, R. M. A, N. M. Bashara, Ellipsometry and polarized light, Elsevier Science B.V., The Netherland, 1987.
- [48] P. Y. Yu, M. Cardona, Fundamentals of Semiconductors, Springer Berlin Heidelberg, Berlin and Heidelberg, 2010. doi:10.1007/978-3-642-00710-1.
- [49] N. J. Harrick, Internal reflection spectroscopy, John Wiley & Sons, USA, 1967.
- [50] H. Neugebauer, In situ vibrational spectroscopy of conducting polymer electrodes, *Macromol. Symp.* **94** (1995) 61–73.
- [51] P. Meisterle, H. Kuzmany, Nauer G., In situ raman spectroscopy of the electrochemical doping process in polyacetylene, *Phys. Rev. B* **29** (1984) 6008.
- [52] S. Klod, F. Ziegls, L. Dunsch, In situ nmr spectroelectrochemistry of higher sensitivity by large scale electrodes, *Anal. Chem.* **81** (2009) 10262–10267.
- [53] A. Petr, L. Dunsch, A. Neudeck, In situ uv-vis esr spectroelectrochemistry, *J. Electroanal. Chem.* **412**.
- [54] A. L. Whitworth, D. Mandler, P. R. Unwin, Theory of scanning electrochemical microscopy (secm) as a probe of surface conductivity, *Phys. Chem. Chem. Phys.* **7** (2005) 384.
- [55] M. A. Edwards, S. Martin, A. L. Whitworth, J. V. Macpherson, P. R. Unwin, Scanning electrochemical microscopy: principles and applications to biophysical systems, *Physiol. Measur.* **27** (2006) R63–R108.
- [56] M. E. Snowden, A. G. Güell, S. C. S. Lai, K. MKelvey, N. Ebejer, M. A. O’Connell, A. W. Colburn, P. R. Unwin, Scanning electrochemical cell microscopy: Theory and experiment for quantitative high resolution spatially-resolved voltammetry and simultaneous ion-conductance measurements, *Anal. Chem.* **84** (2012) 2483–2491.
- [57] S. O. Klemm, J.-C. Schauer, B. Schuhmacher, A. W. Hassel, A micro-

- electrochemical scanning flow cell with downstream analytics, *Electrochim. Acta* **56** (2011) 4315–4321.
- [58] J. P. Kollender, A. I. Mardare, A. W. Hassel, Photoelectrochemical scanning droplet cell microscopy (pe-sdcm), *Chem. Phys. Chem.* **14** (2013) 560–567.
- [59] A. W. Hassel, M. M. Lohrengel, The scanning droplet cell and its application to structured nanometer oxide films on aluminium, *Electrochim. Acta* **42**.
- [60] A. W. Hassel, K. Fushimi, M. Seo, An agar-based silver/silver chloride reference electrode for use in micro-electrochemistry, *Electrochem. Comm.* **1**.
- [61] M. M. Lohrengel, A. Moehring, M. Pilaski, Electrochemical surface analysis with the scanning droplet cell, *Fresenius J. Anal. Chem.* **367** (2000) 334–339.
- [62] B. Horovitz, Infrared activity of peierls systems and application to polyacetylene, *Sol. State Commun.* **41** (1982) 729–734.
- [63] E. Ehrenfreund, Z. Vardeny, O. Brafman, B. Horovitz, Amplitude and phase modes in trans-polyacetylene: Resonant raman scattering and induced infrared activity, *Phys. Rev. B* **36** (1987) 1535–1553.
- [64] G. Zerbi, M. Gussoni, Castiglioni C., Conjugated polymers: novel science and technology of conductive and non linear optically active materials: Vibrational spectroscopy of policonjugated aromatic materials with electrical and non linear optical properties, Kluwer, New York, 1991.
- [65] M. Del Zoppo, C. Castiglioni, P. Zuliani, G. Zerbi, Handbook of Conducting Polymers, 2nd Edition, Skotheim, T. A. and Elsenbaumer, R. L. and Reynolds, J. R., New York, 1988.
- [66] E. A. Ehrenfreund, Z. Vardeny (Eds.), Optical Science, Engineering and Instrumentation '97: Phonon spectroscopy in p-conjugated polymers: the role of the excited electronic states, *SPIE Proceedings*, SPIE, 1997.
- [67] A. Girlando, A. Painelli, Z. G. Soos, Electron–phonon coupling in conjugated polymers: Reference force field and transferable coupling constants for polyacetylene, *J. Chem. Phys.* **98** (1993) 7459.
- [68] N. S. Sariciftci, M. Mehring, K. U. Gaudl, P. Bauerle, H. Neugebauer, A. Neckel, Third generation of conducting polymers: Spectroelectrochemical investigations on viologen functionalized poly (3-alkylthiophenes), *J. Chem. Phys.* **96** (1992) 7164.

- [69] J. Gasiorowski, E. D. Głowacki, B. Hajduk, M. Siwy, M. Chwastek-Ogierman, J. Weszka, H. Neugebauer, N. S. Sariciftci, Doping-induced immobile charge carriers in polyazomethine: A spectroscopic study, *J. Phys. Chem. C* **117** (2013) 2584–2589.
- [70] C.-Y. Nam, D. Su, C. T. Black, High-performance air-processed polymerâfullerene bulk heterojunction solar cells, *Adv. Funct. Mater.* **19** (2009) 3552–3559.
- [71] M. Jørgensen, K. Norrman, S. A. Gevorgyan, T. Tromholt, B. Andreasen, F. C. Krebs, Stability of polymer solar cells, *Adv. Mater.* **24** (2012) 580–612.
- [72] D. d. Leeuw, M. Simenon, A. Brown, R. Einerhand, Stability of n-type doped conducting polymers and consequences for polymeric microelectronic devices, *Synth. Met.* **87** (1997) 53–59.
- [73] K. Takimiya, T. Yamamoto, H. Ebata, T. Izawa, Design strategy for air-stable organic semiconductors applicable to high-performance field-effect transistors, *Sci. Techn. Adv. Mater.* **8** (2007) 273–276.
- [74] T. D. Anthopoulos, G. C. Anyfantis, G. C. Papavassiliou, D. M. d. Leeuw, Air-stable ambipolar organic transistors, *Appl. Phys. Lett.* **90** (2007) 122105.
- [75] J. H. Oh, Y.-S. Sun, R. Schmidt, M. F. Toney, D. Nordlund, M. Konemann, F. Wurthner, Z. Bao, Interplay between energetic and kinetic factors on the ambient stability of n-channel organic transistors based on perylene diimide derivatives, *Chem. Mater.* **21** (2009) 5508–5518.
- [76] A. Pitarch, G. Garcia-Belmonte, I. Mora-Sero, J. Bisquert, Electrochemical impedance spectra for the complete equivalent circuit of diffusion and reaction under steady-state recombination current, *Phys. Chem. Chem. Phys.* **6** (2004) 2983.
- [77] M. Ates, A. S. Sarac, Electrochemical impedance spectroscopic study of polythiophenes on carbon materials, *Polym. Plast. Tech. Eng.* **50** (2011) 1130–1148.
- [78] J.-S. Yoo, I. Song, J.-H. Lee, S.-M. Park, Real-time impedance measurements during electrochemical experiments and their application to aniline oxidation, *Anal. Chem.* **75** (2003) 3294–3300.
- [79] A.-E.-H. Bekkali, I. Thurzo, T. U. Kampen, D. R. Zahn, Impedance spectroscopy study of metal–organic–metal structures, *Appl. Surf. Sci.* **234** (2004) 149–154.
- [80] V. S. Reddy, S. Das, S. K. Ray, A. Dhar, Studies on conduction mechanisms

- of pentacene based diodes using impedance spectroscopy, *J. Phys. D: Appl. Phys.* **40** (2007) 7687–7693.
- [81] R. D. McCullough, R. D. Lowe, Enhanced electrical conductivity in regioselectively synthesized poly(3-alkylthiophenes), *J. Chem. Soc. Chem. Comm.* (1) (1992) 70.
- [82] N. F. Mott, The theory of crystal rectifiers, *Proc. Roy. Soc. A: Math. Phys. Eng. Sci.* **171** (1939) 27–38.
- [83] W. Schottky, Zur halbleiterttheorie der sperrschicht- und spitzengleichrichter, *Zeit. Phys.* **113** (1939) 367–414.
- [84] M. S. A. Abdou, F. P. Orfino, Y. Son, S. Holdcroft, Interaction of oxygen with conjugated polymers: Charge transfer complex formation with poly(3-alkylthiophenes), *J. Am. Chem. Soc.* **119** (1997) 4518–4524.
- [85] H. Nishimura, M. Iizuka, M. Sakai, M. Nakamura, K. Kudo, Poly(3-hexylthiophene) field-effect transistor with controllable threshold voltage, *Jap. J. Appl. Phys.* **44** (2005) 621–625.
- [86] N. Sato, *Electrochemistry at metal and semiconductor electrodes*, Elsevier, Amsterdam and New York, 1998.
- [87] M. Scharber, N. Sariciftci, Efficiency of bulk-heterojunction organic solar cells, *Prog. Polym. Sci.* doi:10.1016/j.progpolymsci.2013.05.001.
- [88] P. W. M. Blom, V. D. Mihailetschi, L. J. A. Koster, D. E. Markov, Device physics of polymer:fullerene bulk heterojunction solar cells, *Adv. Mater.* **19** (2007) 1551–1566.
- [89] C. J. Brabec, S. Gowrisanker, J. J. M. Halls, D. Laird, S. Jia, S. P. Williams, Polymer-fullerene bulk-heterojunction solar cells, *Adv. Mater.* **22** (2010) 3839–3856.
- [90] J. vanDuren, X. Yang, J. Loos, C. W. T. Bulle-Lieuwma, A. B. Sieval, J. C. Hummelen, R. A. J. Janssen, Relating the morphology of poly(p-phenylene vinylene)/methanofullerene blends to solar-cell performance, *Adv. Funct. Mater.* **14** (2004) 425–434.
- [91] M. Grätzel, Dye-sensitized solar cells, *J. Photochem. Photobiol C Photochem. Rev.* **4** (2003) 145–153.

CURRICULUM VITAE

Jacek Gąsiorowski



Personal Data

Address	(Poland)	ul. Bukowska 130a/7 60-398 Poznań Poland
	(Austria)	Julius Raab Strasse 5-7/413 4040 Linz Austria
Phone number (private)		+43 650 9031760
	(work)	+43 732 2468-8854
E-mail		jacek.gasiorowski@jku.at

Education

02/2009 - present

DOCTORAL PROGRAM IN ENGINEERING AND NATURAL SCIENCES

Topic: "**Doping induced effects in the organic semiconductors and bulk heterojunction solar cells**"

Under supervision of:

o.Univ. Prof. Mag. Dr. DDr. h. c. Niyazi Serdar Sariciftci

Physical Chemistry Department and Linz Institute for Organic Solar Cells (LIOS), Johannes Kepler University of Linz, Austria

Main focus:

- Electrochemical, chemical and photodoping of organic semiconductors and bulk heterojunctions
- Characterization of the electrochemical doping: Electrochemical Scanning Droplet Cell Microscopy (SDCM) and Photoelectrochemical Scanning Droplet Cell Microscopy (PE-SDCM), Cyclic Voltammetry, Electrochemical Impedance Spectroscopy, Spectroelectrochemistry in FTIR/UV-Vis, Ellipsometric spectroelectrochemistry
- Characterization of the chemical and photo doping: in-situ FTIR, Spectroscopic Ellipsometry, Conductivity measurements
- Preparation, optimization and characterization of the polymer based organic solar cells

12/2007 - 12/2008

REGIONE LAZIO SCHOLARSHIP

Topic: "**Flexible hybrid and dye-sensitized solar cells**"

Electronic Engineering Department, University of Rome "Tor Vergata", Rome, Italy

Main focus:

- Dye Sensitized Solar Cell on flexible substrates - preparation, optimization and characterization

06/2006 –08/2007

DIPLOMA THESIS

Topic: “**Organic Solar Cells with fine-tuned morphology and Donor:Acceptor composition by OVPD**”

Under supervision of:

Prof. Małgorzata Śliwińska-Bartkowiak (Adam Mickiewicz University, Poznań, Poland)

Prof. Martha Christina Lux-Steiner (Hahn-Meitner Institut Berlin, Germany)

Dr. Marin Rusu (Hahn-Meitner Institut, Berlin, Germany)

Dr. Konstantinos Fostiropoulos (Hahn-Meitner Institut, Berlin, Germany)

Main focus:

- Development of the Organic Vapor Phase Deposition (OVPD) technique
- Morphology and surface characterization (SEM, XRD) of thin films
- Preparation, optimization and characterization of organic solar cells containing small molecules (phthalocyanines, C₆₀)

10/2002 - 09/2007

DIPLOMA PROGRAM:

Material Engineering – specialisation: Nanotechnology

Physics Department, Adam Mickiewicz University, Poznań,
Poland

PUBLICATIONS

2013

22. C. Yumusak, J. Gasiowski, N. S. Sariciftci „**Solution processed organic field effect transistor based on low band gap polymer PBDTTT-c**” *Synth. Met.* submitted

21. J. Gasiowski, J. P. Kollender, K. Hingerl, N. S. Sariciftci, A. I. Mardare, A. W. Hassel "**Photoelectrochemical scanning droplet cell microscopy for localized photovoltaic investigations on organic semiconductors**" *Phys. Chem. Chem. Phys.* submitted

20. J. Gasiowski, S. Boudiba, K. Hingerl, C. Ulbricht, V. Fattori, F. Tinti, N. Camaioni, R. Menon, S. Schlager, L. Boudida, N. S. Sariciftci, D. A. M. Egbe "**Anthracene-Containing Conjugated Polymer Showing Four Optical Transitions Upon Doping: a Spectroscopic Study**" *Adv. Opt. Mat.* submitted

19. C. Reanprayoon, P. Thamyongkit, J. Gasiowski, N. S. Sariciftci "**Photosensitizing Porphyrin-Diacetylene towards Bulk Heterojunction Solar Cells**" *RSC Advances* accepted

18. J. Gasiowski, K. Hingerl, R. Menon, T. Plach, K. Wiesauer, C. Yumusak, N. S. Sariciftci "**The dielectric function of undoped and doped MDMO-PPV by ellipsometry in a wide spectral range**" *J. Phys. Chem. C* DOI: 10.1021/jp4061957

17. J. Gasiowski, A. I. Mardare, N. S. Sariciftci, A. W. Hassel "**Characterization of electrochemically doped PBDTTT-c using scanning droplet cell microscopy**" *Electrochim. Acta* DOI:10.1016/j.electacta.2013.07.050

16. T. Kengthanomma, P. Thamyongit, J. Gasiowski, A. Montigne-Ramil, N. S. Sariciftci "**On the potential of porphyrin-spiked triarylamine stars for bulk heterojunction solar cells**" *J. Mat. Chem.* 1 (2013) 10524

15. E. D. Głowacki, G. Voss, K. Demirak, M. Havlicek, N. Suenger, A. C. Okur, U. Monkowius, J. Gasiowski, L. Leonat, E. Tordin, Z. Bozkurt, A. Gerisch, M. Irmia-Vladu, S. Bauer, N. S. Sariciftci "**A facile protect-deprotect route for obtaining indigo pigments as thin films and in organic bulk heterojunctions**" *Chem. Comm.* 49 (2013) 6063

14. V. Zardetto, G. De Angelis, L. Vesce, V. Caratto, C. Mazzuca, J. Gasiorowski, A. Reale, A. Di Carlo, T. Brown **"Formulations and processing of nanocrystalline TiO₂ films for different requirements of plastic, metal and glass dye solar cell applications"** *Nanotech.* 24 (2013) 255401
13. J. Gasiorowski, R. Menon, K. Hingerl, M. Dachev, N. S. Sariciftci **"Surface morphology, optical properties and conductivity changes of poly(3,4-ethylenedioxythiophene):poly(styrenesulfonate) by using additives"** *Thin Sol. Films* 513 (2013) 211
12. E. Portenkirchner, J. Gasiorowski, K. Oppelt, S. Schlager, C. Schwarzingler, H. Neugebauer, G. Knör, N. S. Sariciftci **„Toward efficient electrocatalytic reduction of carbon dioxide to carbon monoxide by a polymerized film of the alkynyl-substituted rhenium (I) complex (5,5'-bisphenylethynyl-2,2'-bipyridyl)Re(CO)₃Cl"** *Chem. Cat. Chem.* 5 (2013) 1790
11. J. Gasiorowski, E. D. Głowacki, B. Hajduk, M. Siwy, M. Chwastek-Ogierman, J. Wieszka, H. Neugebauer, N. S. Sariciftci **"Doping-induced immobile charge carriers in polyazomethine: a spectroscopic study"** *J. Phys. Chem. C* 117 (2013) 2584
10. E. D. Głowacki, M. Irmia-Vladu, M. Kaltenbrunner, J. Gasiorowski, M. White, G. Romanazzi, G. P. Suranna, P. Mastroianni, T. Sekitani, S. Bauer, T. Someya, L. Torsi, N. S. Sariciftci **"Hydrogen bonded semiconducting pigments for air-stable field effect transistors"** *Adv. Mat.* 25 (2013) 1563
9. J. Gasiorowski, A. I. Mardare, N. S. Sariciftci, A. W. Hassel **"Electrochemical characterization of sub-micro-gram amounts of organic semiconductors using scanning droplet cell microscopy"** *J. Electroanal. Chem.* 691 (2013) 77

2012

8. H. Bednarski, J. Gasiorowski, M. Domanski, B. Hajduk, J. Jurusik, B. Jarzabek, J. Wieszka **"Stability of Diodes with Poly(3-hexylthiophene) and Polyazomethines Thin Organic Layer"** *Acta Phys. Pol. A* 122 (2012) 1085
7. M. Grucela-Zajac, M. Filapek, L. Skorcka, J. Gasiorowski, H. Neugebauer, E. Schab-Balcerzak **"Thermal, optical, electrochemical and electrochromic characteristics of novel polyimides bearing the Acridine Yellow moiety"** *Mater. Chem. Phys.* 137 (2012) 221
6. A. Luechai, J. Gasiorowski, A. Petsom, H. Neugebauer, N. S. Sariciftci, P. Thamyongkit **"Photosensitizing porphyrin-triazine compound for bulk heterojunction solar cells"** *J. Mater.*

2009

5. J. Gasiorowski, B. Meana-Esteban, P. Troshin, H. Neugebauer, N.S. Sariciftci „**Elektrochemiczne i optyczne badania pochodnych diimidu naftalenowego: nowego półprzewodnika typu n organicznych ogniw słonecznych**” Conference Proceedings of the 1st National Conference on Photovoltaic, Krynica-Zdrój, Poland, October 9th-11th, 2009

4. M. Rusu, J. Gasiorowski, S. Wiesner, D. Keiper, N. Meyer, M. Heuken, K. Fostiropoulos and M.Ch. Lux-Steiner “**Performance and Transport Properties of Phthalocyanine:Fullerene Organic Solar Cells**” *Springer Proceedings in Physics*, **2009**, Vol. 129 (5), 195-198

2008

3. M. Rusu, S. Wiesner, D. Keiper, J. Gasiorowski, N. Meyer, M. Heuken, K. Fostiropoulos, M.Ch. Lux-Steiner “**Organic Photovoltaic Devices with fine-controlled Donor and Acceptor Composition Profiles**” Proceedings of the 23rd EU-PVSEC in Valencia, Spain, September 1st -5th, 2008

2. M. Rusu, J. Gasiorowski, S. Wiesner, N. Meyer, M. Heuken, K. Fostiropoulos and M.Ch. Lux-Steiner “**Fine tailored interpenetrating donor-acceptor morphology by OVPD for organic solar cells**” *Thin Solid Films* 519 (2008) 7160

2007

1. M. Rusu, J. Gasiorowski, S. Wiesner, N. Meyer, M. Heuken, K. Fostiropoulos, M.Ch. Lux-Steiner “**Organic Solar Cells with fine-tuned Morphology and Donor:Acceptor Composition by OVPD**” Conference Proceedings, 22nd EUPVSEC, Milan, Italy, September 3-7, 2007

INVITED LECTURES

6-15/12/2009

“**New concepts in photovoltaics: from inorganic to organic materials**”

Delta State University, Cleveland (MS), United States of America

CONFERENCES

Oral presentation (First author only)

- 8 –13.09.2013 J. Gasiorowski, K. Hingerl, K. Oppelt, Ch. Cobet and N. S. Sariciftci
”Ellipsometric spectroelectrochemistry - an insight in the optical properties of doped organic semiconductors” 64th Annual Meeting of the International Society of Electrochemistry, Santiago de Queretaro, Mexico
- 12 –16.05.2013 J. Gasiorowski, A. I. Mardare, J. Kollender, N. S. Sariciftci and A. W. Hassel**”Scanning Droplet Cell Microscopy for electrochemical characterization of semiconducting polymers”** 223rd Electrochemical Society Meeting, Toronto, Canada
- 19 –25.08.2012 J. Gasiorowski, A. I. Mardare, H. Neugebauer, N. S. Sariciftci and A. W. Hassel **”High throughput screening of small amounts of organic semiconductors using a scanning droplet cell”** 63rd Annual Meeting of the International Society of Electrochemistry, Prague, Czech Republic
- 15 –17.08.2012 J. Gasiorowski, P. Stadler, A. I. Mardare, A. W. Hassel, M. White, S. Schlager, H. Neugebauer and N. S. Sariciftci **”Electrochemical, chemical and photo-doping in low band gap polymer PBDTTT-c”** 9th International Symposium on Electrochemical Micro & Nanosystem Technology (EMNT 2012), Linz, Austria
- 7-11.10.2009 J. Gasiorowski, B. Meana-Esteban, P. Troshin, H. Neugebauer, N.S. Sariciftci
“Electrochemical and optical studies on different derivatives of naphthalene diimides: new n-type semiconductor for organic solar cells”
1st National Conference on Photovoltaics, Krynica Zdrój, Poland
- 22-29.07.2007 J. Gasiorowski, M. Rusu, M. Ch. Lux-Steiner and M. Śliwińska-Barkowiak
”Organic solar cells with fine tuned morphology and Donor:Acceptor composition by OVPD” Polish-German summer school of nanotechnology „Nanoscience”, Poznań, Poland